Spring 2022

ESTABLISHING PTERIDINE METABOLISM IN A BREAST CANCER CELL MODEL AND QUANTIFICATION OF SILVER NANOPARTICLE INTERACTIONS WITH YEAST CELLS USING MASS SPECTROMETRY

Lindsey Katherine Rasmussen
Missouri University of Science and Technology

Department: Chemistry

ESTABLISHING PTERIDINE METABOLISM IN A BREAST CANCER CELL MODEL AND QUANTIFICATION OF SILVER NANOPARTICLE INTERACTIONS WITH YEAST CELLS USING MASS SPECTROMETRY

by

LINDSEY KATHERINE RASMUSSEN

A DISSERTATION

Presented to the Graduate Faculty of the

MISSOURI UNIVERSITY OF SCIENCE AND TECHNOLOGY

In Partial Fulfillment of the Requirements for the Degree

DOCTOR OF PHILOSOPHY

in

CHEMISTRY

2022

Approved by:

Honglan Shi, Advisor
Yinfa Ma
Paul Nam
Jeffrey Winiarz
David Westenberg

PUBLICATION DISSERTATION OPTION

This dissertation consists of the following three articles, two of them have been published and one was submitted for publication (under review). The publication option is used by following the corresponding scientific journal format.

Paper I, found on pages 18-42, has been published. Lindsey Rasmussen, Zachary Foulks, Casey Burton, Honglan Shi. Establishing pteridine metabolism in a progressive isogenic breast cancer cell model, *Metabolomics*, 18(1): 2022. http://doi.org/10.1007/s11306-021-01861-9.

Paper II, found on pages 43-70, has been submitted to *Metabolomics.* Lindsey Rasmussen, Zachary Foulks, Jiandong Wu, Casey Burton, Honglan Shi. Establishing pteridine metabolism in a progressive isogenic breast cancer cell model – Part II. Under review.

Paper III, found on pages 71-98, has been published. Lindsey Rasmussen, Honglan Shi, Wenyan Liu, Katie B. Shannon. Quantification of silver nanoparticle interactions with yeast *Saccharomyces cerevisiae* studied using single-cell ICP-MS, *Analytical and Bioanalytical Chemistry*, 2022, https://doi.org/10.1007/s00216-022-03937-4.

ABSTRACT

Recent advances in analytical methods have furthered the quantitative insights that can be gleaned from cellular analyses, with applications in cancer and nanoparticle research. In the first part of the research presented, a recently developed HPLC-MS/MS method was advanced to elucidate pteridine metabolism in an isogenic progressive MCF10A breast cancer cell model. The folate-derived pteridine pathway in breast cells was established by individually dosing cell cultures with folic acid and 15 pteridines. Eight potential pteridine biomarkers in breast cancer cells were identified including pterin and isoxanthopterin, which yielded the first *in vitro* evidence for the cellular metabolisms behind previously reported elevated urinary pteridine levels in breast cancer patients, which could eventually lead to the development of a non-invasive cancer screening technique, as well as highlighted key metabolic reactions for further biomarker investigation. In the second part of the research presented, cutting-edge single cell (SC)-ICP-MS was utilized to investigate the interaction of silver nanoparticles (AgNPs), one of the most broadly utilized type of NP, with *Saccharomyces (S) cerevisiae* yeast cells, a potential candidate for green manufacturing of AgNPs. Rapid quantification of cell concentration, silver concentration per cell, and the profile of AgNP distribution in a cell population was used to evaluate dose time, concentration, and size impacts on AgNP uptake and to quantify intracellular versus extracellular AgNP concentrations. This high throughput, ultra-sensitive SC-ICP-MS method is expected to have many potential applications, such as optimization of AgNP green synthesis procedures, drug delivery, and nanotoxicity.

ACKNOWLEDGEMENTS

First and foremost, I want to thank my advisor, Dr. Honglan Shi, for her unending patience, kindness, and encouragement. She has fully supported my non-traditional academic journey and pushed me to aim higher. I will have more opportunities in my career because of her faith in me and persistence to make that a reality. Secondly, I want to thank Dr. Yinfa Ma, who first recruited me to the research group and got me started on this journey. Thirdly, I want to thank my pteridine research coworkers: Dr. Casey Burton, who conceived the research and provided invaluable expertise throughout; and Zachary Foulks, who was my partner on almost every experiment for the two papers of the pteridine metabolism study. I am grateful to have had an incredibly smart, talented, and positive undergraduate student with whom to collaborate.

I also want to thank the rest of my committee members: Dr. Paul Nam, who has provided advice and feedback throughout weekly group meetings, and Dr. David Westenberg and Dr. Jeffrey Winiarz for their support and encouragement. I also want to thank Dr. Katie Shannon, Dr. Wenyan Liu, Dr. Jiandong Wu, Dr. Ke Li, and various individuals at Perkin Elmer for their advice. Additional thanks must be made to the National Institute of Health (NIH), the National Cancer Institute, Perkin Elmer, Inc., the Center for Single Nanoparticle, Single Cell, and Single Molecule Monitoring, the College of Arts, Sciences, and Business (CASB), and Brewer Science, Inc. for funding the research, tuition, and conference travel over the past six years.

Finally, I want to thank the rest of my research group, my coworkers at Brewer Science, and my family and friends for their countless small acts of kindness, support, and sacrifice day-to-day that made this achievement possible.

TABLE OF CONTENTS

Page

PUBLICATION DISSERTATION OPTION iii

ABSTRACT iv

ACKNOWLEDGEMENTS v

LIST OF ILLUSTRATIONS x

LIST OF TABLES xi

NOMENCLATURE xii

SECTION

1. INTRODUCTION 1

1.1. PTERIDINE METABOLISM IN BREAST CANCER 1

1.1.1. Pteridines and Breast Cancer 1

1.1.2. Advantages of HPLC-MS/MS Analysis for Pteridine Study 4

1.1.3. Research Objective – Part 1 6

1.2. SILVER NANOPARTICLE INTERACTIONS WITH YEAST CELLS STUDIED BY SINGLE CELL-ICP-MS 7

1.2.1. Single Cell – ICP-MS 7

1.2.2. Why Study Nanoparticle Interactions with Cells? 14

1.2.3. Research Objective – Part 2 17

PAPER

I. ESTABLISHING PTERIDINE METABOLISM IN A PROGRESSIVE ISOGENIC BREAST CANCER CELL MODEL 18

ABSTRACT 18

1. INTRODUCTION 19

2. EXPERIMENTAL 22

2.1. CHEMICALS AND MATERIALS 22

2.2. HPLC-MS/MS METHOD 23

2.3. CELL CULTURE, FOLIC ACID DOSING, AND SAMPLE PREPARATION 24

2.4. PROTEIN ASSAY 26

2.5. QUALITY CONTROL AND STATISTIC ANALYSIS 26

3. RESULTS AND DISCUSSION 27

3.1. PTERIDINE EXTRACTION AND ANALYSIS METHOD PERFORMANCE 27

3.2. INTRACELLULAR AND EXTRACELLULAR PTERIDINES 27

3.3. CORRELATIONS OF EXTRACELLULAR PTERIDINE LEVELS WITH TUMORIGENICITY 30

3.4. IMPLICATIONS FOR FOLATE-DERIVED PTERIDINE METABOLISM . 32

4. CONCLUSIONS 35

SUPPLEMENTARY INFORMATION 37

ACKNOWLEDGEMENTS 38

REFERENCES 38

II. ESTABLISHING PTERIDINE METABOLISM IN A PROGRESSIVE ISOGENIC BREAST CANCER CELL MODEL – PART II 43

ABSTRACT 43

1. INTRODUCTION 44

2. EXPERIMENTAL 47

2.1. CHEMICALS AND MATERIALS 47

2.2. HPLC-MS/MS METHOD 48

2.3. CELL CULTURE, PTERIDINE DOSING, AND SAMPLE PREPARATION 48

3. RESULTS AND DISCUSSION 50

3.1. DOSING STUDY FOR METABOLIC PATHWAY CONFIRMATION 50

3.1.1. Screening Study for Pteridines Metabolized by Breast Cells 50

3.1.2. 6-Carboxypterin Dosing Results 52

3.1.3. Pterin Derived Metabolic Pathway 53

3.1.4. 7,8-Dihydroxanthopterin and Xanthopterin Dosing Results 55

3.1.5. Sepiapterin Dosing Results 55

3.2. EFFECTS OF TUMORIGENICITY ON PTERIDINE METABOLISMS 56

3.2.1. Pterin Precursor 57

3.2.2. Xanthopterin Precursor 59

3.2.3. Sepiapterin Precursor 60

4. CONCLUSIONS 62

SUPPLEMENTARY INFORMATION 63

ACKNOWLEDGEMENTS 67

REFERENCES 67

III. QUANTIFICATION OF SILVER NANOPARTICLE INTERACTIONS WITH YEAST *SACCHAROMYCES CEREVISIAE* STUDIED USING SINGLE-CELL ICP-MS 71

ABSTRACT 71

1. INTRODUCTION 72

2. MATERIALS AND METHODS 76

2.1. MATERIALS 76

2.2. YEAST CELL CULTURE 77

2.3. SINGLE-CELL ICP-MS METHOD 77

2.4. CELLULAR EXPOSURE TO AGNPS AND SC-ICP-MS ANALYSIS 78

2.5. TRANSMISSION ELECTION MICROSCOPE IMAGING OF AGNP-DOSED YEAST CELLS 80

3. RESULTS AND DISCUSSION 80

3.1. SC-ICP-MS METHOD OPTIMIZATION AND PERFORMANCE 80

3.1.1. Transmission Efficiency Determination 80

3.1.2. Reproducibility and Stability 82

3.1.3. Linear Correlation and Detection Limits 83

3.2. WASHING METHODS AND THEIR IMPACTS ON AGNP AND YEAST CELL INTERACTIONS 84

3.3. DOSING TIME IMPACT ON AGNP UPTAKE 86

3.4. UPTAKE EFFICIENCIES BY DIFFERENT SIZES OF AGNPS AT DIFFERENT DOSING CONCENTRATIONS 87

3.5. INTERNAL UPTAKE VERSUS CELL SURFACE-ADSORBED AGNP 89

4. CONCLUSIONS 91

SUPPLEMENTARY INFORMATION 92

ACKNOWLEDGEMENTS 93

REFERENCES 94

SECTION

2. CONCLUSIONS 99

BIBLIOGRAPHY 102

VITA 111

LIST OF ILLUSTRATIONS

SECTION Page

Figure 1.1. Pterin (left) and lumazine (right). 2

Figure 1.2. Histogram of silver nanoparticle dosed yeast cells. 8

Figure 1.3. Top: Single cell sample introduction system with Asperon^{TM} spray chamber. Bottom: Meinhard HEN single cell nebulizer. 10

PAPER I

Figure 1. Concentrations of pteridines in extracellular media with and without cells.. ... 29

Figure 2. Total extracellular pteridine masses produced per million cells and per microgram protein (n = 2). 30

Figure 3. Folic acid derived pteridine metabolic pathway 33

PAPER II

Figure 1. Pteridine pathway in breast cells based on screening and quantitative studies. 50

Figure 2. Production of pteridine derivatives in different breast cells following dosing with PTE (12.26 µM) for five days (n=3). 58

Figure 3. Production of pteridine derivatives in different breast cells following dosing with SEP (8.43 µM) for five days (n = 3). 62

PAPER III

Figure 1. Gaussian distribution fitting of representative histogram for AgNP-dosed yeast cells. 83

Figure 2. Cell concentrations detected by SC-ICP-MS versus hemacytometer-counted cell concentrations tested on 2 different days. 84

Figure 3. Cellular uptake of 10 nm AgNPs vs exposure time. 87

Figure 4. Uptake concentration versus dosing concentration ag Ag/cell for different sizes of AgNPs. 88

Figure 5. Uptake concentrations and %uptake versus dosing particle concentrations. 89

LIST OF TABLES

PAPER I Page

Table 1. Mass fractions of intracellular vs. extracellular pteridines (total intracellular mass to total extracellular mass) (n = 3) 28

PAPER II

Table 1. Production of cell-derived pteridines following dosing with different pteridine precursors... 51

Table 2. Concentrations (pmol/million cells) of unreacted xanthopterin precursor and 7,8-dihydroxanthopterin product. 60

PAPER III

Table 1. Optimized single-cell ICP-MS parameters. 78

Table 2. Transport efficiencies measured with yeast cell suspensions (intrinsic metal ^{64}Zn was monitored), EQ four-element calibration beads (^{140}Ce in the beads was monitored), and Au NPs (^{107}Au was monitored) in aqueous and matrix-matched solutions. 82

Table 3. Quantitative comparison of cell surface adsorbed and intracellular AgNPs. . .. 86

NOMENCLATURE

Symbol	Description
HPLC-MS/MS	High Performance Liquid Chromatography – Tandem Mass Spectrometry
MCF10A (A)	Nontumorigenic breast cell line
MCF10AT (T)	Premalignant/tumorigenic breast cell line, also MCF10AneoT
MCF10CA1a (C)	Tumorigenic/metastatic breast cell line
m/z	Mass-to-charge ratio
DTT	Dithiothreitol
XOR	Xanthine oxidoreductase
FR	Folate receptor
GTP	Guanine triphosphate
SC-ICP-MS	Single Cell – Inductively Coupled Plasma – Mass Spectrometry
NP	Nanoparticle
AgNP	Silver Nanoparticle
TE	Transport efficiency

1. INTRODUCTION

1.1. PTERIDINE METABOLISM IN BREAST CANCER

1.1.1. Pteridines and Breast Cancer. Pteridines are bicyclic nitrogen compounds consisting of one pyrimidine and one pyrazine ring with various functional groups. They are ubiquitous in nature and act as color compounds in a wide variety of animals such as the wings of butterflies (Watt, 1967, 1972), skins of amphibians and reptiles (Brejcha et al., 2019; Odate et al., 1959), and the scales of fish (Braasch et al., 2007). They are also present in the human body as vitamins and cofactors (Burton et al., 2016a; Fukushima and Shiota, 1974; Tomšíková et al., 2013) with functions in areas such as vasodilation (Alp and Channon, 2004; Chalupsky et al., 2015; Crabtree et al., 2009; Gao et al., 2009; Gross and Levi, 1992) and immune response (Kośliński et al., 2011; Murr et al., 1999; Schoedon et al., 1987; Weiss et al., 1993). Analogs to pteridines are the lumazines, which have a similar structure, but a carbonyl group instead of an amide group at the C-2 position (Figure 1.1). Lumazines are generated from the pteridines by a deaminase, although the specific one responsible *in vivo* has not been identified (Fan et al., 2013; Jayaraman et al., 2016; Murugesan et al., 2017; Rembold and Simmersbach, 1969). Pteridines have been studied extensively while lumazines have been typically excluded, but both are present in the biological system (Burton and Ma, 2017).

In 1977, it was first reported that pterin-6-aldehyde, aka 6-formylpterin, levels were elevated in the cell media of cancer cells and in the urine of cancer patients (Halpern et al., 1977), prompting study into the use of pteridines as biomarkers for cancer over the past 45 years (Burton and Ma, 2017; Kośliński et al., 2011; Ma and Burton,

2013; Stea et al., 1978; Stea et al., 1981; Tomšíková et al., 2013). However, investigations were complicated low pteridine levels, complex biological environments, absence of an ultra-sensitive detection method, and the instability of pteridines under various analytical methods (Burton and Ma, 2017, 2019; Kośliński et al., 2011; Tomšíková et al., 2013). Therefore, the metabolic pathways and mechanisms are not well understood. Pteridine concentrations can be altered by the cell type (Goldberg and Koller, 1991; Kośliński et al., 2011), cancer stage (Rasmussen et al., 2022a; Stea et al., 1978), and sample type analyzed (ie, cellular extract, serum, urine, etc.) (Tomšíková et al., 2013). Therefore, if pteridines are to be used as biomarkers for cancer detection, it is necessary to understand how pteridine metabolisms are altered in the presence of each specific cancer, and how these changes may be best detected.

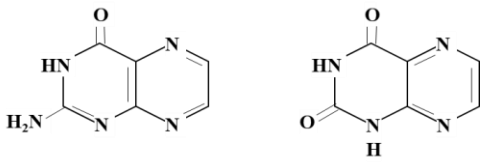

Figure 1.1. Pterin (left) and lumazine (right).

Breast cancer is a unique case for pteridine metabolism study. Multiple previous studies, several of which have been within our research group in the Department of Chemistry at Missouri University of Science and Technology, have shown altered pteridine levels in the urine of breast cancer patients, specifically, elevated levels of isoxanthopterin and xanthopterin (Burton et al., 2014, 2016b; Gamagedara et al., 2011). However, the relationship between the altered urinary pteridine levels and the breast

cancer effects on the pteridine metabolisms are not understood. The objective of this investigation was to interrogate how pteridine metabolisms may be altered by breast cells with tumorigenicity to determine if the concentrations are directly tied to alterations occurring in the cells themselves or elsewhere in the body such as the kidneys.

One of the enzymes that has been shown to act on pteridines in the metabolic pathway is the xanthine oxidoreductase (XOR) enzyme (Blau et al., 1996; Oettle and Reibnegger, 1999; Rembold et al., 1971). It is a non-specific enzyme that reacts with several pteridine substrates including pterin, xanthopterin, 6-hydroxylumazine, and lumazine (Blau et al., 1996; Oettle and Reibnegger, 1999; Rembold et al., 1971). This enzyme specifically has reduced activity in cancerous breast cells, and therefore is suspected to be a primary intracellular actor for the altered pteridine levels in breast cells (Battelli et al., 2015; Fini et al., 2011; Fini et al., 2008; Linder et al., 2005).

Another feature of breast cancer tumors is the correlation of folate receptor (FR) expression and breast cancer (Hansen et al., 2017; Necela et al., 2015) wherein it has been found to be a better predictor for cancer severity than tumor size or grade, nodal status, and estrogen receptor (Hartmann et al., 2007). Pteridines are mainly derived from two major precursors in the body: folic acid and guanine triphosphate (GTP) (Burton and Ma, 2017; Burton et al., 2016a; Fukushima and Shiota, 1974; Kośliński et al., 2011; Tomšíková et al., 2013). GTP-derived pteridines have been studied extensively, especially with respect to neopterin and biopterin (Kośliński et al., 2011; Tomšíková et al., 2013). However, the folic acid side of the pathway has been less studied (Burton et al., 2016a; Rasmussen et al., 2022a), and yet, folic acid-derived pteridines are likely to be directly impacted by tumorigenicity due to breast cancer's altered folate metabolism. In

this study, the pteridine panel was focused on the folic acid-derived pteridines as these were hypothesized to be impacted most by tumorigenicity in the breast cell model.

1.1.2. Advantages of HPLC-MS/MS Analysis for Pteridine Study.

Several types of analytical methods have been used to investigate pteridines (Burton and Ma, 2017; Han et al., 1999; Kośliński et al., 2011; Tomšíková et al., 2013) including a variety of chromatographic methods such as TLC (Halpern et al., 1977; Stea et al., 1978), high performance liquid chromatography (HPLC-MS/MS) (Burton et al., 2015; Rasmussen et al., 2022a), HPLC-QTOF-MS (Burton et al., 2015), CE-LIF (Gamagedara et al., 2011; Gibbons et al., 2009), and HPLC-FD (Cañada-Cañada et al., 2009; Kośliński et al., 2014; Tomšíková et al., 2014). However, variation in results can occur due to the instability of certain pteridines by oxidation with exposure to air or degradation with exposure to light (Kośliński et al., 2011; Off et al., 2005; Tomšíková et al., 2013). This has led to differences in results just based on the analytical methods used (Burton and Ma, 2017) such as the 5 - 30 x higher concentrations of detected isoxanthopterin and xanthopterin in the urine of cancer patients using CE-LIF (Gamagedara et al., 2011) versus HPLC-MS/MS, which the authors attributed to possible coelution of interferences or differences in analyte oxidation states in the CE-LIF method (Burton et al., 2013). In addition, certain methods are better suited for specific classes of pteridines such as fully oxidized pteridines that fluoresce and so FD works well for their analysis while the tetra- and di- hydroforms generate low signal (Tomšíková et al., 2014; Tomšíková et al., 2013), which has led to a variety of oxidative pretreatments being developed and applied for pteridine analysis (Tomšíková et al., 2013). However, as shown by Burton, et al. (2016b), these oxidative pretreatments may cause quantitative inaccuracies, especially for the

reduced forms like 7,8-dihydroxanthopterin, and therefore analytical methods where pteridines are analyzed in their natural oxidation states may be advantageous for quantitation (Burton et al., 2016b).

The analysis method for quantification of pteridines in MCF10A breast cells developed by our research group kept pteridines in their natural form by addition of 0.1% dithiothreitol (DTT) which prevented the autooxidation of certain pteridines as shown by Burton, et al. (2015) in a previous study of pteridines in A549 cells. Stability of the compounds over the analysis period allowed for accurate quantification of the pteridine concentrations in the study.

HPLC-MS/MS is specifically well-suited for analysis of pteridines in their natural form since the reduced forms do not need to be oxidized for analysis (Burton et al., 2016b). The Luna phenyl-hexyl column and corresponding method parameters separate 15 pteridines in less than seven minutes, which is fast and allows for high throughput analysis, such as the current pteridine investigation of biological samples (Burton et al., 2016b). It is particularly useful for resolution of the xanthopterin and isoxanthopterin peaks, which are isomers, and therefore have the same [M + H] mass to charge ratio (m/z) of 180 when analyzed by mass spectrometry. Separation of the compounds prior to analysis allows for quantification of each peak. This is particularly advantageous for this study since both compounds have been identified as potential biomarkers of breast cancer in the urine of breast cancer patients (Burton et al., 2014, 2016b; Gamagedara et al., 2011).

Once the analytes are separated by the column, the sample is then ionized by electrospray ionization (ESI) and introduced into the mass analyzer. The instrumentation

used in this study is a triple quadrupole mass spectrometer wherein the analytes are separated in the first quadrupole by their parent ion m/z, [M + H]. In the second quadrupole, they are bombarded with N_2 gas to fragment the molecules into daughter ions. The daughter ions are then separated again by the third quadrupole before being detected. Only molecules that have both the specified parent and fragment ion m/z's will be detected and appear on the chromatogram for analysis. Analytes can be further discriminated by the retention time at which they appear, which is dependent on the corresponding column and conditions used. Two transitions for each molecule are monitored in the method and the most sensitive one is used for quantitation while the less sensitive one serves as confirmation. When validated with a known standard, compounds in a sample can be identified with confidence and analyzed.

1.1.3. Research Objective – Part 1. The purpose of this investigation was to detect how pteridine levels were altered with breast cancer in a progressive, isogenic MCF10A cell model consisting of the cell lines MCF10A (nontumorigenic), MCF10AT (premalignant/tumorigenic, also MCF10AneoT), and MCF10CA1a (tumorigenic/metastatic). An HPLC-MS/MS method previously developed in our research group was validated and utilized for the study (Burton et al., 2016b), and a protocol for the extraction and analysis of both intracellular and extracellular pteridines was optimized.

Cell samples were dosed with various levels of folic acid or pteridine precursor for specified periods of time and then analyzed for pteridine concentrations. Pteridines where concentrations in one cell line statistically differed from one or both of the other cell lines using Anova two-factor with replication test or paired t-test with two-tailed

distribution ($p < 0.05$) were considered to be potential biomarkers of breast cancer. Dosing with different pteridine precursors was utilized to confirm part of the proposed pteridine pathway in breast cells, parts of which have been proposed based on studies *in vitro* (Rembold et al., 1971), in other cell types (Fukushima and Shiota, 1974; Stea et al., 1978), or in urine (Blau et al., 1996; Burton et al., 2016a; Cañada-Cañada et al., 2009), but have not been previously reported in breast cells.

1.2. SILVER NANOPARTICLE INTERACTIONS WITH YEAST CELLS STUDIED BY SINGLE CELL-ICP-MS

1.2.1. Single Cell – ICP-MS. Single cell (SC) – inductively coupled plasma (ICP) – mass spectrometry is an emerging technique developed recently and is a derivation of the single particle (SP) – ICP – MS technique (Corte-Rodríguez et al., 2020). It is a time-resolved analytical method wherein all signals from a single mass-to-charge ratio (m/z) are detected during the analysis period. Cell suspensions are prepared at low concentrations so that statistically, at a low enough flow rate, one cell is introduced for analysis at a time so that each signal pulse detected by the instrument corresponds to one cell, and the intensity of the signal corresponds to the amount of that element in that cell. At the end of sample analysis, a histogram of cellular events versus mass is generated, providing the distribution of the selected mass in the cell population (Figure 1.2).

Conventional ICP-MS analysis of the metal content of cell samples is to acid digest a sample into a solution and then that solution is analyzed with ICP-MS. The digestion of a cell suspension to a single solution prior to analysis means that only the average concentration of the selected element in the cell population can be determined,

which is disadvantageous wherein the heterogeneity of the cell population cannot be resolved. Therefore, SC-ICP-MS solves this gap by changing the sample introduction setup on the front of the instrument and, commercially, the data analysis software so that the distribution of an element within a cell population can be elucidated (Corte-Rodríguez et al., 2020).

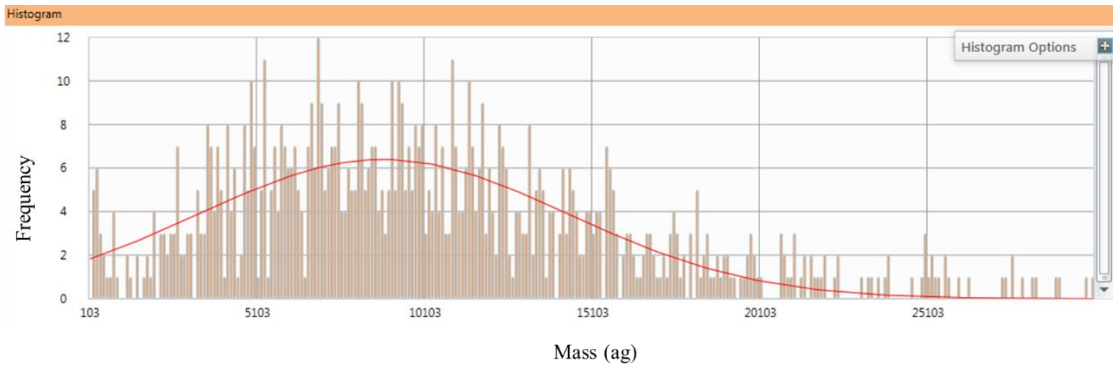

Figure 1.2. Histogram of silver nanoparticle dosed yeast cells.

Single cell analysis in literature covers a wide range of techniques in which SC-ICP-MS is one of them (Corte-Rodríguez et al., 2020; Miyashita et al., 2017; Mueller et al., 2014; Wei et al., 2020; Yin et al., 2019). Reviews typically separate the more narrow field of SC-ICP-MS analysis into three categories: (1) SC-ICP-MS (also referred to as time resolved (TR) -ICP-MS) wherein typically a quadrupole MS is utilized in conjunction with a pneumatic pump or microfluidic device sample introduction system, (2) laser ablation (LA) -ICP-MS where one cell at a time is ablated into the mass spectrometer, and (3) mass cytometry (SC-ICP-TOF-MS) (Corte-Rodríguez et al., 2020; Miyashita et al., 2017; Mueller et al., 2014; Yin et al., 2019; Yu et al., 2020). Mass cytometry is a commercialized technique developed by CyTOF®. Similar to SC-ICP-MS,

it uses a proprietary pneumatic pump sample introduction system (Corte-Rodríguez et al., 2020; Miyashita et al., 2017). The main difference in the two techniques is the use of a time-of-flight (TOF) mass spectrometer wherein data for multiple elements are simultaneously collected whereas one element is analyzed at a time when using a quadrupole MS (Miyashita et al., 2017; Mueller et al., 2014). However, almost all literature using this technique is focused on immunophenotyping or mass-tag cellular barcoding (MCB), with very few reported uses for the analysis of nanoparticle uptake in single cells (Ivask et al., 2017; Malysheva et al., 2021; Miyashita et al., 2017; Mueller et al., 2014). The current project utilized SC-ICP-MS with a single quadrupole mass spectrometor, and so the remaining discussion will focus on this specific technique and applications.

Sample introduction is a key differentiator of single cell analysis, and therefore different setups are being continually designed and evaluated (Corte-Rodríguez et al., 2020; Wang et al., 2017; Yu et al., 2020). Conventional ICP-MS sample introduction systems typically operate at higher sample flow rates (ie, 0.45 µL/min) and their design can cause cells to burst during nebulization prior entering the plasma. In contrast, the goal of any pneumatic single cell sample introduction system is to keep the cells intact until they reach the plasma. In this way, the element in a whole cell is ionized and introduced into the mass spectrometer almost simultaneously so that a detected pulse of ions by the instrument corresponds to the amount of that element in a single cell. A variety of custom and novel designs have been described in the past with a couple becoming commercially available from CyTOF®, Glass Expansion, and Perkin Elmer (Corte-Rodríguez et al.,

2020; Miyashita et al., 2017; Wang et al., 2017; Yu et al., 2020). The sample introduction setup from Perkin Elmer was evaluated in this research project.

The cell suspension is prepared at a concentration of ideally 100,000 cells/mL and is introduced into the instrument using a specialized high-efficiency sample introduction system containing a capillary nebulizer and a large, tapered sample chamber (Figure 1.3).

Figure 1.3. Top: Single cell sample introduction system with Asperon™ spray chamber. Bottom: Meinhard HEN single cell nebulizer.

The sample flows slowly at approximately 0.15 µL/min and the nitrogen (~0.25-0.5 L/min) and argon (0.7 L/min) gas flows are optimized so that the cells remain intact during the nebulization process until they reach the plasma, at which point, the sample is ionized ideally into its basic atomic elements. The optimal flow rate and gas flows are dependent on the cellular analyte's composition (Corte-Rodríguez et al., 2020) wherein cells with stronger cell walls or membranes, such as bacteria (Shen et al., 2019) and yeast cells (Rasmussen et al., 2022b), will more easily stay intact during the nebulization

process while thinner membrane cells like red blood cells are more prone to bursting upon nebulization (Cao et al., 2020; Tanaka et al., 2020). The overall rate at which the cells are introduced and eventually detected by the instrument is referred to as the transport efficiency (TE), and it is a critical parameter in the optimization of the SC-ICP-MS method, as well as a key advantage of the technique (Corte-Rodríguez et al., 2020).

To demonstrate, when a standard nanoparticle suspension is tested using the single particle sample introduction system (ie, a larger diameter nebulizer at a 0.45 µL/min flow rate and a cyclonic spray chamber which is design to separate larger droplets from the nebulized mist) the transport efficiency is typically 7-9%, whereas when the same nanoparticle suspension is tested using the single cell sample introduction system, the transport efficiency is typically 40-60%. When the same cell suspension is tested using the two techniques, the cellular transport efficiency may still reach approximately 7-9%, *if the cells stay intact at all*, using the SP setup whereas the TE will typically be about 30-40% with a higher confidence of intact cells using the SC setup.

The TE is dependent on the sample introduction parameters, analyte type, and instrument conditions. It can fluctuate day-to-day and so must be determined at the beginning of each experiment. There are multiple ways in which TE can be determined, and due to the newness of the technique, no “gold standard” method has been developed. One objective of this research project was evaluating parameters that may affect transport efficiency and potential best methods and practices for accurately quantifying TE. Three main approaches have been previously proposed: nanoparticle suspensions (Merrifield et al., 2018), cellular suspensions (Rasmussen et al., 2022b; Shen et al., 2019), and polystyrene bead suspensions (Merrifield et al., 2018; Rasmussen et al., 2022b).

Each TE determination method has its pros and cons. The use of nanoparticle suspensions for determination of TE stems from the current “gold standard” method used in SP analysis (Montoro Bustos et al., 2015; Montoro Bustos et al., 2018). Typically, the TE of gold nanoparticles (AuNPs) approximately 40-60 nm in diameter are tested at the beginning of an experiment and the TE determined is assumed to be accurate for the following analytes (Merrifield et al., 2018). AuNP standard suspensions are commercially available and easy to work with, with no interferences on the ICP-MS. However, in SC analysis, the TE of the nanoparticles may differ from that of cell samples due to their much smaller size, which can allow them to be transported at a higher efficiency and yield a non-representative TE for cellular analysis (Corte-Rodríguez et al., 2020). The second method to detect TE for SC-ICP-MS is using the cells. The cell concentration of a representative suspension of the cellular analyte is determined using a secondary method such as hemacytometry or flow cytometry, and then the TE calculated is derived from the concentration by monitoring an intrinsic metal in the cells (Rasmussen et al., 2022b; Shen et al., 2019). While this method ensures that TE is based on the behavior of the analyte itself, eliminating the uncertainty of if a nanoparticle suspension accurately yields a similar TE to the cellular suspension, it is not practical for all cell types. Cells that are not easily counted by hemacytometry or flow cytometry, such as those that readily aggregate or are extremely small, is a challenge for the TE determination both in terms of the initial determination of the cell concentration and under SC analysis. Therefore, this approach is not ideal for all cell types. The third method of TE detection is using lanthanide-doped polystyrene beads that are approximately 2.5 µm in diameter (Merrifield et al., 2018). They were originally

developed for use as standards in mass cytometry which is a form of single cell analysis using a time-of-flight mass spectrometer. Due to the similar size of the beads with cells, they can behave more similarly to the cells than nanoparticles for determination of TE and eliminate the potential error from cell counting (Corte-Rodríguez et al., 2020; Merrifield et al., 2018). In addition, the lanthanide metals also do not have any interferences for ICP-MS detection. However, in practice, the standard is not always accurate wherein it has been reported, as well as personally experienced during this project, that sometimes a preparation will yield an erroneous ~5-10% TE result and the standard has to be reprepared frequently (Leipold et al., 2017). Therefore, as part of method development, which technique is the most accurate and repeatable for a certain cell type must be determined.

After sample introduction, a quadrupole ICP-MS is used in single ion monitoring (SIM) mode in which a single mass is analyzed during the entire sampling period, which allows for each cell to be detected as a single pulse signal whose intensity correlates to the concentration of the metal analyte in each cell. The pulses detected over the course of the analysis time can then be converted to a histogram of the frequency of each mass concentration detected. Prior to commercialization of this technique, the pulse signals were converted to the histograms manually using the raw ICP-MS data, but now software has been developed where this analysis is performed automatically by the software and results are reported as such (Corte-Rodríguez et al., 2020; Ho and Chan, 2010). Due to the small size of the cells, results are typically reported in attograms (ag, 10^{-18} g) per cell and the results are binned, such as 100 ag increments, depending on what is practical for the analyte to derive a useful histogram.

As with all analytical techniques, SC-ICP-MS has its pros and cons when it comes to cellular analysis, and therefore its use depends on the application. While this technique introduces a key advantage over conventional ICP-MS analysis of cells wherein the heterogeneous distribution of an element in a cell population can be discriminated, only one element can be analyzed at a time, which is a disadvantage when several elements need to be monitored. In that case, acid digestion and analysis of a cell population by conventional ICP-MS techniques or use of mass cytometry, which can do SC analysis of multiple elements at once due to its use of a TOF-MS instead of a quadrupole MS, may be more applicable (Corte Rodríguez et al., 2017; Mueller et al., 2014). However, mass cytometry uses a specialized, expensive, separate instrument that requires specialized training and is cost prohibitive to implement in a laboratory setting that does not have a high throughput need for this analysis, whereas an existing ICP-MS can be setup to run SC analyses with minimal operator training, making it much cheaper and easier to implement.

1.2.2. Why Study Nanoparticle Interactions with Cells? Nanoparticles are typically defined as particles that are less than 100 nm in at least one dimension, and their small size can introduce unique properties to a material that many not otherwise occur at the atomic or macro scale (Bahadar et al., 2016; Kettler et al., 2014). For example, a generic piece of gold has a unique, shiny color at the macro level. However, when gold is in its colloidal nanoparticle form of less than 100 nm in diameter, the particles interact differently with light, causing the solution to be a reddish color. Commercially, nanoparticles can have a wide variety of applications from the anti-bacterial properties of silver nanoparticles embedded in materials (Rosli et al., 2021) to the improved electrical

properties of carbon nanotubes (Taghavi et al., 2013) to the UV protective properties of titanium dioxide and zinc oxide in sunscreen (Bahadar et al., 2016) to the use of lipid or polymeric nanoparticles for targeted drug delivery (Bahadar et al., 2016; Taghavi et al., 2013; Tenchov et al., 2021).

With the growth of the nanoparticle industry comes the hazards of how nanoparticle waste will impact the environment and how nanoparticles can impact the short-term and long-term health of users or people exposed to them (Bahrulolum et al., 2021; Bondarenko et al., 2013; Taghavi et al., 2013). Due to nanoparticles' smaller size, they can react differently in the body when inhaled, ingested, or absorbed (Bahadar et al., 2016; Taghavi et al., 2013). The interactions of nanoparticles with cells can depend on several variables including size, shape, and composition of the nanoparticle (Kettler et al., 2014), the environment or media in which the nanoparticle interacts with the cell (Kettler et al., 2016; Kettler et al., 2014), and the type of cell, tissue, or organism with which the nanoparticles are interacting (Bahadar et al., 2016; Bondarenko et al., 2013; Kettler et al., 2014). Not only does this complicate predicting and understanding how nanoparticles interact either in the environment or with regards to human body, but also introduces variation in research results where even the media chosen in an experiment can change how nanoparticles interact with cells, limiting the application scope of each study as well as preventing a regulated way to evaluate nanoparticle safety prior to production (Bahadar et al., 2016; Kettler et al., 2014; Taghavi et al., 2013).

A secondary environmental and health hazard aspect of the nanoparticle industry is the harsh chemicals which are used to manufacture the nanoparticles (Ahmed et al., 2016; Bahrulolum et al., 2021). This has led to the growing interest in "green

manufacturing" in which biological resources are utilized to synthesize the nanoparticles (Ahmed et al., 2016; Almatroudi, 2020; Badhusha and Mohideen, 2016; Bahrulolum et al., 2021; Zhang et al., 2016). For example, the functional groups of proteins on and inside of cells such as yeast or bacteria or even plant extracts can act as nucleation points on which nanoparticles can be grown when the ion of interest, such as gold or silver, is added to the cell suspension (Ahmed et al., 2016; Badhusha and Mohideen, 2016; Chen et al., 2017; Li et al., 2018; Sujith et al., 2008; Sujith et al., 2009). While not yet developed on a large scale, use of these methods at the laboratory level are well reported and continually investigated (Ahmed et al., 2016; Bahrulolum et al., 2021).

Due to the various ways in which nanoparticles can interact with cells, a parallel development of analytical metrology has arisen in the same time frame to improve both the characterization of the nanoparticles themselves and their effects (Ashraf et al., 2020; FitzGerald and Johnston, 2021; Hoseinzadeh et al., 2017; Mueller et al., 2014; Wei et al., 2020; Yu et al., 2020). While this list is expansive, the relevant area for this research project is quantification of nanoparticle uptake both on and in cells, for which SC-ICP-MS is well suited (Corte-Rodríguez et al., 2020; Mueller et al., 2014; Yu et al., 2020). In the area of drug delivery, this type of analysis is needed to better optimize the uptake of drugs. It has previously been reported that of the drug delivery methods developed, less than 1% of the drug actually makes it to its target *in vivo* (Wilhelm et al., 2016). SC-ICP-MS can provide valuable quantitative data to assist in the research to optimize uptake of the drugs, such as cisplatin for cancer treatment (Corte Rodríguez et al., 2017). In addition, SC-ICP-MS can be used to analyze the uptake of nanoparticles or heavy metals in algae cells for environmental analysis applications (Merrifield et al., 2018). Thirdly,

SC-ICP-MS could also be used to optimize nanoparticle green manufacturing for optimal yield (Rasmussen et al., 2022b).

1.2.3. Research Objective – Part 2. The purpose of this investigation was to evaluate how SC-ICP-MS could be used to monitor the uptake of nanoparticles by cells using silver nanoparticles and yeast cells a model. *Saccharomyces cerevisiae* has been reported as a potential candidate for green synthesis of silver nanoparticles (Badhusha and Mohideen, 2016; Bahrulolum et al., 2021; Chen et al., 2017; Li et al., 2018) while silver nanoparticles are one of the most commercially utilized type of nanoparticle (Bahrulolum et al., 2021; Bondarenko et al., 2013). Therefore, developing methods for optimizing green manufacturing of AgNPs could be hugely beneficial, and the current project objective was to investigate if SC-ICP-MS could potentially be applicable to supporting this endeavor, as well as development of a method that could be used by the nanoparticle engineering industry.

PAPER

I. ESTABLISHING PTERIDINE METABOLISM IN A PROGRESSIVE ISOGENIC BREAST CANCER CELL MODEL*

Lindsey Rasmussen[1], Zachary Foulks[1], Casey Burton[1,2], Honglan Shi[1]

[1]Department of Chemistry, Missouri University of Science and Technology, 400 W 11th Street, Rolla, MO 65409, USA

[2]Phelps Health, Rolla, MO 65401, USA

ABSTRACT

Introduction: Pteridines include folate-derived metabolites that have been putatively associated with certain cancers in clinical studies. However, their biological significance in cancer metabolism and role in cancer development and progression remains poorly understood.

Objectives: The purpose of this study was to examine the effects of tumorigenicity on pteridine metabolism by studying a panel of 15 pteridine derivatives using a progressive breast cancer cell line model with and without folic acid dosing.

Methods: The MCF10A progressive breast cancer model, including sequentially derived MCF10A (benign), MCF10AT (premalignant), and MCF10CA1a (malignant) cell lines were dosed with 0, 100, and 250 mg/L folic acid. Pteridines were analyzed in

---

* Reproduced with permission from Springer Nature

both intracellular and extracellular contexts using an improved high-performance liquid chromatography—tandem mass spectrometry method.

Results: Pteridines were located predominately in the extracellular media. Folic acid dosing increased extracellular levels of pterin, 6-hydroxylumazine, xanthopterin, 6-hydroxymethylpterin, and 6-carboxypterin in a dose-dependent manner. In particular, pterin and 6-hydroxylumazine levels were positively correlated with tumorigenicity upon folate dosing.

Conclusions: Folic acid is a primary driver for pteridine metabolism in human breast cell. Higher folate levels contribute to increased formation and excretion of pteridine derivatives to the extracellular media. In breast cancer, this metabolic pathway becomes dysregulated, resulting in the excretion of certain pteridine derivatives and providing in vitro evidence for the observation of elevated pteridines in the urine of breast cancer patients. Finally, this study reports a novel use of the MCF10A progressive breast cancer model for metabolomics applications that may readily be applied to other metabolites of interest.

Keywords: Pterin, Breast cancer, Folic acid, Folate-derived pteridine metabolism, MCF10A cell line, HPLC-MS/MS

1. INTRODUCTION

Pteridines have captivated humans for millennia as the brilliant pigments found on the wings of moths and butterflies (Braasch et al., 2007; Brejcha et al., 2019; Odate et al., 1959; Watt, 1972). More recently, they have garnered new interest as important

metabolic intermediates in the pathways of various cofactors and vitamins (Kośliński et al., 2011; Ma & Burton, 2013). Notably, pteridines and their derivatives are excreted in urine where they have been abundantly detected from cancer patients, driving interest in their application as novel cancer biomarkers (Burton et al., 2013, 2016b; Gamagedara et al., 2011; Ma & Burton, 2013; Shantaram et al., 2012). However, efforts to develop pteridine derivatives as cancer biomarkers have been challenged by their poorly established biological significance in cancer metabolism and progression. This limited understanding has been imposed primarily by analytical limitations relating to accurately detecting this diverse family of metabolites found intracellularly at trace concentrations. However, recent advancements in pteridine analysis have provided new opportunities to explore pteridine metabolism in disease contexts.

Pteridines are derived from guanosine triphosphate (GTP) and folic acid. The former gives rise to neopterin and biopterin derivatives which have been extensively studied as biologically significant intermediates in human health and disease (Blau et al., 1996; Burton et al., 2016a; Kośliński et al., 2011). Meanwhile, the metabolism of folate-derived pteridines and their possible linkages to GTP-derived pteridines remain poorly understood, though the conversion of folic acid to 6-formylpterin, to 6-carboxypterin, to pterin, and then to isoxanthopterin, is well documented (Blau et al., 1996; Burton et al., 2016a; Off et al., 2005). It has also reported that dihydrofolate reductase (DHFR) can convert folic acid to 7,8-dihydrofolic acid to tetrahydrofolic acid, which can then be converted to 5,6,7,8-tetrahydropterin either non-enzymatically or by xanthine oxidoreductase (XOR) (Gao et al., 2009). The 5,6,7,8-tetrahydropterin can then act as a precursor from which other pteridine derivatives and lumazines can be formed via the

XOR enzyme (Rembold et al., 1971). However, no comprehensive studies on breast cancer at the cellular level have been conducted to the author's knowledge. It is unknown if the elevated isoxanthopterin levels observed in the urine of breast cancer patients is a direct result of the tumor itself or some other source in vivo (Burton et al., 2014, 2016b; Gamagedara et al., 2011).

Breast cancer presents a useful model for investigating pteridine metabolism for several reasons. First, several clinical studies have reported elevated levels of urinary pteridines in women with newly diagnosed breast cancer compared to healthy controls, with particular interest given to xanthopterin, isoxanthopterin, and neopterin as prospective biomarkers (Burton et al., 2014, 2016b; Gamagedara et al., 2011; Kośliński et al., 2011). Second, a possible explanation for the elevated pteridines involves the well-documented relationship between folate and breast cancer. Specifically, folate receptor (FR) expression has been conclusively correlated with breast cancer tumorigenicity while dietary intake of folate has been shown to modulate the risk of developing breast cancer (Hansen et al., 2017; Hartmann et al., 2007; Necela et al., 2015; Ross et al., 1994). Notably, FR expression has even been shown to be more predictive than tumor size, nodal status, estrogen receptor, and tumor grade for breast cancer prognosis (Hartmann et al., 2007). Third, XOR, a key enzyme in the pteridine biosynthetic pathway, is markedly reduced or even absent in breast tumors, impacting cancer progression and survival rates (Bortolotti et al., 2021; Cook et al., 1997; Fini et al., 2008, 2011; Hansen et al., 2017; Linder et al., 2005; Taibi et al., 2009). Finally, the MCF10A progressive breast cancer model offers a series of sequentially derived cell lines that model the stepwise progression of breast cancer toward a malignant phenotype. This simplified system can

uniquely enable metabolomics research in a clinically relevant disease progression model without interference from the systemic effects and the biological heterogeneity typically encountered in clinical contexts. For these reasons, breast cancer presents an intriguing disease model for elucidating pteridine metabolism in cancer.

In this study, cellular pteridines were measured in a MCF10A derived progressive isogenic breast cancer cell model to examine how pteridine metabolism is affected by increasing tumorigenicity with and without folic acid dosing. To the best of our knowledge, this study reported the first instance of an isogenic breast cancer cell model being used to investigate the pteridine biosynthetic pathway.

2. EXPERIMENTAL

2.1. CHEMICALS AND MATERIALS

Pterin, xanthopterin, 7,8-dihydroxanthopterin, isoxanthopterin, 6-biopterin, sepiapterin, neopterin, monapterin, 6-carboxypterin, 6-hydroxymethylpterin, 6,7-dimethylpterin, 6-methylpterin, lumazine, 6-hydroxylumazine, and 7-hydroxylumazine were purchased from Schircks Laboratory (Jona, Switzerland). Folic acid, dithiothreitol, ammonium hydroxide, LC-MS grade formic acid, methanol, acetonitrile, and cell culture media (contains DMEM/F-12 supplemented with 5% Horse Serum, 20 ng/mL EGF, 10 µg/mL bovine insulin, 0.5 mg/mL hydrocortisone, 100 ng/mL cholera toxin, 100 µg/mL calcium chloride, 0.05% trypsin-EDTA (trypsin), and 50 U/mL penicillin-streptomycin) were purchased from Fisher Scientific (New Jersey, USA). Ultrapure water was produced from a Milli-Q Advantage® A10 and Millipore Elix® water purification system. Three

sequentially derived MCF10A series of human breast cancer cell lineages including MCF10A (benign), MCF10AT (premalignant), and MCF10CA1a (malignant), hereafter referred to as A, T, and C, respectively, were provided by the Cell Resources Core of the Barbara Ann Karmanos Cancer Institute (Detroit, MI, USA).

Individual pteridine stock standard solution was prepared in ultrapure water with 3.7% of 2 N ammonium hydroxide as described by Burton et al., (2016b). A stock standard mixture solution containing 5 mg/L of each pteridine was then prepared by combining the individual standard solutions and diluted in ultrapure water. This solution was then aliquoted into smaller quantities and stored at - 80 °C until used for experiments.

2.2. HPLC-MS/MS METHOD

A Shimadzu ultra-fast liquid chromatography (UFLC) system (Columbia, MD) that included a degasser (DGU30A3), two pumps (LC-20 AD XR), a temperature controlled autosampler (SIL-20AC XR) and a column oven (CTO-20 A) coupled with an AB Sciex 4000Q Trap mass spectrometer (Foster City, CA, USA) was used to quantify pteridines and the derivatives in all experiments. The analytes were separated using a Luna phenyl-hexyl column (3.0 μm, 3.0 × 150 mm) with an attached guard column (Phenomenex, Torrance, CA, USA). The high-performance liquid chromatography-tandem mass spectrometry (HPLC-MS/MS) analysis method was based on a previously published method (Burton et al., 2016b) with some modifications with the final method conditions as: The binary gradient flow profile (mobile phase A: 0.025% (v/v) formic acid in 99% water/1% acetonitrile; mobile phase B: methanol) was modified as follows:

from 0 to 2 min mobile phase B increased linearly from 7 to 20%; kept at 20% B from 2 to 4 min; then quickly increased B to 80% from 4 to 5 min and remained at 80% from 5 to 7 min before dropping B back to 7%; and equilibrated it for 3 min before next injection. Injection volume of 50 µL, oven temperature of 40 °C, and the mobile phase flow rate of 0.45 mL/min remained the same as the published method (Burton et al., 2016b). Mass spectrometer conditions of positive electrospray ionization (ESI) with multiple reaction monitoring (MRM) mode for quantification were also optimized as follows: nitrogen gas used for curtain gas, collision gas, ion source gas 1, and ion source gas 2 pressures were 45, 6, 45, and 40 psi, respectively; IonSpray voltage was 5500 V; Ion source temperature was 600 ºC; Entrance Potential was 10 V. Ion pair of MRM and mass voltages for each compound were optimized and are denoted in Online Resource Table S1.

2.3. CELL CULTURE, FOLIC ACID DOSING, AND SAMPLE PREPARATION

Cells were cultivated in 100 mm cell culture dishes in the cell culture media as described above by following the protocol provided by the cell supplier in a cell culture incubator maintained at 37 °C and 5% carbon dioxide. For folic acid dosing experiments, modified growth media containing selected concentrations of folic acid (0, 100, or 250 mg/L) was used to culture the cells. Cells were cultured in the modified media for 4-5 days before harvesting. 50 µL of cell culture media was collected for extracellular pteridine analysis prior to harvesting cells for intracellular pteridine analysis. The cells were harvested by first discarding the media and washing the cells once with 2 mL of trypsin quickly, then adding 2 mL of trypsin solution and incubating at 37 °C and 5%

carbon dioxide until the cells were detached from the dish. The trypsin was then diluted with an equal amount of culture media to inhibit the proteolytic activity of trypsin. The cells were transferred to 15 mL centrifuge tubes and centrifuged at 130 × *g* for 10 min at room temperature. The supernatant was then carefully removed, and the cells were washed twice with 2 mL phosphate-buffered saline (PBS). During the final wash, the cells were counted with a hemacytometer, and a small aliquot of the cell suspension was also collected to determine the protein concentration of the samples. After the final wash, the cells were processed for extraction of pteridines.

The pteridine extraction procedure was based on the procedure used for A549 lung cancer cells (Burton et al., 2015) with some modification. Briefly, the cells were resuspended in 200 µL of extraction solvent containing 80% methanol, 20% ultrapure water, 5 mM ammonium hydroxide, and 0.1% (w/v) dithiothreitol (DTT). The cell samples were sonicated in an ice bath for 1 min before being snap-frozen in liquid nitrogen for 4 min. After thawing, the lysate was allowed to sit at room temperature for 30 min to ensure complete precipitation of proteins. The samples were then centrifuged at 20,000 × *g* for 20 min at 4 °C to remove the precipitate. The supernatants were filtered with a 0.22 µm Nylon membrane filter and diluted to appropriate concentrations for HPLC-MS/MS analysis.

For extracellular media sample analysis, a 50 µL aliquot of the media sample was collected prior to detaching the cells from the culture dish. It was directly diluted 4 times with the extraction solvent and processed through the same precipitation procedure as the intracellular samples to precipitate any possible protein residue. The sample was then diluted as needed and analyzed by HPLC-MS/MS.

2.4. PROTEIN ASSAY

Protein assays were performed using a Pierce™ Coomassie (Bradford) Protein Assay Kit. A cell suspension aliquot from each sample was collected after cells had been washed and counted, followed by centrifugation at 130 × *g* for 10 min at room temperature. The supernatant was discarded and replaced with ultrapure water. After resuspension, the cell samples were sonicated in an ice water bath for 1 min. Cell lysates were then distributed in triplicate into a Corning 96-well Solid Black microplate in 150 µL volumes. Bovine serum albumin standards were used to make a calibration curve prepared at a concentration range of 1 to 75 µg/mL in ultrapure water and distributed in 150 µL triplicates into the microplate. A 150 µL volume of the Coomassie Reagent solution was then added to each of the wells, and absorbance was measured at 595 nm after 10 min of incubation at room temperature.

2.5. QUALITY CONTROL AND STATISTIC ANALYSIS

Good laboratory practice and quality controls were performed throughout all the experiments. The HPLC-MS/ MS method was optimized and validated before used for samples analysis. Protein assay protocol was also validated before sample analysis. Instrument calibration, calibration curve linear range, detection limit of each analyte, reproducibility, blank, sample matrix spike recovery were all tested to ensure good method performance. Spike recoveries for all the analytes were tested at low and high spike concentrations to cover the analyte concentration ranges in the samples. For each batch of sample analysis, a minimum of one reagent blank, one duplicate or triplicate, and one quality control standard were included for every 10 to 15 samples. For counting

the cells, cells were counted 3 times and the average results were used for calculation. Anova test (two-factor with replication, $p < 0.05$) was used to evaluate statistical differences of pteridine levels for different cells and under different folic acid dosing concentrations.

3. RESULTS AND DISCUSSION

3.1. PTERIDINE EXTRACTION AND ANALYSIS METHOD PERFORMANCE

In this study, pteridines were extracted from breast cancer cell lysates and extracellular media using a method previously developed for pteridine analysis in lung cancer cells with further optimization. Extracted pteridines were separated and detected using a further improved HPLC-MS/MS method based on a previously developed method for urinary pteridine analysis (Burton et al., 2016b). Overall, the method performances are comparable or better than the previously published method. However, neopterin and monapterin were not resolved, which may be attributed to the slight performance difference of the column and/or higher proportion of organic solvent content used in our modified extraction method. As a result, monapterin and neopterin were integrated together as a single peak, given the negligible levels of monapterin in samples.

3.2. INTRACELLULAR AND EXTRACELLULAR PTERIDINES

Interestingly, only intracellular 6-hydroxymethylpterin was reliably detected from undosed cell lysates. However, subsequent dosing of cells with folic acid yielded significant levels of extracellular pteridines in the cell media (Table 1). Mass fractions of

extracellular pteridines compared to intracellular pteridines exceeded 90%, and for most pteridines, exceeded 99%, following folic acid dosing. This finding indicated that the extracellular pteridines in the expressed media would afford better analytical detection, and correspondingly, a better target for studying pteridines in cancer metabolism, than intracellular pteridines extracted from cell lysates.

Table 1. Mass fractions of intracellular vs. extracellular pteridines (total intracellular mass to total extracellular mass) (n = 3).

Cell Line	Dosed Folic Acid Concentration (mg/L)	Mass Fraction of intracellular/extracellular (%)					
		PTE	6-MP	XAN	6-HLUM	6-HMP	6-CAP
MCF10A	0	ND	ND	<0.03	ND	8.20	ND
MCF10AT	0	ND	ND	<3.45	<0.30	11.12	ND
MCF10CA1a	0	ND	ND	<0.59	<1.90	15.91	ND
MCF10A	100	<0.09	0.28	0.60	<0.26	0.60	0.14
MCF10AT	100	<0.08	0.26	2.70	2.74	2.78	0.08
MCF10CA1a	100	<0.05	<0.00	<6.20	0.22	0.52	0.06
MCF10A	250	<0.05	2.91	0.53	<9.95	0.89	2.00
MCF10AT	250	<0.07	1.51	<0.09	<0.1	0.62	0.42
MCF10CA1a	250	<0.03	0.61	<0.08	<0.07	0.58	0.54

If pteridine concentration was below detection limit for intracellular sample, detection limit value was used for intracellular concentration and is indicated as "<". ND means pteridine was not detectable in neither intracellular nor extracellular samples

In order to determine whether the extracellular pteridines observed following folate dosing were produced in the cell media or by the cells, extracellular pteridine levels were compared in dosed media with and without cells. Dosing cell media alone with folic acid resulted in increased levels of pterin, 6-hydroxymethylpterin, 6-methylpterin, and 6-carboxypterin in a dose-dependent manner (Figure 1), but the rest of the pteridines were not detectable without cells present. The formation of these pteridine derivatives in the absence of cells likely represented folate degradation and subsequent

interconversion of pteridine derivatives by physical processes. However, dosing cells with folic acid led to additional increases of extracellular pterin, 6-hydroxymethylpterin, and 6-carboxypterin compared to dosed cell media alone under the same conditions. This finding, except 6-methylpterin, which did not increase in the presence of cells, suggested a cell-dependent pteridine metabolism that favored extracellular transport of these pteridines after synthesis in or on the cells. Further supporting this line of evidence, dosed cells had significantly elevated levels of extracellular xanthopterin (Online Resource Figure S1) and 6-hydroxylumazine (Figure 2) without any observed contribution from dosed media.

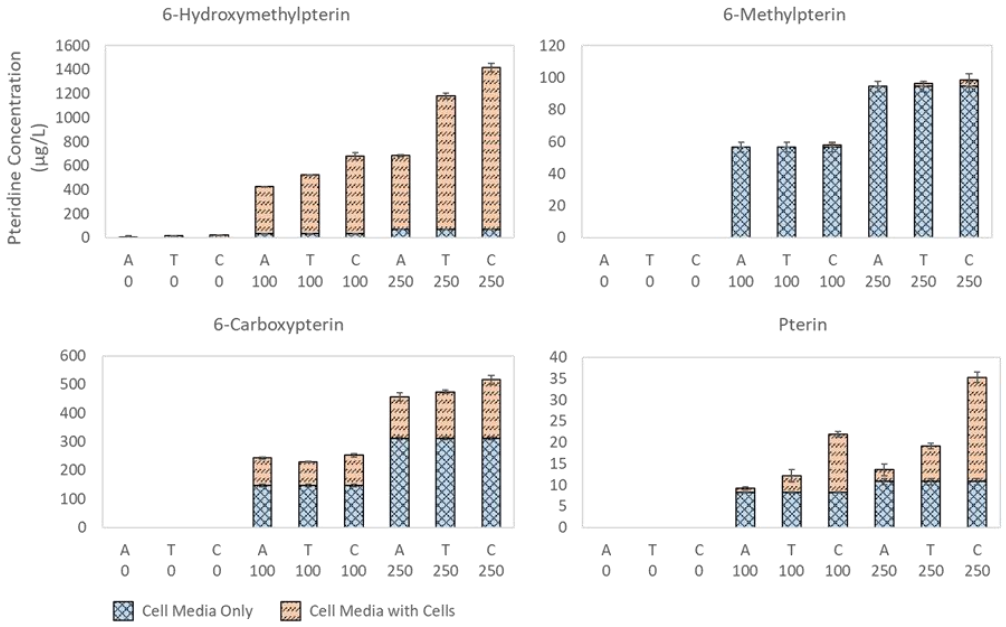

Figure 1. Concentrations of pteridines in extracellular media with and without cells. A, T, C refers to MCF10A (benign), MCF10AT (premalignant), and MCF10CA1a (malignant) cell lines, respectively. Folic acid dosing concentrations were 0, 100, and 250 mg/L.

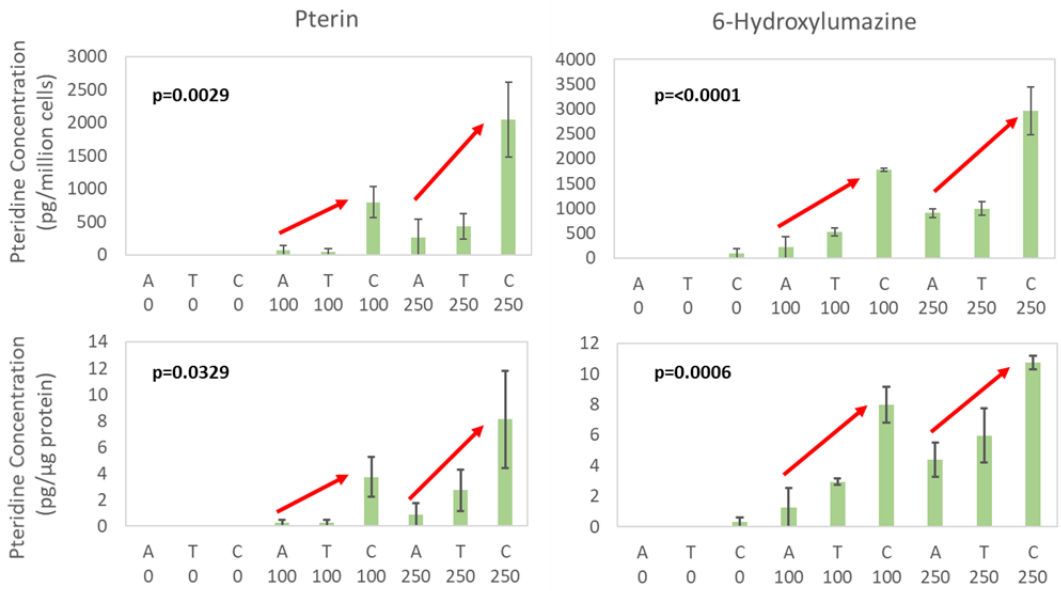

Figure 2. Total extracellular pteridine masses produced per million cells and per microgram protein (n = 2). Arrows indicate statistically significant correlation between pteridine concentrations and cell line tumorigenicity ($p < 0.05$, two-factor ANOVA). A, T, C refers to MCF10A (benign), MCF10AT (premalignant), and MCF10CA1a (malignant) cell lines, respectively. Folic acid dosing concentrations were 0, 100, and 250 mg/L. Error bars indicate relative percent difference (RPD).

As a result of these findings, all subsequent experiments were focused on extracellular pteridine analysis after folic acid dosing.

3.3. CORRELATIONS OF EXTRACELLULAR PTERIDINE LEVELS WITH TUMORIGENICITY

Extracellular pterin and 6-hydroxylumazine displayed a statistically significant correlation with tumorigenicity (Anova: Two-factor with replication test, $p < 0.05$) (Figure 2) following folic acid dosing. Statistical significance was maintained when pteridine concentrations were corrected for either cell concentration or protein concentration. The folate-dependent release of pterin reported here corroborated the

results of an earlier study that reported higher levels of urinary pterin following a two-week period of daily folate supplementation (Burton et al., 2016a). Given that 6-hydroxylumazine was not included in this earlier study, further work on urinary pteridines may benefit from its inclusion as a prospective cancer biomarker.

The correlation of 6-hydroxylumazine with breast cancer tumorigenicity further suggests tumorigenic deaminase activity in the MCF10A breast cancer cell model. This finding is significant because lumazines, which are close derivatives to pteridines with a carbonyl group at the C-2 position instead of an amino group, are also enzymatic substrates of XOR (Rembold et al., 1971). This understanding taken together with the consideration that lumazines have generally been excluded from cancer biomarker research suggests that lumazines present an understudied class of metabolites.

Elevated levels of urinary isoxanthopterin have been reported in patients with breast cancer (Burton et al., 2014, 2016b). In the current study, isoxanthopterin was observed in the extracellular media from the tumorigenic cell lines, albeit at highly variable levels near the method detection limit. It was either not detectable or at a very low level (similar level of the detection limit) in the benign cell extracellular media. This observation may be better understood through the biosynthesis of isoxanthopterin in humans, which occurs primarily through the conversion of pterin to isoxanthopterin by XOR (Blau et al., 1996). The basal MCF10A cell line, constituting benign fibrocystic disease, is reported to have relatively high levels of XOR activity compared with other tissues, in which comparatively higher levels of isoxanthopterin would be expected in the presence of sufficient substrate (Fini et al., 2008). However, the low pterin concentrations observed in the basal MCF10A cell line instead indicated poor substrate availability,

which may have limited production of isoxanthopterin, despite increased XOR activity. Moreover, isoxanthopterin production would be expected to be comparatively low in the tumorigenic cell lines which have been reported to have negligible or absent XOR activity. In this way, these findings suggest that pterin may be produced directly by breast cancer cells, whereupon it may be subsequently converted elsewhere in the body to isoxanthopterin (Blau et al., 1996; Bortolotti et al., 2021).

3.4. IMPLICATIONS FOR FOLATE-DERIVED PTERIDINE METABOLISM

A key focus of this study was to elucidate the pteridine biosynthetic pathway in breast cancer with an emphasis on the folate-derived pteridines, which has been summarized below in Figure 3. Briefly, folic acid can degrade into 6-formylpterin through physical and enzymatic processes (Blau et al., 1996; Burton et al., 2016a; Gao et al., 2009; Off et al., 2005; Rembold et al., 1971). However, subsequent degradation and interconversion in breast cancer tissue remains poorly understood. In this study, pterin, 6-hydroxylumazine, xanthopterin, 6-carboxypterin, and 6-hydroxymethylpterin were all significantly elevated in the presence of cells dosed with folic acid in a dose-dependent manner ($p < 0.05$).

A significantly higher ratio of 6-hydroxymethylpterin to 6-carboxypterin was observed across all three breast cancer cell lines. This finding differs from an earlier study examining extracellular pteridines from healthy human breast fibroblast cells dosed with 6-formylpterin, in which higher levels of 6-carboxypterin were observed (Stea et al., 1978). Burton et al. (2016a) also noted increased levels of urinary 6-carboxypterin following daily folate supplementation, although 6-hydroxymethylpterin was not

included in their study. Given that the enzyme XOR has been previously implicated in the conversions of 6-formylpterin to 6-carboxypterin and 6-hydroxymethylpterin, it appears likely that differential XOR activity modulates the conversion of folates to either 6-hydroxymethylpterin or 6-carboxypterin. Future studies examining pteridine metabolism in disease contexts should therefore include measurements of XOR activity to better understand its role in pteridine metabolism.

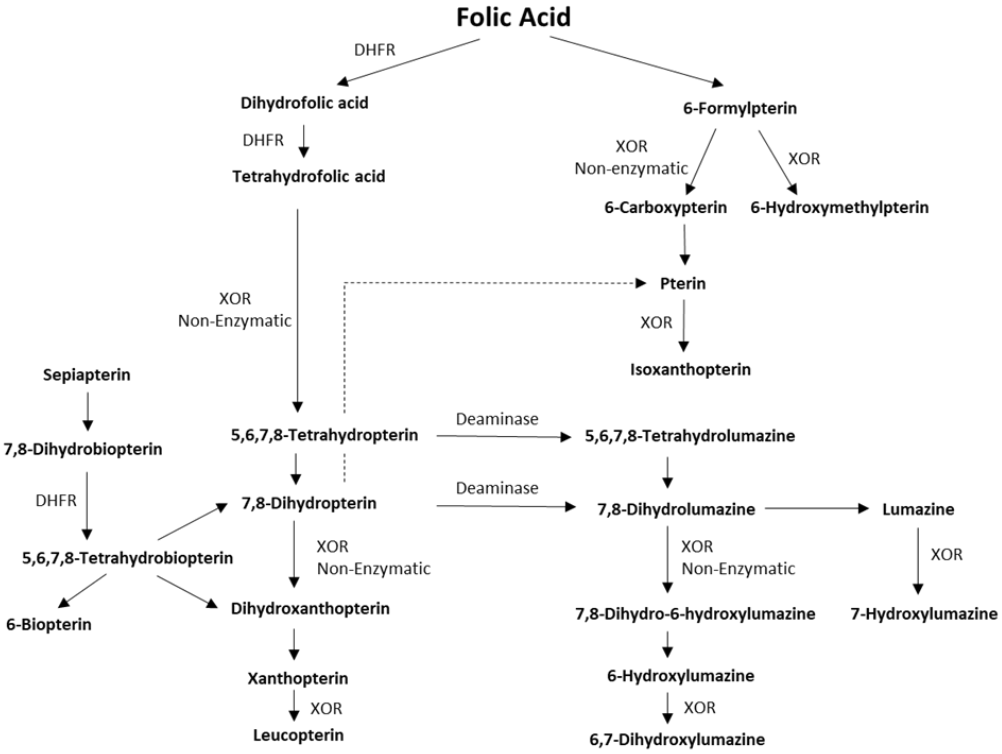

Figure 3. Folic acid derived pteridine metabolic pathway.

Furthermore, the folate-dependent metabolism of 6-hydroxymethylpterin and 6-carboxypterin was not related to tumorigenicity in this study, supporting earlier work. For example, prior *in vitro* studies examining 6-hydroxymethylpterin in healthy and

cancerous human skin fibroblasts, as well as other healthy animal cell lines, have shown that physiological metabolism of 6-hydroxymethylpterin varies significantly across cell and tissue types without any apparent association with tumorigenicity (Clynes & O'Neill, 1980; Goldberg & Koller, 1991; Halpern et al., 1977; Stea et al., 1978). Similarly, prior clinical studies involving women with newly diagnosed breast cancers and benign fibrocystic masses failed to describe any association between 6-carboxypterin and 6-hydroxymethylpterin and presence of cancer (Burton et al., 2013, 2014, 2016b).

The compound 6-carboxypterin is known to be subsequently converted to the downstream pteridine derivatives, pterin and isoxanthopterin, which have been described in the preceding section. Interestingly, extracellular xanthopterin was also found to be significantly elevated with folate dosing in the current study. Folic acid has not previously been known to degrade into xanthopterin through physical processes, which was supported in the present study by the lack of xanthopterin in cell media alone dosed with folic acid. Therefore, the folate-dependent xanthopterin levels observed here were cell-mediated and separate from non-enzymatic folate degradation (Burton et al., 2016a; Off et al., 2005; Stea et al., 1978). However, Rembold et al. (1971) previously demonstrated that tetrahydrofolic acid can form xanthopterin and pterin non-enzymatically in Tris-HCL buffer (Rembold et al., 1971). The reduction of folic acid to tetrahydrofolic acid is mediated by DHFR, an enzyme that would have been appreciably present in the breast cancer cells, but not the cell media. Moreover, cellular DHFR is upregulated in the presence of extracellular folic acid, which may account for the observed dose-dependent xanthopterin response to folic acid (Chalupsky et al., 2015; Gao et al., 2009). Finally, tetrahydrofolic acid can be converted to 6-hydroxylumazine in the

presence of pterin deaminase independent of XOR activity (Rembold et al., 1971). Hence, tumorigenic expression of DHFR, a clinically important breast cancer receptor, may explain not only the folate-dependent levels of xanthopterin observed here, but also the tumorigenic association of 6-hydroxylumazine. Future work using isotopic labels would be capable of ultimately determining whether the folate-derived pteridine ring is directly incorporated into the resulting xanthopterin and 6-hydroxylumazine or whether their folate-dependent responses result from metabolic crosstalk and regulation.

4. CONCLUSIONS

In this study, pteridine derivatives were measured in a cellular progressive breast cancer model with and without folic acid dosing. Folic acid was found to be a principal driver for pteridine metabolism in human breast cell, resulting in increased formation and ultimately excretion to the extracellular media. Folate dosing resulted in a range of extracellular pteridines with previously established and newly reported derivations from folic acid, including pterin, 6-hydroxylumazine, xanthopterin, 6-hydroxymethylpterin, and 6-carboxypterin. Breast cancer tumorigenicity was further found to impact specific conversions within the pteridine biosynthetic pathway, with pterin and 6-hydroxylumazine exhibiting a strong correlation with tumorigenicity. The excretion of these compounds to the extracellular media provides *in vitro* evidence for previous observations of certain elevated pteridines in the urine of breast cancer patients. Further work on determining the individual steps within the biosynthetic pathway using individual pteridine derivatives may afford additional understanding on the role of

pteridine metabolism in cancer progression. In particular, the current work was inconclusive with regard to isoxanthopterin, where additional work may provide further insights on its apparent increase in urine. In summary, the current study provided new insights into the interconnectivity of the pteridine biosynthetic pathway and its alteration in breast cancer development and progression. Finally, the novel use of the MCF10A progressive breast cancer model in this study afforded a simplified biological system in which to investigate cancer metabolism and may be readily applied to other metabolites and disease systems.

SUPPLEMENTARY INFORMATION

Table S1. Optimized mass detector conditions.

Compound	Abbreviation	MRM (m/z)	DP (V)	CE (V)	CXP (V)
Pterin	PTE	164.2 > 118.7	45	29	6.8
		164.2 > 120.8	45	30	10.8
		164.2 > 91.6	45	42.2	14.9
Lumazine	LUM	165.1 > 92.8	66	39	4
		165.1 > 68.9	66	53	11.3
6-Methylpterin	6-MP	178.2 > 132.7	58.3	31	7.3
		178.2 > 105.8	58.3	39.3	8.3
Xanthopterin	XAN	180 > 134.8	82	30.7	12.4
		180 > 162.9	82	26	9.5
Isoxanthopterin	ISO	180.2 > 134.7	60	31.4	7.4
		180.2 > 162.8	60	25.8	9.4
7-Hydroxylumazine	7-HLUM	181 > 109.9	63	31	5.4
		181 > 54.9	63	52	8.6
6-Hydroxylumazine	6-HLUM	181 > 163.9	77	22.4	9.3
		181 > 107.8	77	34.9	8
7,8-Dihydroxanthopterin	XH_2	182.1 > 153.9	42	23	9.2
		182.1 > 125.8	42	30	24
6,7-Dimethylpterin	6,7-DMP	192.1 > 105.7	61.1	39.8	5.2
		192.1 > 164.8	61.1	29.9	9.7
		192.1 > 67.8	61.1	48.9	10.9
6-Hydroxymethylpterin	6-HMP	194.1 > 175.9	59	21	10.9
		194.1 > 105.9	59	36	5
6-Carboxypterin	6-CAP	208 > 189.9	46	17.7	12
		208 > 163.9	46	22.2	9.5
6-Biopterin	6-BIO	238.2 > 219.8	57	21.9	13.6
		238.2 > 177.7	57	27.3	10.1
Sepiapterin	SEP	238.1 > 191.8	48	22.8	11.9
		238.1 > 164.8	48	30.3	9.6
Neopterin	NEO	254.2 > 205.8	60.8	25.3	12.4
		254.2 > 235.8	60.8	21.2	14.8
Monapterin	MNP	254.2 > 205.8	55.3	26	12.9
		254.2 > 235.8	55.3	20.1	14.5

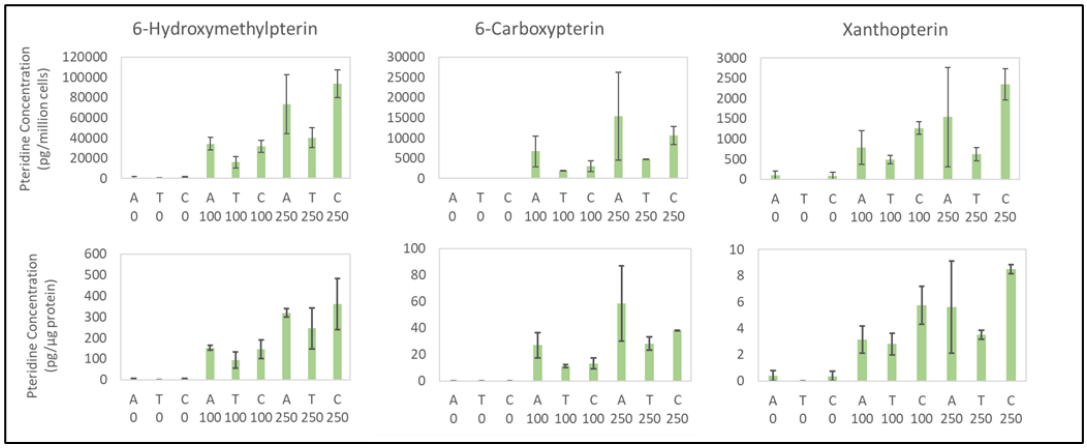

Figure S2. Total extracellular pteridine derivative masses (ng) (n=2). A, T, C refers to MCF10A (benign), MCF10AT (premalignant), and MCF10CA1a (malignant) cell lines, respectively. Folic acid dosing concentrations were 0, 100, and 250 mg/L. Error bars indicate relative percent difference (RPD) of duplicated samples.

ACKNOWLEDGEMENTS

The authors would like to thank Barbara Ann Karmanos Cancer Institute for providing the MCF10A series of cell lines. We appreciate the assistances of Dr. Paul Nam and Dr. Wenyan Liu on analytical method and instrument troubleshooting. Special thanks are also given to Dr. Yinfa Ma for editing this paper.

REFERENCES

Blau, N., De Klerk, J.B.C., Thöny, B., Heizmann, C.W., Kierat, L., Smeitink, J.A.M. and Duran, M. (1996) Tetrahydrobiopterin Loading Test in Xanthine Dehydrogenase and Molybdenum Cofactor Deficiencies. *Biochemical and Molecular Medicine* **58,** 199-203. https://doi.org/10.1006/bmme.1996.0049

Bortolotti, M., Polito, L., Battelli, M.G. and Bolognesi, A. (2021) Xanthine oxidoreductase: One enzyme for multiple physiological tasks. *Redox Biology* **41**. https://doi.org/10.1016/j.redox.2021.101882

Braasch, I., Schartl, M. and Volff, J.-N. (2007) Evolution of pigment synthesis pathways by gene and genome duplication in fish. *BMC Evolutionary Biology* **7**. https://doi.org/10.1186/1471-2148-7-74

Brejcha, J., Bataller, J.V., Bosáková, Z., Geryk, J., Havlíková, M., Kleisner, K., Maršík, P. and Font, E. (2019) Body coloration and mechanisms of colour production in Archelosauria: the case of deirocheline turtles. *Royal Society Open Science* **6**. https://doi.org/10.1098/rsos.190319

Burton, C., Shi, H. and Ma, Y. (2013) Simultaneous Detection of Six Urinary Pteridines and Creatinine by High-Performance Liquid Chromatography-Tandem Mass Spectrometry for Clinical Breast Cancer Detection. *Analytical Chemistry* **85,** 11137-11145. https://doi.org/10.1021/ac403124a

Burton, C., Shi, H. and Ma, Y. (2014) Normalization of urinary pteridines by urine specific gravity for early cancer detection. *Clinica Chimica Acta* **435,** 42-47. https://doi.org/10.1016/j.cca.2014.04.022

Burton, C., Shi, H. and Ma, Y. (2016a) Daily variation and effect of dietary folate on urinary pteridines. *Metabolomics* **12,** 1-10. https://doi.org/10.1007/s11306-016-1019-4

Burton, C., Shi, H. and Ma, Y. (2016b) Development of a high-performance liquid chromatography – Tandem mass spectrometry urinary pterinomics workflow. *Analytica Chimica Acta* **927,** 72-81. https://doi.org/10.1016/j.aca.2016.05.005

Burton, C., Weng, R., Yang, L., Bai, Y., Liu, H. and Ma, Y. (2015) High-throughput intracellular pteridinic profiling by liquid chromatography–quadrupole time-of-flight mass spectrometry. *Analytica Chimica Acta* **853,** 442-450. https://doi.org/10.1016/j.aca.2014.10.044

Chalupsky, K., Kračun, D., Kanchev, I., Bertram, K. and Görlach, A. (2015) Folic Acid Promotes Recycling of Tetrahydrobiopterin and Protects Against Hypoxia-Induced Pulmonary Hypertension by Recoupling Endothelial Nitric Oxide Synthase. *Antioxidants & Redox Signaling* **23,** 1076-1091. https://doi.org/10.1089/ars.2015.6329

Clynes, M.M. and O'Neill, C. (1980) Folic acid degradation is not a property specific to cancer cells in culture. *Cancer Letters* **10,** 133-140. https://doi.org/10.1016/0304-3835(80)90036-1

Cook, W.S., Chu, R., Saksela, M., Raivio, K.O. and Yeldandi, A.V. (1997) Differential immunohistochemical localization of xanthine oxidase in normal and neoplastic human breast epithelium. *International Journal of Oncology* **11,** 1013-1017. https://doi.org/10.3892/ijo.11.5.1013

Fini, M.A., Monks, J., Farabaugh, S.M. and Wright, R.M. (2011) Contribution of Xanthine Oxidoreductase to Mammary Epithelial and Breast Cancer Cell Differentiation In Part Modulates Inhibitor of Differentiation-1. *Molecular Cancer Research* **9,** 1242-1254. https://doi.org/10.1158/1541-7786.MCR-11-0176

Fini, M.A., Orchard-Webb, D., Kosmider, B., Amon, J.D., Kelland, R., Shibao, G. and Wright, R.M. (2008) Migratory activity of human breast cancer cells is modulated by differential expression of xanthine oxidoreductase. *Journal of Cellular Biochemistry* **105,** 1008-1026. https://doi.org/10.1002/jcb.21901

Gamagedara, S., Gibbons, S. and Ma, Y. (2011) Investigation of urinary pteridine levels as potential biomarkers for noninvasive diagnosis of cancer. *Clinica Chimica Acta* **412,** 120-128. https://doi.org/10.1016/j.cca.2010.09.015

Gao, L., Chalupsky, K., Stefani, E. and Cai, H. (2009) Mechanistic Insights into Folic Acid-dependent Vascular Protection: Dihydrofolate reductase-mediated Reduction in Oxidant Stress in Endothelial Cells and Angiotensin II-Infused Mice. *Journal of molecular and cellular cardiology* **47,** 752-760. https://doi.org/10.1016/j.yjmcc.2009.07.025

Goldberg, M. and Koller, M. (1991) Concentrations and Patterns of Released Pterins of Various Animal Cell Cultures. *Journal of Veterinary Medicine Series A* **38,** 49-53. https://doi.org/10.1111/j.1439-0442.1991.tb00983.x

Halpern, R., Halpern, B.C., Stea, B., Dunlap, A., Conklin, K., Clark, B., Ashe, H., Sperling, L., Halpern, J.A., Hardy, D. and Smith, R.A. (1977) Pterin-6-aldehyde, a cancer cell catabolite: identification and application in diagnosis and treatment of human cancer. *Proceedings of the National Academy of Sciences of the United States of America* **74,** 587-591. https://doi.org/10.1073/pnas.74.2.587

Hansen, M.F., Jensen, S.Ø., Füchtbauer, E.-M. and Martensen, P.M. (2017) High folic acid diet enhances tumour growth in PyMT-induced breast cancer. *British Journal of Cancer* **116,** 752-761. https://doi.org/10.1038/bjc.2017.11

Hartmann, L.C., Keeney, G.L., Lingle, W.L., Christianson, T.J.H., Varghese, B., Hillman, D., Oberg, A.L. and Low, P.S. (2007) Folate receptor overexpression is associated with poor outcome in breast cancer. *International Journal of Cancer* **121,** 938-942. https://doi.org/10.1002/ijc.22811

Kośliński, P., Bujak, R., Daghir, E. and Markuszewski, M.J. (2011) Metabolic profiling of pteridines for determination of potential biomarkers in cancer diseases. *ELECTROPHORESIS* **32,** 2044-2054. https://doi.org/10.1002/elps.201000664

Linder, N., Lundin, J., Isola, J., Lundin, M., Raivio, K.O. and Joensuu, H. (2005) Down-Regulated Xanthine Oxidoreductase Is a Feature of Aggressive Breast Cancer. *Clinical Cancer Research* **11,** 4372-4381. https://doi.org/10.1158/1078-0432.CCR-04-2280

Ma, Y. and Burton, C. (2013) Pteridine detection in urine: the future of cancer diagnostics? *Biomarkers in Medicine* **7,** 679-681. https://doi.org/10.2217/bmm.13.88

Necela, B.M., Crozier, J.A., Andorfer, C.A., Lewis-Tuffin, L., Kachergus, J.M., Geiger, X.J., Kalari, K.R., Serie, D.J., Sun, Z., Aspita, A.M., O'Shannessy, D.J., Maltzman, J.D., McCullough, A.E., Pockaj, B.A., Cunliffe, H.E., Ballman, K.V., Thompson, E.A. and Perez, E.A. (2015) Folate Receptor-α (FOLR1) Expression and Function in Triple Negative Tumors. *PLOS ONE* **10,** 1-19. https://doi.org/10.1371/journal.pone.0122209

Odate, S., Tatebe, Y., Obika, M. and Hama, T. (1959) Pteridine Derivatives in Reptilian Skin. *Proceedings of the Japan Academy* **35,** 567-570. https://doi.org/10.2183/pjab1945.35.567

Off, M.K., Steindal, A.E., Porojnicu, A.C., Juzeniene, A., Vorobey, A., Johnsson, A. and Moan, J. (2005) Ultraviolet photodegradation of folic acid. *Journal of Photochemistry and Photobiology B: Biology* **80,** 47-55. https://doi.org/10.1016/j.jphotobiol.2005.03.001

Rembold, H., Metzger, H. and Gutensohn, W. (1971) Catabolism of Pteridine Cofactors: III. On the introduction of an oxygen function into position 6 of the pteridine ring. *Biochimica et Biophysica Acta* **230,** 117-126. https://doi.org/10.1016/0304-4165(71)90059-6

Ross, J.F., Chaudhuri, P.K. and Ratnam, M. (1994) Differential regulation of folate receptor isoforms in normal and malignant tissues in vivo and in established cell lines. Physiologic and clinical implications. *Cancer* **73,** 2432-2443.

Shantaram, M., Bhaktha, G., Kumta, S. and Aziz, M.A. (2012) Evaluation of Urinary 6-Hydroxymethylpterin in Malignancies. *International Journal of Analytical, Pharmaceutical, and Biomedical Sciences* **1,** 71-74.

Stea, B., Backlund, P.S., Berkey, P.B., Cho, A.K., Halpern, B.C., Halpern, R.M. and Smith, R.A. (1978) Folate and Pterin Metabolism by Cancer Cells in Culture. *Cancer Research* **38,** 2378-2384.

Taibi, G., Carruba, G., Cocciadiferro, L., Granata, O.M. and Nicotra, C.M.A. (2009) Low Levels of Both Xanthine Dehydrogenase and Cellular Retinol Binding Protein Are Responsible for Retinoic Acid Deficiency in Malignant Human Mammary Epithelial Cells. *Annals of the New York Academy of Sciences* **1155,** 268-272. https://doi.org/10.1111/j.1749-6632.2008.03687.x

Watt, W.B. (1972) Xanthine Dehydrogenase and Pteridine Metabolism in *Colias* Butterflies. *Journal of Biological Chemistry* **247,** 1445-1451. https://doi.org/10.1016/S0021-9258(19)45578-6

II. ESTABLISHING PTERIDINE METABOLISM IN A PROGRESSIVE ISOGENIC BREAST CANCER CELL MODEL – PART II

Lindsey Rasmussen[1], Zachary Foulks[1], Jiandong Wu[2], Casey Burton[1,3,4], Honglan Shi[1,3]

[1]Department of Chemistry, Missouri University of Science and Technology, Rolla, MO 65409, USA

[2]Department of Chemical and Biochemical Engineering, Missouri University of Science and Technology, Rolla, MO 65409, USA

[3]Center for Biomedical Research, Missouri University of Science and Technology, Rolla, MO 65409, USA

[4]Phelps Health, Rolla, MO 65401, USA

ABSTRACT

Introduction: Determining the biological significance of pteridines in cancer development and progression remains an important step in understanding the altered levels of urinary pteridines seen in certain cancers. Our companion study revealed that several folate-derived pteridines and lumazines correlated with tumorigenicity in an isogenic, progressive breast cancer cell model, providing direct evidence for the tumorigenic origin of pteridines.

Objectives: This study sought to elucidate the pteridine biosynthetic pathway in a progressive breast cancer model via direct pteridine dosing to determine how pteridine metabolism changes with tumorigenicity.

Methods: First, MCF10AT breast cancer cells were dosed individually with 15 pteridines to determine which pteridines were being metabolized and what metabolic products were being produced. Second, pteridines that were significantly metabolized

were dosed individually across the progressive breast cancer cell model (MCF10A, MCF10AT, and MCF10ACA1a) to determine the relationship between each metabolic reaction and breast cancer tumorigenicity.

Results: Several pteridines were found to have altered metabolism in breast cancer cell lines, including pterin, isoxanthopterin, xanthopterin, sepiapterin, 6-biopterin, lumazine, and 7-hydroxylumazine ($p < 0.05$). In particular, isoxanthopterin and 6-biopterin concentrations were differentially expressed ($p < 0.05$) with respect to tumorigenicity following dosing with pterin and sepiapterin, respectively. Finally, the pteridine biosynthetic pathway in breast cancer cells was proposed based on these findings.

Conclusion: This study, along with its companion study, demonstrates that pteridine metabolism becomes disrupted in breast cancer tumor cells. This work highlights several key metabolic reactions within the pteridine biosynthetic pathway that may be targeted for further investigation and clinical applications.

Keywords: Pteridine, Breast cancer, Pteridine metabolism, MCF10A cell line, HPLC-MS/MS, Biomarker

1. INTRODUCTION

Pteridines are metabolic intermediates in the biosynthetic pathways of various cofactors and vitamins (Burton *et al.*, 2016a; Crabtree *et al.*, 2009; Fukushima and Shiota, 1974; Gross and Levi, 1992). Elevated levels of urinary pteridines have been reported in patients with certain cancers (Burton *et al.*, 2013, 2016b; Gamagedara *et al.*,

2011; Kośliński *et al.*, 2011; Ma and Burton, 2013; Shantaram *et al.*, 2012), prompting interest in elucidating the role of pteridines in cancer metabolism. However, previous efforts to study the potential tumorigenic origin of pteridines have been met with analytical challenges, including trace cellular concentrations, a multitude of pteridine derivatives with diverse chemical functionality, multiple structural isomers, and rapid autooxidation and degradation of certain pteridine derivatives (Burton and Ma, 2017, 2019; Kośliński *et al.*, 2011; Ma and Burton, 2013). Recent advances in pteridine quantification in relevant biological matrices have newly enabled comprehensive investigations into the pteridine biosynthetic pathway in cellular disease models (Burton *et al.*, 2015).

To this end, our team recently explored how tumorigenicity affects pteridine metabolism using a novel isogenic, progressive breast cancer cell model consisting of sequentially derived cell lines that models the clinical progression towards metastatic breast cancer (Rasmussen *et al.*, 2022). In our companion study, we reported that extracellular levels of pterin and 6-hydroxylumazine were correlated with tumorigenicity following dosing with folic acid, one of the two primary precursors to the pteridine biosynthetic pathway. This work provided direct evidence for the tumorigenic origin of elevated pteridines seen in urine, and particularly in breast cancer (Burton *et al.*, 2014, 2016b; Gamagedara *et al.*, 2011). However, the manner in which the pteridine biosynthetic pathway may differ in breast tumor cells and the molecular mechanisms responsible for these changes remain to be determined.

Moreover, several downstream pteridines were observed to have altered extracellular levels following folic acid dosing in our companion study, such as 6-

carboxypterin, 6-hydroxymethylpterin, and xanthopterin, that were not otherwise correlated with tumorigenicity (Rasmussen *et al.*, 2022). Furthermore, other downstream pteridines derived from folic acid were not otherwise detected following folic acid dosing in the companion study. For example, isoxanthopterin, which has been reported to be elevated in the urine of breast cancer patients (Burton *et al.*, 2014, 2016b) and is the direct product of pterin (Blau *et al.*, 1996; Fukushima and Shiota, 1974; Rembold *et al.*, 1971). It is likely that dosing cells with folic acid, as a primary precursor to the pteridine biosynthetic pathway, may have been insufficient to produce detectable changes in secondary and tertiary metabolic products further downstream in the pathway. This study therefore sought to investigate the metabolism of downstream pteridines in a progressive breast cancer model by directly dosing cells with intermediate pteridines.

In addition, the companion study was limited in scope in that it strictly examined folate-derived pteridines, whereas previous work has demonstrated crosstalk between the folic acid and guanosine triphosphate (GTP) entry points to the pteridine biosynthetic pathway (Burton *et al.*, 2016a; Oettle and Reibnegger, 1999; Rembold and Simmersbach, 1969). For example, urinary levels of 6-biopterin, xanthopterin, and neopterin were decreased in healthy individuals following a two-week folate supplementation (Burton *et al.*, 2016a). Similarly, multiple pteridines throughout the pathway have been established as substrates for xanthine oxidoreductase (XOR) (Blau *et al.*, 1996; Oettle and Reibnegger, 1999; Rembold *et al.*, 1971) and pterin deaminase, which is responsible for the conversion of pteridines to lumazines (Fan *et al.*, 2013; Jayaraman *et al.*, 2016; Rembold and Simmersbach, 1969). The XOR enzyme has been shown to have altered activity in breast cancer cells (Battelli *et al.*, 2015; Fini *et al.*, 2011; Fini *et al.*, 2008;

Linder *et al.*, 2005), which may explain the observations made in our companion study and provide suitable targets for additional investigation in this study. In this way, the current study further sought to investigate pteridine metabolism in a broader context that included key pteridines and lumazines derived from both GTP and folic acid. While previous studies have variously examined the clinical and biological significance of pteridines in breast cancer in urine (Burton *et al.*, 2016a, b; Gamagedara *et al.*, 2011) and cumulative effects of folate dosing in a progressive breast cancer cell model (Rasmussen *et al.*, 2022), the elucidation of the pteridine biosynthetic pathway in progressive breast cancer has not yet been achieved. This study advanced this objective by sequentially dosing cells with pteridine intermediates using a progressive breast cancer cell model to determine pathway connectivity.

2. EXPERIMENTAL

2.1. CHEMICALS AND MATERIALS

The MCF10A progressive breast cancer cell model, which consisted of three sequentially derived human epithelial breast cell lineages comprising nontumorigenic MCF10A (A), premalignant/tumorigenic MCF10AT (T), and tumorigenic/metastatic MCF10CA1a (C), was obtained from the Bargara Ann Karmanos Cancer Institute (Detroit, MI, USA) at Wayne State University, and matches the disease model used in our recent companion study (Rasmussen *et al.*, 2022). Dithiothreitol, ammonium hydroxide, LC-MS grade formic acid, acetonitrile, methanol, and cell culture media were also all from the same resource of our recent study (Rasmussen *et al.*, 2022). Ultrapure

water was obtained from a Milli-Q Advantage® A10 and Millipore Elix® water purification system. All the pteridine standards, including leucopterin, were also purchased from Schircks Laboratory (Jona, Switzerland). The stock standard solutions of each pteridine were also prepared in the same way. Leucopterin was prepared at 1 mg/L in ultrapure water with 3.7% 2 N ammonium hydroxide measured quantitatively in this study owing to its poor solubility.

2.2. HPLC-MS/MS METHOD

The HPLC-MS/MS method to determine pteridine derivatives was the same with our recent companion study (Rasmussen *et al.*, 2022) with slight modifications, as described in the supplemental information (Tables S1 and S2). A procedural calibration method was used for HPLC-MS/MS analysis to minimize matrix effects and improve method accuracy. Briefly, different concentrations of pteridine standards were added in the cell culture media and processed through the same procedure as the sample preparation, and then diluted and analyzed as the same process of the sample analysis. Leucopterin was added to the method in a later phase of the study. It was only used for compound identification and confirmation purposes, not for quantitative analysis due to poor solubility of this standard.

2.3. CELL CULTURE, PTERIDINE DOSING, AND SAMPLE PREPARATION

Cells from each of the A, T, and C cell lines were cultivated in 100 mm cell culture dishes in 6 mL of cell culture media as described in our recent publication (Rasmussen *et al.*, 2022) by following the protocol provided by the cell supplier.

Pteridine dosing experiments were conducted using modified growth media containing 2 mg/L of the selected individual pteridine standard. In addition, two types of control samples, one consisting of dosed cell media without cells and the other one with cells but no pteridine dosing, were also processed in parallel for each batch of experiments. All the treatments were triplicated or duplicated. Cells and corresponding control samples were cultured for five days before harvesting. Cell media was harvested as 1 mL aliquots, and either used directly for extracellular pteridine analysis or stored at -80 °C until analysis, by following the same sample preparation and HPLC-MS/MS analysis method (Rasmussen *et al.*, 2022). The cells were harvested and counted as described in our companion study (Rasmussen *et al.*, 2022).

Two phases of experiments were performed in this study. First, T breast cancer cells were dosed individually with 15 pteridines. These step-by-step tests confirmed which pteridines were being metabolized and what metabolic products were being produced in each individual step of the metabolic pathway. Second, pteridines that were significantly metabolized from the phase 1 experiments were chosen to test in the phase 2 experiments by dosing each pteridine individually across all three progressive breast cancer cell lines (A, T, and C) to determine the relationship between each metabolic reaction and breast cancer tumorigenicity.

3. RESULTS AND DISCUSSION

3.1. DOSING STUDY FOR METABOLIC PATHWAY CONFIRMATION

3.1.1. Screening Study for Pteridines Metabolized by Breast Cells.

Fifteen pteridines were dosed separately in breast cells (T cells) and downstream pteridines were monitored to determine pathway connectivity. Dosed concentrations of five pteridines, including pterin, xanthopterin, sepiapterin, lumazine, and 6-hydroxylumzine, were significantly reduced after five days (Table 1). 6-Hydroxymethylpterin was detected in all extracellular media of the cell samples in a concentration range of 0.08 – 0.17 μM, which is in agreement with Rasmussen, *et al.* (2022) where 6-hydroxymethylpterin was detected in T cells at low concentrations without additional dosed folic acid.

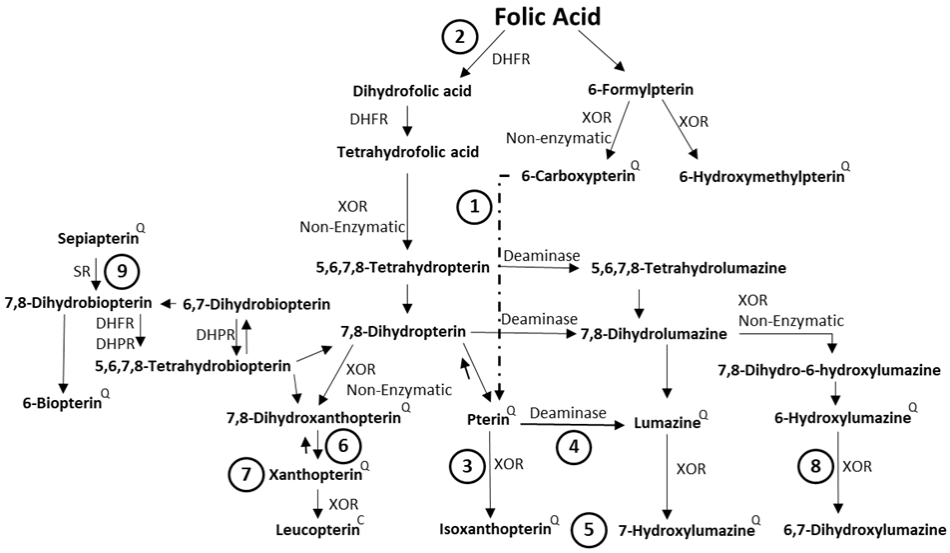

Figure 1. Pteridine pathway in breast cells based on screening and quantitative studies. Circled numbers indicate pathways evaluated and discussed in this study. (Q) and (C) indicate compounds analyzed quantitatively and confirmatively, respectively, in the pteridine panel.

Table 1. Production of cell-derived pteridines following dosing with different pteridine precursors. Samples were dosed for 5 days with each initial pteridine concentration at 2 mg/L. Reported concentrations have been normalized relative to pteridines measured in dosed media without cells.

Dosed Pteridine* (Abbreviation)	**µM**	**Cell Samples: Control Media (%)**	**Product Pteridines (Abbreviation) In Cell Samples**	**µM**
Pterin (PTE)	12.3	3	Isoxanthopterin (ISO) 7-Hydroxylumazine (7-HLUM) 6-Hydroxylumazine (6-HLUM)	7.52 0.108 0.005
Xanthopterin (XAN)	11.2	5	7,8-Dihydroxanthopterin (XH_2)	0.157
Sepiapterin (SEP)	8.43	43	6-Biopterin (BIO) 7,8-Dihydroxanthopterin (XH_2) 7-Hydroxylumazine (7-HLUM) Isoxanthopterin (ISO) Xanthopterin (XAN) 6-Hydroxylumazine (6-HLUM)	0.299 0.241 0.141 0.091 0.069 0.057
Lumazine (LUM)	12.2	0	7-Hydroxylumazine (7-HLUM)	7.34
6-Hydroxylumazine (6-HLUM)	11.1	38		
Undosed		N/A	6-Hydroxymethylpterin** (6-HMP)	0.169

* Additional pteridines that were dosed, but otherwise not significantly metabolized by cell samples, are not included in this table. They are 6-Methylpterin (6-MP), Isoxanthopterin, 7-Hydroxylumazine, 7,8-Dihydroxanthopterin, 6,7-Dimethylpterin (6,7-DMP), 6-Hydroxymethylpterin, 6-Carboxypterin (6-CAP), 6-Biopterin, Neopterin (NEO), Monapterin (MNP).
**6-Hydroxymethylpterin detected in all samples at similar concentrations, including in control cells without pteridine dosing, therefore not considered as direct product of dosed pteridines.

The various pteridine products observed following dosing with the pteridine precursors, as shown in Table 1, align with the established pteridine biosynthetic pathway (Figure 1) (Burton *et al.*, 2016a; Crabtree *et al.*, 2009; Kośliński *et al.*, 2011; Rasmussen *et al.*, 2022; Rembold *et al.*, 1971). Several pteridine derivatives, including 6-hydroxymethylpterin, 7-hydroxylumazine, isoxanthopterin, 6-biopterin, 6-methylpterin, 6,7-dimethylpterin, neopterin, and monapterin, were not significantly metabolized by the breast cancer cells, indicating that these pteridine derivatives may be terminal endpoints within the pteridine biosynthetic pathway or that these pteridine derivatives may not be actively transported into breast cancer cells. Evidence for the latter may include 7,8-dihydroxanthopterin, a precursor to xanthopterin, and 6-carboxypterin, a precursor to

pterin (Burton *et al.*, 2016a; Rasmussen *et al.*, 2022; Rembold *et al.*, 1971), which were not shown to be significantly metabolized in these experiments. The detailed results from each dosing experiment are discussed below.

3.1.2. 6-Carboxypterin Dosing Results. Pterin may be formed from folic acid either (1) nonenzymatically through the photocatalysis of folic acid or (2) through a multistep enzymatic process involving dihydrofolate reductase and XOR (Burton *et al.*, 2016a; Rasmussen *et al.*, 2022; Rembold *et al.*, 1971).

Folic Acid →→ 6-Carboxypterin → Pterin (pathway 1)

Folic Acid → (DHFR) →→ Pterin (pathway 2)

In this experiment, 6-carboxypterin was not significantly metabolized by the premalignant T cell line and no additional pterin was observed following dosing with 6-carboxypterin. This finding generally agreed with that of our companion study where folic acid dosing yielded substantial amounts of 6-carboxypterin and only 10-35 μg/L of pterin (Rasmussen *et al.*, 2022). Both studies were performed under dark conditions to minimize the photocatalytic degradation of folic acid to 6-carboxypterin and ultimately pterin (Rasmussen *et al.*, 2022). These findings together suggest that the metabolic pathway from folic acid to pterin in breast cancer cells proceeds primarily through enzymatic processes involving dihydrofolic acid as an intermediate (pathway 2) and not through physical processes involving 6-carboxypterin as an intermediate (pathway 1). This understanding would further explain the minimal change in urinary pterin following folate supplementation in healthy individuals reported by Burton, *et al* (2016a).

3.1.3. Pterin Derived Metabolic Pathway. *Pterin dosing*. In this experiment, pterin dosing afforded isoxanthopterin along with trivial levels of 6-hydroxylumazine and 7-hydroxylumazine. The conversion of pterin to isoxanthopterin has been previously established as an enzymatic reaction involving XOR both clinically in humans (Blau *et al.*, 1996) and *in vitro* using XOR enzyme derived from rat liver (Rembold *et al.*, 1971). This experiment confirmed this reaction step (pathway 3) by directly dosing pterin precursor into the breast cancer cell culture.

$$\text{Pterin} \xrightarrow{\text{XOR}} \text{Isoxanthopterin} \qquad \text{(pathway 3)}$$

In our companion study, isoxanthopterin was not detected at significant levels following folate dosing; however, the amount of pterin precursor generated with folic acid dosing in that study was approximately 10 - 35 μg/L whereas the pterin precursor dose used in the current study was 2 mg/L. In this way, the negligible effects of daily folate supplementation for two weeks on urinary isoxanthopterin (Burton *et al.*, 2016a) are likely the result of the poor conversion efficiency of folic acid to pterin.

Pterin dosing yielded a small fraction (0.08%) of 6-hydroxylumazine. This unexpected finding may suggest a reverse equilibrium between pterin and 7,8-dihydropterin. The latter may be deaminated to 7,8-dihydrolumazine and ultimately to 6-hydroxylumazine through previously established reactions (Rembold *et al.*, 1971). However, 7,8-dihydropterin was not monitored in this study due to lack of chemical standard, and its reaction rate constant and whether it is enzymatically controlled has not been previously reported. We also dosed 6-hydroxylumazine directly in the cell culture, and the 6-hydroxylumazine was significantly metabolized by the T cells with only 38% of the dosed amount remaining after five days (Table 1). However, no metabolic products

were detected in our pteridine panel, which excluded 6,7-dihydroxylumazine, the predicted metabolic product (Figure 1, pathway 8) (Rembold *et al.*, 1971) due to a lack of commercially available standard. This rapid conversion of 6-hydroxylumazine to the downstream product(s) may explain its low yield with pterin dosing.

Lumazine dosing. Lumazine strongly converted to 7-hydroxylumazine (pathway 4), with a molar conversion rate of 60%, agreeing with a previous study that 7-hydroxylumazine is the direct product of lumazine (Rembold *et al.*, 1971). In addition, while lumazine was not detected in the T cell line when dosed with pterin, subsequent pterin dosing in the highly tumorigenic C cell line yielded lumazine (pathway 4), which is discussed in Section 3.2.1.

$$\text{Pterin} \xrightarrow{\text{Deaminase}} \text{Lumazine} \xrightarrow{\text{XOR}} \text{7-Hydroxylumazine} \qquad \text{(pathway 4)}$$

Isoxanthopterin dosing. Isoxanthopterin was not metabolized in the cell samples in the screening experiment. In a prior work by Rembold *et al*. (1969), a pterin deaminase was shown *in vitro* to deaminate 5,6,7,8-tetrahydropterin, 7,8-dihydropterin, pterin, and isoxanthopterin to 5,6,7,8-tetrahydrolumazine, 7,8-dihydrolumazine, lumazine, and 7-hydroxylumazine, respectively. However, in this experiment, dosed isoxanthopterin was not metabolized by the cells, indicating that the hypothesized deaminase responsible for generating the lumazines in the breast cells does not act on isoxanthopterin. Therefore, it is proposed that generation of 7-hydroxylumazine in breast cells dosed with pterin is due to pterin conversion to lumazine (pathway 4) and not from deamination of isoxanthopterin (pathway 5).

$$\text{Pterin} \xrightarrow{\text{XOR}} \text{Isoxanthopterin} \xrightarrow{\text{Deaminase}} \text{7-Hydroxylumazine} \qquad \text{(pathway 5)}$$

3.1.4. 7,8-Dihydroxanthopterin and Xanthopterin Dosing Results.

7,8-Dihydroxanthopterin dosing. Dosed 7,8-dihydroxanthopterin was not significantly metabolized by the T cell line. Instead, similar ratios of 7,8-dihydroxanthopterin and xanthopterin were observed in dosed cells and media (2:1 and 2.6:1, respectively). This may be attributed to the spontaneous autooxidation of 7,8-dihydroxanthopterin to xanthopterin (Blau *et al.*, 1996; Burton *et al.*, 2016a; Rembold *et al.*, 1971).

$$\text{7,8-Dihydroxanthopterin} \xrightarrow{\text{Nonenzymatic}} \text{Xanthopterin} \qquad \text{(pathway 6)}$$

Xanthopterin dosing. Cells dosed with xanthopterin resulted in qualitatively higher levels of leucopterin (Figure S1). This finding agreed with previously reported results that leucopterin is a metabolic product of xanthopterin when its metabolism was studied *in vitro* using XOR enzyme derived from rat liver (Rembold *et al.*, 1971) and butterflies (Watt, 1972). Xanthopterin dosing also yielded marginal amounts (1.41%) of 7,8-dihydroxanthopterin. This finding suggested that while 7,8-dihydroxanthopterin incompletely oxidizes to xanthopterin, as already seen here, that some 7,8-dihydroxanthopterin may be recovered from as yet undetermined processes (pathway 7).

$$\text{7,8-Dihydroxanthopterin} \rightleftarrows \text{Xanthopterin} \xrightarrow{\text{XOR}} \text{Leucopterin} \qquad \text{(pathway 7)}$$

3.1.5. Sepiapterin Dosing Results. The sepiapterin dosing experiment resulted in significant increases of multiple pteridine derivatives, including 6-biopterin, 7,8-dihydroxanthopterin, 7-hydroxylumazine, isoxanthopterin, xanthopterin, and 6-hydroxylumazine (Table 1). The multiplicity of metabolic products seen here can be attributed to the so-called salvage pathway in which exogenous sepiapterin is reduced to 7,8-dihydrobiopterin by sepiapterin reductase (Figure 1, pathway 9) and subsequently reduced to 5,6,7,8-tetrahydrobiopterin by dihydrofolate reductase (Alp and Channon,

2004; Crabtree *et al.*, 2009; Nichol *et al.*, 1983; Tomšíková *et al.*, 2013). A two-step spontaneous oxidation of 5,6,7,8-tetrahydrobiopterin with 7,8-dihydrobiopterin as an intermediate yields 6-biopterin. Moreover, nonenzymatic side chain cleavage of 5,6,7,8-tetrahydrobiopterin can yield 7,8-dihydropterin (Walter *et al.*, 1997). The latter may be spontaneously oxidized to pterin and subsequently converted to isoxanthopterin by XOR, as shown in this study and others (Rembold *et al.*, 1971; Tomšíková *et al.*, 2013; Walter *et al.*, 1997). The intermediate 7,8-dihydropterin may also be converted to 7,8-dihydroxanthopterin by XOR (Rembold *et al.*, 1971). Similarly, 6-hydroxylumazine and 7-hydroxylumazine may be produced from 7,8-dihydropterin and pterin, as seen in the current study and elsewhere (Rembold *et al.*, 1971).

In this way, a full accounting of the observed metabolic products of sepiapterin may be understood through its salvage to 5,6,7,8-tetrahydrobiopterin. Given the clinical significance of many of these pteridine derivatives in various epithelial cancers, this finding may be particularly important in understanding their biological significance in cancer development and the potential role of 5,6,7,8-tetrahydrobiopterin metabolism in particular.

3.2. EFFECTS OF TUMORIGENICITY ON PTERIDINE METABOLISMS

While the screening study in phase 1 was designed to determine the metabolic products of various pteridine precursors within the T cell line, the quantitative study in phase 2 was designed to determine the relationship between individual metabolic reactions and breast cancer tumorigenicity across the progressive breast cancer cell model. For these experiments, three exogeneous pteridine precursors, including pterin,

xanthopterin, and sepiapterin, were dosed in the A, T, and C cell lines and the amounts of precursor consumed and products formed were quantified. These pteridine precursors were selected based on the multiplicity of products covered, their clinical significance as potential cancer biomarkers, and to better elucidate their biosynthetic pathways in breast tumors.

3.2.1. Pterin Precursor. Exogeneous pterin was efficiently converted to isoxanthopterin with an 86.26% and 88.44% molar conversion in the nontumorigenic A cell line and premalignant T cell lines, respectively. Less conversion was observed (66%) in the tumorigenic C cell line (Table S3). When normalized to cell concentrations **(**Figure 2), isoxanthopterin was marginally higher in T and C cell lines ($p < 0.05$, Student's t-test), 6-hydroxymethylpterin and lumazine were significantly higher in C cell lines ($p < 0.05$, Student's t-test), and 6-hydroxylumazine generally trended with tumorigenicity although no pairwise comparisons were statistically significant. Notably, the amount of unmetabolized pterin in C cells after five days was significantly higher than in A and T cells ($p < 0.05$, Student's t-test). This finding, taken together with the elevated levels of pterin in tumorigenic breast cancer cells following folic acid dosing reported in our companion study (Rasmussen *et al.*, 2022), strongly implicates altered XOR enzymatic activity. As previously noted, XOR mediates a myriad of pteridine and lumazine reactions, including the conversion of pterin to isoxanthopterin. While XOR activity was not directly measured in the present study, its activity has previously been shown to be inversely correlated with breast cancer tumorigenicity using the same progressive breast cancer cell model (Fini *et al.*, 2011; Fini *et al.*, 2008). In this case, suppressed enzymatic activity in tumor cells would be expected to result in less efficient conversion of pterin, as

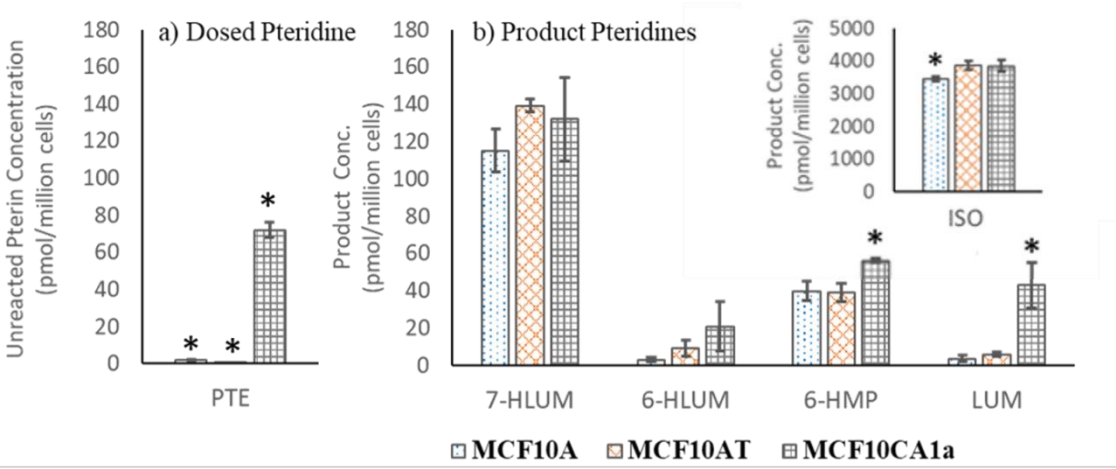

c)

Molar Reaction Recoveries	MCF10A	MCF10AT	MCF10CA1a
ISO produced	86.26%	88.44%	66.09%
Other pteridines produced	< 5%	< 5%	< 5%
Total recovery	**89.34%**	**91.98%**	**70.59%**

Figure 2. Production of pteridine derivatives in different breast cells following dosing with PTE (12.26 µM) for five days (n=3). a) Concentration (pmol/million cells) of unreacted PTE in different breast cells; b) Concentrations (pmol/million cells) of pteridine derivatives produced following dosing with PTE in different breast cells; c) molar reaction recoveries following PTE dosing.

* $p < 0.05$, two-tailed Student's t-test.

seen here and in our companion study (Rasmussen *et al.*, 2022). In addition, the tumorigenic increase of lumazine and, to a lesser extent, 6-hydroxylumazine, but not 7-hydroxylumazine, is suggestive of tumorigenic deaminase activity. As previously discussed, pterin may be deaminated to lumazine and subsequently hydroxylated to 7-hydroxylumazine by XOR (Figure 1). In this way, suppressed XOR activity and elevated deaminase activity in tumorigenic breast cells would promote pterin conversion to lumazine, but hinder the subsequent reaction, resulting in higher levels of the lumazine intermediate. Similarly, pterin may be reduced to 7,8-dihydropterin, whereupon it may be

deaminated and converted to 6-hydroxylumazine before being ultimately converted to 6,7-dihydroxylumazine by XOR (Figure 1). In this way, the combination of increased deaminase activity and suppressed XOR activity can account for the majority of the metabolic products seen here. Finally, the marginal increases observed for isoxanthopterin and 6-hydroxymethylpterin in tumorigenic C cells suggest more complicated pathways, potentially involving novel feedback mechanisms and metabolic reactions. Taken together, these findings present an accounting of altered pterin metabolism in breast cancer, invoking multiple enzymatic processes and providing a tumorigenic origin for several pteridine derivatives.

3.2.2. Xanthopterin Precursor. More than 95% of the exogeneous xanthopterin precursor was metabolized by the A and T cell lines, while 77% was consumed by the tumorigenic C cell line (Table 2). The difference between the A and T cell lines and the C cell line was statistically significant ($p < 0.05$, Student's t-test). Notably, most of the consumed xanthopterin could not be accounted for by the monitored pteridine derivatives. Previous work has identified leucopterin as a primary metabolic product of xanthopterin (Rembold *et al.*, 1971; Watt, 1972). Although leucopterin was not quantitatively determined in the current study, it was produced in this dosing experiment and confirmed by HPLC-MS/MS method matching elution times and ionization ion pairs with leucopterin standard, as shown in the chromatograms in Figure S1. Furthermore, the observed decrease in xanthopterin consumption in the C cell line provides indirect evidence for the conversion of the exogeneous xanthopterin to leucopterin, which is mediated by XOR. In this way, suppressed XOR activity in the tumorigenic C cell line would limit conversion of the exogeneous xanthopterin to

leucopterin, as observed here. These findings ultimately suggest that xanthopterin, and potentially leucopterin, may exhibit altered metabolism in breast tumors.

Table 2. Concentrations (pmol/million cells) of unreacted xanthopterin precursor and 7,8-dihydroxanthopterin product. Total reaction recovery (% molar concentration) of detected pteridines to initial xanthopterin dose (11.165 μM) for 5 days (n=3). Standard deviations are denoted in parentheses.

	Pteridine	**MCF10A**	**MCF10AT**	**MCF10CA1a**
Unreacted Precursor (pmol/million cells)	XAN	104.30 (7.86)	73.63 (17.62)	1391.75 (126.62)
Detected Product (pmol/million cells)	XH_2	179.02 (17.82)	65.54 (63.70)	112.75 (95.09)
Reaction Recovery (%)				
Unreacted Precursor	XAN	3.66 (0.28)	1.46 (0.35)	23.14 (2.11)
Detected Product	XH_2	6.29 (0.63)	1.30 (1.26)	1.91 (1.58)
	Sum	9.95 (0.90)	2.75 (1.61)	25.05 (3.69)
	LEU*	Detected	Detected	Detected

*Leucopterin confirmed, but not quantified

3.2.3. Sepiapterin Precursor. Exogeneous sepiapterin was virtually consumed (<2% remaining) across all three cell lines (Table S4). The amount of unmetabolized sepiapterin remaining was significantly higher in the T cell line ($p < 0.05$, Student's t-test). Exogeneous sepiapterin yielded a multiplicity of metabolic products, including 6-biopterin, 7,8-dihydroxanthopterin, isoxanthopterin, 6-hydroxylumazine, 7-hydroxylumazine, lumazine, and xanthopterin. Five of these metabolic products, shown in Figure 3, were found to have significantly altered levels in the tumorigenic C cell line ($p < 0.05$, Student's t-test). Interestingly, pterin was not generated at detectable levels, although it is likely that the levels were below detection limits and that it was readily

converted to isoxanthopterin, lumazine, and 7-hydroxylumazine. 6-Hydroxylumazine was only statistically discriminated between the T and C cell lines ($p < 0.05$, Student's t-test) and non-statistically discriminated between the A and C cell lines ($p = 0.065$, Student's t-test) while in our previous study, all three cell lines were correlated with tumorigenicity. However, there are several more metabolic steps between sepiapterin and 6-hydroxylumzaine than from folic acid, as well as derivation from a GTP-derived precursor, which may indicate that biomarker levels may be affected by available precursors, which supports previous report from Burton, et al. (2016a) wherein increasing available folate levels altered urinary pteridine levels.

Although this study was not designed to assess the individual intermediates within this section of the pteridine pathway, there are several enzymes implicated in this pathway, including XOR, SR, DHFR, DHPR, and pterin deaminase that may be useful targets for further investigation. Similarly, expansion of the pteridine panel to include reduced and semi-reduced pteridine derivatives may shed additional insights into the intermediate pathways of both pteridines and lumazines. Pterin deaminase, hypothesized to be responsible for the conversion of pteridines to lumazines. In this way, further work on elucidating the molecular mechanisms for the differentiation of these metabolic products and their corresponding enzymes in breast tumor cells may provide useful insights into the role of pteridines as breast cancer biomarkers.

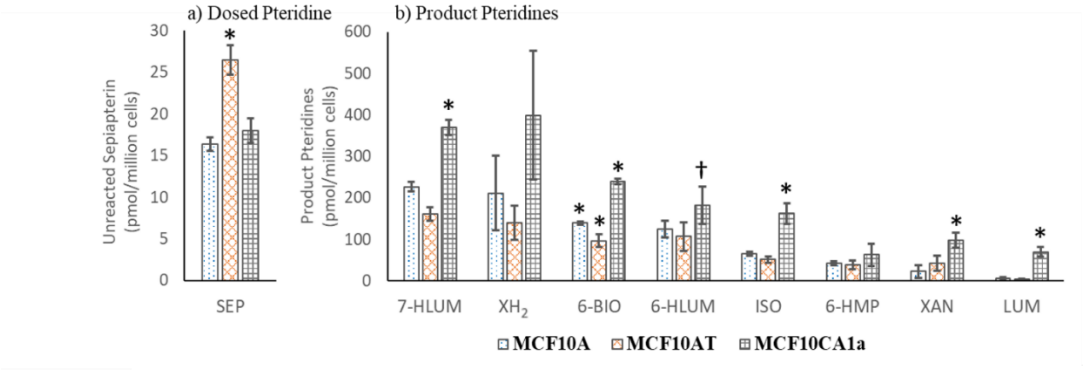

c)

Molar Reaction Recoveries	MCF10A	MCF10AT	MCF10CA1a
7-HLUM produced	10.32%	7.70%	9.34%
XH_2 produced	9.65%	6.63%	10.06%
6-BIO produced	6.36%	4.60%	6.04%
6-HLUM produced	5.68%	5.09%	4.59%
Other pteridines produced	< 5%	< 5%	< 5%
Total recovery	**36.94%**	**29.89%**	**38.77%**

Figure 3. Production of pteridine derivatives in different breast cells following dosing with SEP (8.43 µM) for five days (n = 3). a) Concentration (pmol/million cells) of unreacted SEP in different breast cells; b) Concentrations (pmol/million cells) of pteridine derivatives produced following dosing with SEP in different breast cells; c) molar reaction recoveries following SEP dosing.

* $p < 0.05$, two-tailed Student's t-test.

† Only the T and C cell lines were significantly different, $p < 0.05$, two-tailed Student's t-test.

4. CONCLUSIONS

In this study, the pteridine biosynthetic pathway in progressive breast cancer was investigated by dosing cells directly with pteridine intermediates and monitoring the dosed precursors and the metabolic products. Five pteridines, including pterin, xanthopterin, sepiapterin, lumazine, and 6-hydroxylumazine were found to be metabolized by breast cancer cells. Further investigation into the metabolism of pterin,

xanthopterin, and sepiapterin revealed differential patterns of pteridine metabolites as a function of breast cancer tumorigenicity. Specifically, several pteridines, including pterin, isoxanthopterin, xanthopterin, sepiapterin, 6-biopterin, lumazine, and 7-hydroxylumazine were reported to have significantly altered concentrations ($p < 0.05$, Student's t-test) across the progressive breast cancer model. Pteridine concentrations were found to generally peak in the most aggressive MCF10CA1a cell line, although, sepiapterin, 6-biopterin, and isoxanthopterin were also significantly altered in the mildly aggressive MCF10AT cell line. In this way, the present work built upon our recent companion study to provide direct evidence for the tumorigenic origin of pteridines in breast cancer. These findings together provide an important biological basis for the accounts of elevated urinary pteridines reported in women with breast cancer. Overall, the current study provided new insights into the pteridine biosynthetic pathway and its role in breast cancer development and progression, identifying multiple pteridine metabolites and reactions that warrant further investigation as clinical biomarkers.

SUPPLEMENTARY INFORMATION

HPLC-MS/MS Method: The HPLC-MS/MS method to determine pteridine derivatives was the same as our recent companion study (Rasmussen et al., 2022) with slight modifications. Briefly, chromatographic separation was achieved using a Shimadzu ultra-fast liquid chromatography (UFLC) system (Columbia, MD) with two pumps (LC-20 AD XR), a degasser (DGU-30A3), a temperature controlled autosampler (SIL-20AD XR), and a column oven (CTO-20A) using a Luna phenyl-hexyl column (3.0 µm, 3.0 ×

150 mm) with an attached guard column (Phenomenex, Torrance, CA). A binary gradient flow profile was used (mobile phase A: 0.025% (v/v) formic acid in 99% water/1% acetonitrile; mobile phase B: methanol) with a 50 µL injection volume, oven temperature of 40 °C, and a flow rate of 0.45 mL/min. An AB Sciex 4000 QTrap mass spectrometer (Foster City, CA, USA) was coupled to the liquid chromatography for pteridine quantitation. Optimized mass spectrometer conditions and voltages are denoted in Tables S1 and S2.

Table S1. Positive electrospray ionization (ESI) mass spectrometer conditions with multiple reaction monitoring (MRM) mode.

Parameter	Value
Curtain Gas	45 psi
Collision Gas	6 psi
Ion Source Gas 1	45 psi
Ion Source Gas 2	40 psi
IonSpray Voltage	5500 V
Ion Source Temperature	600 °C
Entrance Potential	10 V

Table S2. Optimized mass spectrometer conditions.

Compound	Abbreviation	MRM (m/z)	DP (V)	CE (V)	CXP (V)
Pterin	PTE	164.2 > 119.1	47	31	6
		164.2 > 121.1	47	31	6
		164.2 > 92.1	47	43	15
Lumazine	LUM	165.2 > 93.0	58	40	4
		165.2 > 69.0	58	57	11
6-Methylpterin	6-MP	178.1 > 133.1	53	30	7
		178.1 > 106.0	53	39	5
Xanthopterin	XAN	180.1 > 135.1	47	32	7
		180.1 > 163.1	47	25	9
Isoxanthopterin	ISO	180.1 > 135.0	69	31	7
		180.1 > 163.0	69	25	9
7-Hydroxylumazine	7-HLUM	181.1 > 110.0	54	31	5
		181.1 > 55.1	54	51	9
6-Hydroxylumazine	6-HLUM	181.1 > 164.0	60	22	9
		181.1 > 108.0	60	34	5
7,8-Dihydroxanthopterin	XH_2	182.1 > 154.1	51	22	9
		182.1 > 126.1	51	31	6
6,7-Dimethylpterin	6,7-DMP	192.2 > 106.0	60	38	5
		192.2 > 165.1	60	30	10
		192.2 > 68.0	60	48	11
6-Hydroxymethylpterin	6-HMP	194.1 > 176.1	44	20	11
		194.1 > 105.9	44	36	5
6-Carboxypterin	6-CAP	208.2 > 190.1	65	18	12
		208.2 > 164.1	65	22	10
6-Biopterin	6-BIO	238.2 > 220.2	50	18	14
		238.2 > 178.2	50	27	10
Sepiapterin	SEP	238.2 > 192.1	79	22	11
		238.2 > 165.1	79	30	10
Neopterin	NEO	254.2 > 206.1	50	25	13
		254.2 > 236.2	50	20	15
Monapterin	MNP	254.2 > 206.1	54	24	12
		254.2 > 236.2	54	17	16
Leucopterin*	LEU	196.2 > 168.1	64	24	10
		196.2 > 140.1	64	28	29

*Used for compound identification and confirmation only.

Table S3. Molar ratios (%) of detected pteridines to initial dosed of pterin (12.26 µM) for 5 days (n=3). Standard deviations are denoted in parentheses.

Pteridine	**MCF10A**	**MCF10AT**	**MCF10CA1a**
PTE*	0.04 (0.01)	0.01 (0.01)	1.24 (0.07)
ISO	86.26 (2.20)	88.44 (3.32)	66.09 (2.88)
7-HLUM	2.87 (0.290	3.20 (0.08)	2.12 (0.29)
LUM	0.09 (0.04)	0.14 (0.03)	0.74 (0.22)
6-HLUM	0.08 (0.03)	0.20 (0.07)	0.40 (0.17)
Sum	89.34 (2.58)	91.98 (3.50)	70.59 (3.63)

*Dosed pteridine

Table S4. Molar ratios (%) of detected pteridines to initial moles dosed of sepiapterin (8.43 µM) for 5 days (n=3).

Pteridine	**MCF10A**	**MCF10AT**	**MCF10CA1a**
SEP*	0.75 (0.04)	1.26 (0.08)	0.45 (0.04)
7-HLUM	10.32 (0.53)	7.70 (0.77)	9.34 (0.46)
XH_2	9.65 (4.08)	6.63 (1.97)	10.06 (3.92)
BIO	6.36 (0.16)	4.60 (0.73)	6.04 (0.19)
6-HLUM	5.68 (0.89)	5.09 (1.65)	4.59 (1.14)
ISO	2.93 (0.21)	2.44 (0.35)	4.08 (0.62)
XAN	1.00 (0.69)	2.00 (0.84)	2.47 (0.45)
LUM	0.25 (0.17)	0.16 (0.08)	1.75 (0.29)
Sum	36.94 (6.77)	29.89 (6.47)	38.77 (7.11)
LEU**	Detected	Detected	Detected

*Dosed pteridine
**Leucopterin confirmed, but not quantified

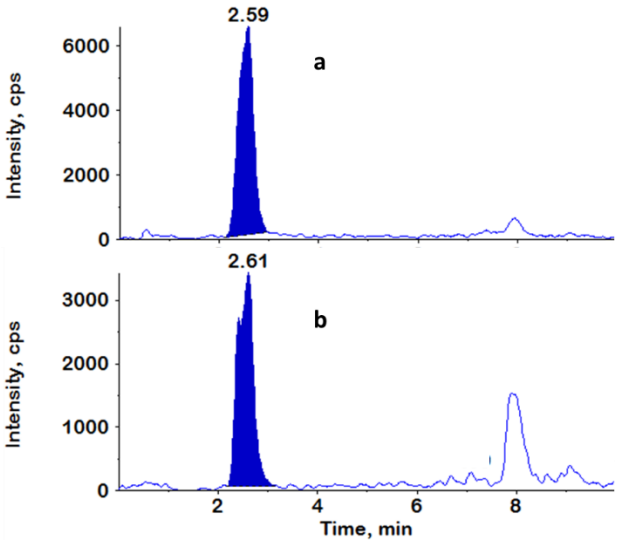

Figure S1. Leucopterin chromatograms. A) Leucopterin standard in solvent matrix. B) Leucopterin peak detected in xanthopterin dosed MCF10A cells.

ACKNOWLEDGEMENTS

The authors would like to thank Barbara Ann Karmanos Cancer Institute for providing the MCA10A series of cell lines. We appreciate the assistances of Dr. Paul Nam on analytical method and instrument troubleshooting. This study was funded by National Institute of Health (NIH), National Cancer Institute, award number R03CA219337.

REFERENCES

Alp, N.J. and Channon, K.M. (2004) Regulation of Endothelial Nitric Oxide Synthase by Tetrahydrobiopterin in Vascular Disease. *Arteriosclerosis, Thrombosis, and Vascular Biology* **24,** 413-420. 10.1161/01.atv.0000110785.96039.f6

Battelli, M.G., Polito, L., Bortolotti, M. and Bolognesi, A. (2015) Xanthine oxidoreductase in cancer: more than a differentiation marker. *Cancer Medicine* **5,** 546-557. 10.1002/cam4.601

Blau, N., De Klerk, J.B.C., Thöny, B., Heizmann, C.W., Kierat, L., Smeitink, J.A.M. and Duran, M. (1996) Tetrahydrobiopterin Loading Test in Xanthine Dehydrogenase and Molybdenum Cofactor Deficiencies. *Biochemical and Molecular Medicine* **58,** 199-203.https://doi.org/10.1006/bmme.1996.0049

Burton, C. and Ma, Y. (2017) The role of urinary pteridines as disease biomarkers. *Pteridines* **28,** 1-21. https://doi.org/10.1515/pterid-2016-0013

Burton, C. and Ma, Y. (2019) Current Trends in Cancer Biomarker Discovery Using Urinary Metabolomics: Achievements and New Challenges. *Current Medicinal Chemistry* **26,** 5-28. 10.2174/0929867324666170914102236

Burton, C., Shi, H. and Ma, Y. (2013) Simultaneous Detection of Six Urinary Pteridines and Creatinine by High-Performance Liquid Chromatography-Tandem Mass Spectrometry for Clinical Breast Cancer Detection. *Analytical Chemistry* **85,** 11137-11145. https://doi.org/10.1021/ac403124a

Burton, C., Shi, H. and Ma, Y. (2014) Normalization of urinary pteridines by urine specific gravity for early cancer detection. *Clinica Chimica Acta* **435,** 42-47. https://doi.org/10.1016/j.cca.2014.04.022

Burton, C., Shi, H. and Ma, Y. (2016a) Daily variation and effect of dietary folate on urinary pteridines. *Metabolomics* **12,** 1-10. https://doi.org/10.1007/s11306-016-1019-4

Burton, C., Shi, H. and Ma, Y. (2016b) Development of a high-performance liquid chromatography‐Tandem mass spectrometry urinary pterinomics workflow. *Analytica Chimica Acta* **927,** 72-81. https://doi.org/10.1016/j.aca.2016.05.005

Burton, C., Weng, R., Yang, L., Bai, Y., Liu, H. and Ma, Y. (2015) High-throughput intracellular pteridinic profiling by liquid chromatography‐quadrupole time-of-flight mass spectrometry. *Analytica Chimica Acta* **853,** 442-450. https://doi.org/10.1016/j.aca.2014.10.044

Crabtree, M.J., Tatham, A.L., Hale, A.B., Alp, N.J. and Channon, K.M. (2009) Critical Role for Tetrahydrobiopterin Recycling by Dihydrofolate Reductase in Regulation of Endothelial Nitric-oxide Synthase Coupling. *The Journal of Biological Chemistry* **284,** 28128-28136. https://doi.org/10.1074/jbc.M109.041483

Fan, H., Hitchcock, D.S., Seidel, R.D., Hillerich, B., Lin, H., Almo, S.C., Sali, A., Shoichet, B.K. and Raushel, F.M. (2013) Assignment of Pterin Deaminase Activity to an Enzyme of Unknown Function Guided by Homology Modeling and Docking. *Journal of the American Chemical Society* **135,** 795-803. 10.1021/ja309680b

Fini, M.A., Monks, J., Farabaugh, S.M. and Wright, R.M. (2011) Contribution of Xanthine Oxidoreductase to Mammary Epithelial and Breast Cancer Cell Differentiation In Part Modulates Inhibitor of Differentiation-1. *Molecular Cancer Research* **9,** 1242-1254. https://doi.org/10.1158/1541-7786.MCR-11-0176

Fini, M.A., Orchard-Webb, D., Kosmider, B., Amon, J.D., Kelland, R., Shibao, G. and Wright, R.M. (2008) Migratory activity of human breast cancer cells is modulated by differential expression of xanthine oxidoreductase. *Journal of Cellular Biochemistry* **105,** 1008-1026.10.1002/jcb.21901

Fukushima, T. and Shiota, T. (1974) Biosynthesis of Biopterin by Chinese Hamster Ovary (CHO K1) Cell Culture. *Journal of Biological Chemistry* **249,** 4445-4451.

Gamagedara, S., Gibbons, S. and Ma, Y. (2011) Investigation of urinary pteridine levels as potential biomarkers for noninvasive diagnosis of cancer. *Clinica Chimica Acta* **412,** 120-128. https://doi.org/10.1016/j.cca.2010.09.015

Gross, S.S. and Levi, R. (1992) Tetrahydrobiopterin synthesis. An absolute requirement for cytokine-induced nitric oxide generation by vascular smooth muscle. *Journal of Biological Chemistry* **267,** 25722-25729.

Jayaraman, A., Thandeeswaran, M., Priyadarsini, U., Sabarathinam, S., Nawaz, K.A.A. and Palaniswamy, M. (2016) Characterization of unexplored amidohydrolase enzyme−pterin deaminase. *Applied Microbiology and Biotechnology* **100,** 4779-4789. 10.1007/s00253-016-7513-9

Kośliński, P., Bujak, R., Daghir, E. and Markuszewski, M.J. (2011) Metabolic profiling of pteridines for determination of potential biomarkers in cancer diseases. *ELECTROPHORESIS* **32,** 2044-2054. https://doi.org/10.1002/elps.201000664

Linder, N., Lundin, J., Isola, J., Lundin, M., Raivio, K.O. and Joensuu, H. (2005) Down-Regulated Xanthine Oxidoreductase Is a Feature of Aggressive Breast Cancer. *Clinical Cancer Research* **11,** 4372-4381. 10.1158/1078-0432.ccr-04-2280

Ma, Y. and Burton, C. (2013) Pteridine detection in urine: the future of cancer diagnostics? *Biomarkers in Medicine* **7,** 679-681. https://doi.org/10.2217/bmm.13.88

Nichol, C.A., Lee, C.L., Edelstein, M.P., Chao, J.Y. and Duch, D.S. (1983) Biosynthesis of tetrahydrobiopterin by de novo and salvage pathways in adrenal medulla extracts, mammalian cell cultures, and rat brain in vivo. *Proceedings of the National Academy of Sciences* **80,** 1546-1550. 10.1073/pnas.80.6.1546

Oettle, K. and Reibnegger, G. (1999) Pteridines as inhibitors of xanthine oxidase: structural requirements. *Biochimica et Biophysica Acta* **1430,** 387-395.

Rasmussen, L., Foulks, Z., Burton, C. and Shi, H. (2022) Establishing pteridine metabolism in a progressive isogenic breast cancer cell model. *Metabolomics* **18**. 10.1007/s11306-021-01861-9

Rembold, H., Metzger, H. and Gutensohn, W. (1971) Catabolism of Pteridine Cofactors: III. On the introduction of an oxygen function into position 6 of the pteridine ring. *Biochimica et Biophysica Acta* **230,** 117-126. https://doi.org/10.1016/0304-4165(71)90059-6

Rembold, H. and Simmersbach, F. (1969) Catabolism of pteridine cofactors II. A specific pterin deaminase in rat liver. *Biochimica et Biophysica Acta* **184,** 589-596.

Shantaram, M., Bhaktha, G., Kumta, S. and Aziz, M.A. (2012) Evaluation of Urinary 6-Hydroxymethylpterin in Malignancies. *International Journal of Analytical, Pharmaceutical, and Biomedical Sciences* **1,** 71-74.

Tomšíková, H., Tomšík, P., Solich, P. and Nováková, L. (2013) Determination of pteridines in biological samples with an emphasis on their stability. *Bioanalysis* **5,** 2307-2326. https://doi.org/10.4155/bio.13.194

Walter, R., Blau, N., Schaffner, A., Schneemann, M., Speich, R., Stocker, R., Naujeck, B. and Schoedon, G. (1997) Inhalation of the Nitric Oxide Synthase Cofactor Tetrahydrobiopterin in Healthy Volunteers. *American Journal of Respiratory and Critical Care Medicine* **156,** 2006-2010. 10.1164/ajrccm.156.6.96-12084

Watt, W.B. (1972) Xanthine Dehydrogenase and Pteridine Metabolism in *Colias* Butterflies. *Journal of Biological Chemistry* **247,** 1445-1451. https://doi.org/10.1016/S0021-9258(19)45578-6

III. QUANTIFICATION OF SILVER NANOPARTICLE INTERACTIONS WITH YEAST *SACCHAROMYCES CEREVISIAE* STUDIED USING SINGLE-CELL ICP-MS*

Lindsey Rasmussen[1], Honglan Shi[1,2,3], Wenyan Liu[1,3], Katie B. Shannon[4]

[1]Department of Chemistry, Missouri University of Science and Technology, 400 West 11th Street, Rolla, MO 65409, USA

[2]Center for Single Nanoparticle, Single Cell, and Single Molecule Monitoring (CS3M), Missouri University of Science and Technology, Rolla, MO 65409, USA

[3]Center for Research in Energy and Environment, Missouri University of Science and Technology, Rolla, MO, USA

[4]Biological Sciences, Missouri University of Science and Technology, Rolla, MO 65409, USA

ABSTRACT

Silver nanoparticles (AgNPs) have been used in many fields due to their anticancer, antimicrobial, and antiviral potential. Single-cell ICP-MS (SC-ICP-MS) is an emerging technology that allows for the rapid characterization and quantification of a metal analyte across a cell population in a single analysis. In this study, a new rapid and sensitive SC-ICP-MS method was developed to quantitatively study the interactions of AgNPs with yeast *Saccharomyces cerevisiae*. The method can quantify the cell concentration, silver concentration per cell, and profile the nanoparticle distribution in a yeast cell population. AgNP dosing time, concentration, and AgNP size were

---

* Reproduced with permission from Springer Nature

quantitatively evaluated for their effects on AgNP-yeast cell interactions. The results showed that the initial uptake of AgNPs was rapid and primarily driven by the mass of Ag per cell. The optimal dosing particle concentrations for highest uptake were approximately 1820, 1000, and 300 AgNPs/cell for 10, 20, and 40 nm AgNPs, respectively. Furthermore, this study also validated a washing method for the application to a microorganism for the first time and was used to quantitatively determine the amount of cell surface–adsorbed AgNPs and intracellular AgNPs. These results indicated that the mass (Ag in ag/cell) ratios of intracellular vs cell surface-adsorbed AgNPs were similar for different AgNP sizes. This high throughput and ultrasensitive SC-ICP-MS method is expected to have many potential applications, such as optimization of methods for green synthesis of AgNPs, nanotoxicity studies, and drug delivery. This is the first quantification study on the interactions of AgNPs and *S. cerevisiae* using SC-ICP-MS.
Keywords: Silver nanoparticle, Yeast cell, Single-cell ICP-MS, Uptake of AgNP by yeast cell, Surface-adsorbed AgNP, Intracellular AgNP

1. INTRODUCTION

The incorporation of nanotechnology into daily life is growing with applications in commercial products, antibacterial materials, and drug delivery [1–4]. Better understanding of the interaction mechanisms between nanoparticles and cells is becoming more important. The effects of nanoparticle waste on the environment such as potential toxic effects on aquatic and plant organisms or air quality are an area of research with many unknowns [1, 5]. Research and development of “green manufacturing methods”

using fungi, bacterial, and plant substrates for nanotechnology production to reduce the environmental impact of the sector has also grown substantially [3, 6, 7]. The exact modes of antibacterial action of nanoparticles on cells are still not fully defined as they can differ based on the cell type, nanoparticle type, and experimental conditions [5, 8, 9]. In drug delivery, the percentage of nanoparticle-based drug that is actually delivered to the target tumor location can be less than 1%, showing that there is still substantial room for optimization of these techniques [10]. More recently, nanoparticles, including silver nanoparticles (AgNPs), have been shown to neutralize COVID-19 viruses [11] and have also been applied to masks and air filters to inactivate Coronaviruses [12]. Therefore, with the growth of the nanotechnology sector and research into these various areas, there has been concurrent development of analytical techniques to facilitate the advancement of nanotechnology. There is no single technology that can fully characterize nanoparticle interactions with a biological system or the environment. Various combinations of different techniques are the practical approaches currently. Spectroscopy, various types of electron microspectroscopic images, and ICP-MS are the major analytical techniques that have been used in this field [13–15]. ICP-MS-based analytical techniques for the detection of metal content in cells [16] such as single-cell (SC) ICP-MS [17–22], including SC-ICP-TOF–MS (also referred to as mass cytometry) [23, 24], LA-ICP-MS [25–28], and microfluidic device-coupled ICP-MS [29] are advancing very rapidly to study nanoparticle and cell interaction mechanisms, nanotoxicity, drug development, and delivery at the single-cell level. More recently, an ICP-OES method was also used for silver nanoparticle speciation after sequential extraction of the solid materials [30].

Comprehensive reviews and comparisons of different techniques and their applications in single-cell analyses have been reviewed extensively [13, 14, 31–35].

SC-ICP-MS is a cutting-edge technology that can help yield insights into the gaps of nanoparticle knowledge as has been previously described [16, 20–22]. Conventional ICP-MS analysis of the metal content in cells is limited to measurements of the average amount per cell in a cell population after acid digestion [16, 21]. The key advantage of the SC-ICP-MS technology is that it rapidly provides the distribution of the metal content within a cell population, allowing for the discrimination of differences due to cell heterogeneity [16, 18, 19, 21]. The analysis is time-resolved, uses a low flow rate high-efficiency nebulizer, and each cell is detected as a single pulse signal. The intensity of the pulse signal is proportional to the mass of the element in each individual cell, and the frequency of the pulse signals is proportional to the cell concentration. This allows for the quantitation of metal ion uptake, metal-based nanoparticle uptake or intrinsic metal, such as Zn or Cu, concentration measurement in each cell [18, 19, 21]. In addition, the single-cell sampling setup and the software can be easily implemented (in comparison to purchasing a new instrument) into an existing ICP-MS in a laboratory, with minimal cost and operator training required for operation. Though it is still at the infancy step of the SC-ICP-MS technology development, it is expected that this technique will advance very quickly and will highly benefit research and applications, especially in the fields of nanomedicine, drug delivery, green synthesis of nanoparticles, and nanotoxicity study.

AgNP is one of the most broadly used nanomaterials. It is particularly popular in agrochemicals (pesticides, insecticides, fungicides, fertilizer), nanomedicines, and drug delivery. Its green synthesis is also an active research field. Yeast *Saccharomyces (S.)*

cerevisiae cells have been used for AgNP green synthesis [36–38] and is also a popular cell type for nanomaterial-cell interaction mechanism study and other nanotoxicity studies [39–41]. It is reported that AgNPs readily adhere to the yeast cell wall and are also taken up intracellularly [15, 42–44]. Chen et al. [37] also demonstrate how *S. cerevisiae* coupled to AgNPs could be used to remove heavy metals from wastewater while also providing antibacterial functions. While the majority of previous toxicity research focuses on evaluating the dosing-toxicity relationship between nanoparticles and cells, comparisons between studies are difficult due to variation in experimental variables such as limited datapoints per study, measurement methods, nanoparticle properties, experimental conditions, and cell type [13, 45, 46]. Kettler et al. demonstrated that even differences in the dosing medium used in a study could have significant effects on the observed uptake [9]. Although studies have reported the interactions of AgNPs with yeast cells [15, 42–44] and the mechanism with different techniques, a rapid and highly sensitive SC-ICP-MS quantification method is still lacking and needed for quantitative and comprehensive study of the broadly used AgNPs and yeast cells.

The objectives of this study are to develop a rapid, ultrasensitive SC-ICP-MS quantification method to study AgNP and yeast cell interactions, to quantitatively measure the amount of cell surface adsorbed and intracellular AgNPs, and to optimize conditions of AgNP uptake by yeast cells. This method can be used to support the variety of applications stated above for this common NP-cell model. The method is expected to benefit the potential application of *S. cerevisiae* as a green synthesis substrate, cell model for nanotoxicity, or drug delivery research, etc. To the authors' best knowledge, this is

the first quantification study on the interactions of AgNPs and *S. cerevisiae* under different conditions using SC-ICP-MS.

2. MATERIALS AND METHODS

2.1. MATERIALS

Citrate-stabilized AgNP standard suspensions (10, 20, 40, 70, and 100 nm at 0.02 mg/mL) were purchased from Nanocomposix (San Diego, CA, USA). *S. cerevisiae* (S288c) was obtained from ATCC. The cell strain was BY4743 with genotype *MATa/α his3Δ1/his3Δ1 leu2Δ0/ leu2Δ0 LYS2/lys2Δ0 met15Δ0/MET15 ura3Δ0/ura3Δ0*. Sodium hydroxide; sodium thiosulfate ($Na_2S_2O_3 \cdot 5H_2O$); and YPD medium containing tryptone, yeast extract, and dextrose were obtained from Fisher Scientific (Fair Lawn, NJ, USA). 2-(N-Morpholino)ethanesulfonic acid (MES) hydrate, ethylenediaminetetraacetic acid (EDTA), and potassium ferricyanide ($K_3Fe(CN)_6$ were purchased from Sigma-Aldrich (St. Louis, MO, USA). Dextrose was purchased from MP Biomedicals (Solon, OH, USA). Ultrapure water (18.2 MΩ-cm) was produced by an Elix-3 water purification system from Millipore (Billerica, MA, USA). EQ four-element calibration beads, polystyrene beads (2.5 μm) containing known concentrations of the metal elements Ce, Eu, Ho, and Lu in aqueous suspension, were purchased from Fluidigm (San Francisco, CA, USA).

2.2. YEAST CELL CULTURE

For each experiment, one colony of yeast cells was cultured in a sterile cell culture flask with 30 mL of YPD medium (50 g/L in ultrapure H_2O) at room temperature on a rotor at 12 rotations per minute for the necessary time. The cells were then sent into log phase by resuspending cells in about 50 mL of fresh YPD medium, and incubating on the rotor for an additional 1.5–2 h. At the end of this time period, the cell sample was transferred to centrifuge tubes, centrifuged (5 min at 500 *g*), and then washed 3 times using 10 mL ultrapure H_2O per wash and recentrifuged after each wash. The samples were centrifuged a fourth time and resuspended in 1 mL of ultrapure H_2O. All resuspended cell samples were then combined into one vial to make a cell stock suspension. A hemacytometer was used to count the concentration of the cell stock suspension for the subsequent use in the next experimental step.

2.3. SINGLE-CELL ICP-MS METHOD

For all experiments, a Nexion300D ICP-MS (PerkinElmer, Shelton, CT), the same sample introduction system and Syngistix Single-Cell Application software used for a previous study of toxic algae treatment by copper-based algaecide [19], was utilized. Additionally, a single-cell Micro DX autosampler was added to the system and used for the SC-ICP-MS analysis. ICP-MS parameters, including autosampler specific parameters, are shown in Table 1. ^{107}Ag was monitored for AgNP and cell interaction and ^{64}Zn was monitored as an intrinsic metal in cells for cell concentration determination. The sample chamber was maintained at approximately 33 °C for all experiments. Transport efficiency (TE) measurement methods were evaluated by using 40 nm gold nanoparticles, yeast

cells, and EQ four-element calibration beads. EQ four-element calibration beads were then selected and used to measure TE before each experiment at 110,000 beads/mL per vendor recommendation. Calibration curves consisted of 20 nm, 40 nm, 70 nm, and 100 nm citrate-stabilized AgNPs at ~ 10^5 NPs/mL.

Table 1. Optimized single-cell ICP-MS parameters.

Parameter	**Value**
Manual sampling flow rate	15 – 20 µL/min
Nebulizer	Meinhard TRP-90-A0.05
Spray chamber	Asperon Single-Cell
Injector	Quartz, 2.0 mm id
RF power	1600 W
Nebulizer gas flow	0.54 L/min
Makeup gas flow	0.7 L/min
Analytes	^{64}Zn, ^{107}Ag
Transport efficiency	30-40 %[a]
Sample analysis time	100 s
Dwell time	50 µs
Sample loop size[b]	100 µL
Auto-sampler sample flow rate[b]	15 µL/min
Sample vials[b]	Micro96 well plate (polypropylene, 2 mL)
Carrier solution[b]	H_2O
Working solution[b]	H_2O
Autosampler rinse 1[b]	1% HNO_3, 5% H_2O_2
Autosampler rinse 2[b]	H_2O

[a]Measured daily or each batch of experiment
[b]Autosampler specific parameters

2.4. CELLULAR EXPOSURE TO AGNPS AND SC-ICP-MS ANALYSIS

Dosing with AgNPs was mainly conducted at 10^7 cells/ mL concentration in 10 mL of dosing medium, unless otherwise noted in certain experiments. Dosing medium was 0.2% (w/v) MES hydrate + 0.2% (w/v) dextrose in ultrapure H_2O, adjusted to a pH of 6.8 using NaOH. Different concentrations and sizes of AgNPs were added in this dosing medium. Each sample dosing level was prepared in triplicate. The samples were then capped and placed on a rotor for a specified exposure time (experiment dependent)

at 12 rotations/min. The cell samples were then washed by following a published procedure [37] for three times by centrifugation (10 min first centrifugation, 5 min for second and third washes) at 500 *g* using 10 mL ultrapure H_2O per wash in order to completely remove dosing medium and any residual free-floating silver nanoparticles. For experiments to remove surface-adsorbed AgNPs, the cell samples were washed with PBS buffer containing 20 mM $K_3Fe(CN)_6$ and 20 mM $Na_2S_2O_3 \cdot 5H_2O$. This published procedure [47] that removes surface-adsorbed nanoparticles from human T-lymphocyte cells via a chemical etch process was validated to work for yeast cells in this study. After the washing step, the samples were resuspended in 1 mL of ultrapure H_2O. To completely remove any residual supernatant, each sample was transferred to a 1.5 mL centrifuge tube. Using a low-speed mini-centrifuge, the samples were centrifuged for about 20 s, and then, the supernatant was removed. If needed, samples were placed in a refrigerator to save for analysis or continued for the next step of the analysis. The cells were resuspended in 1 mL H_2O and vortex-mixed for about 10 s. This stock sample suspension was used to dilute to analysis concentrations (~ 10^5 cells/mL) in 0.26 mM EDTA aqueous solution in 15-mL centrifuge tubes. Samples were vortex-mixed immediately before analysis by SC-ICPMS. Histograms were fitted using Syngistix Gaussian distribution, and the maximum of the distribution was utilized for result comparison. While the software directly reported Ag mass (ag) per cell, the particle number per cell was calculated by dividing the mass per cell by the mass of each AgNP.

2.5. TRANSMISSION ELECTION MICROSCOPE IMAGING OF AGNP-DOSED YEAST CELLS

Transmission electron microscopy (TEM) was used to confirm the impact of the different washing processes and to check the status of AgNPs on the surface of the cells. The unstained AgNP-dosed yeast cells were deposited on TEM grids (Ted Pella, Inc. 300 mesh, Prod # 01843-F), freshly glow discharged with a plasma cleaner for 3 min, and left to incubate for 3 min. Subsequently, excess sample suspension was gently wicked away from the grids with a filter paper, and the grids were air-dried at room temperature. A FEI Tecnai F20 transmission electron microscope (FEI, Hillsboro, OR, USA) was used for obtaining TEM images of dosed cells at an accelerating voltage of 200 kV.

3. RESULTS AND DISCUSSION

3.1. SC-ICP-MS METHOD OPTIMIZATION AND PERFORMANCE

3.1.1. Transmission Efficiency Determination. No universal TE detection standard method is currently reported for SC-ICP-MS analysis. We tested TE by three different methods to evaluate the accurate method for TE determination of yeast cells using the SC-ICP-MS analysis, as there have been several different methods reported with inconsistent results for TE detections of the SC-ICP-MS methods for algae cells [18, 19]. We first used the yeast cells themselves to determine TE by monitoring the intrinsic metal ^{64}Zn, similar to the method used in a recently published paper [19]. Zn is present in high enough quantity in individual yeast cells to be detected by SC-ICP-MS. When we used the yeast cells in water to detect TE, a low TE (18%) was obtained. EDTA has been reported to prevent cell aggregation [19, 48]. By adding a small concentration of

EDTA (0.26 mM) to the final dilution of samples, the TE of the yeast cells increased to about 38% (Table 2). We also checked the cell integrities by collecting a sample post-nebulization and observing the cells using a microscope. The cells were intact after nebulization. EQ four-element beads in water at vendor-recommended concentrations (1.1×10^5 beads/mL) were then tested to determine TE by monitoring the metal element ^{140}Ce in the beads. Since the beads are approximately 2.5 μm in diameter, it has been considered in a previous study that they are more analogous to cells than nanoparticle suspensions due to their similar size and density [18]. The TE measured using the beads was found to be similar with the TE obtained by using the yeast cell suspension at the approximate concentration 1.0×10^5 cells/mL in 0.26 mM EDTA solution (Table 2). We also tested the TEs using 40 nm AuNP suspensions in water with and without EDTA. The TE from AuNP suspensions with EDTA was much higher (> 90%) than the TEs using yeast cells. The TE was also higher when the AuNPs were in water without EDTA, although better than that obtained by using the AuNPs with matrix-matched EDTA present. Our test results here did not agree well with other previously reported results where matrix-matched suspensions of AuNPs were utilized for TE determination [18]. Therefore, TE determination for the SC-ICP-MS analysis should be specific for the cell type and the matrix as part of method development. Though the most accurate method to determine TE should be the cells being analyzed, the TE determined by the beads for yeast cells in this study is similar or the same with those obtained by using yeast cells with EDTA present. Using the beads is a simpler way to determine TE compared with the cells because cells need to be freshly cultured and counted each time. Therefore, the EQ

four-element beads were utilized for TE measurement (measured daily for each experiment) in this study.

Table 2. Transport efficiencies measured with yeast cell suspensions (intrinsic metal ^{64}Zn was monitored), EQ four-element calibration beads (^{140}Ce in the beads was monitored), and Au NPs (^{107}Au was monitored) in aqueous and matrix-matched solutions.

Sample (matrix)	Concentration	Transport Efficiency (%)(n=3)
AuNPs (water)	107,500 (particles/mL)	47.13±0.98
AuNPs (0.26 mM EDTA in water)	107,500 (particles/mL)	96.85±2.12
EQ four element beads (water)	$1.1x10^5$ (beads/mL)_	42.06±2.60
Yeast cells (water)	10^5 (cells/mL)	18.35±0.81
Yeast cells (0.26 mM EDTA in water)	10^5 (cells/mL)	38.04±5.49

3.1.2. Reproducibility and Stability. The stability of yeast cell TEs over 9 h with measurements taken every 1.5 h with hemacytometer-counted cell suspensions was found to be acceptable at 44.2 ± 2.8%. Reproducibility of the method was tested through an experiment where 3 separate cell cultures were grown from 3 different colonies. Each colony was dosed with 10, 20, and 40 nm AgNPs at 3000, 1000, and 300 AgNPs/cell, respectively, for approximately 3 h. The %RSDs of the maximum of the Gaussian distributions were less than 6% for the same cell culture (n = 3) across all three AgNP sizes tested. The %RSDs of results from all three cells cultures (n = 9) were less than 8% for all three AgNP sizes tested (Figure S3).

While ag Ag/cell results were generally Gaussian, the fitting to the maximum of the cell distribution using the Gaussian fit software setting obtained highly repeatable results with an %RSD of 5.3% (n = 3) (Figure 1).

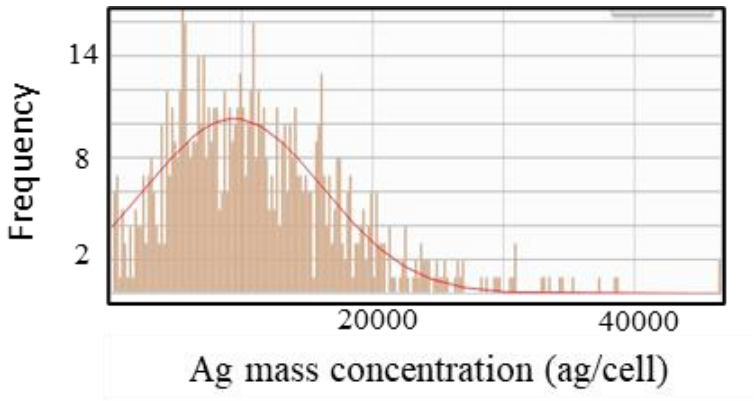

Figure 1. Gaussian distribution fitting of representative histogram for AgNP-dosed yeast cells. Dosed 2300 AgNPs/cell, AgNP size is 10 nm.

3.1.3. Linear Correlation and Detection Limits. Yeast cell concentrations were measured at a concentration range from 1000 to 1,000,000 cells/mL by both the SC-ICP-MS method and by counting the cells with a hemacytometer. It should be noted that only the stock cell suspension was counted by hemacytometer, and the lower concentrations were calculated from the different dilutions because this counting method is not accurate for counting low concentrations of cells. It showed good linear correlation from 1,000,000 cells/mL down to 1000 cells/mL (Figure 2). Therefore, the cell concentration detection limit was estimated to be 1000 cells/mL. While not specifically evaluated in this study, this detection limit could theoretically be improved with longer analysis time. The mass detection limit of Ag per cell for AgNPs was based on AgNP calibration curves (10, 20, 40, 70, 100 nm) collected from multiple experiments, and representative detection limits were calculated using the ICH guidelines [49].

$$\mathrm{DL} = \frac{3.3(\sigma)}{\text{slope of calibration curve}} \quad (1)$$

where σ = standard deviation of the y-intercepts for the AgNP calibration curve, and DL is the mass detection limit (ag Ag/cell).

The silver detection limit was approximately 78 ag/cell. For smaller nanoparticles (10 and 20 nm) below or near the detection limit, it was necessary for multiple nanoparticles to be present on or in the cell for the cell to be detected by the SC-ICP-MS when monitoring the analyte ^{107}Ag. Therefore, the detection limit was equivalent to approximately 14 of 10 nm and 2 of 20 nm AgNPs/cell.

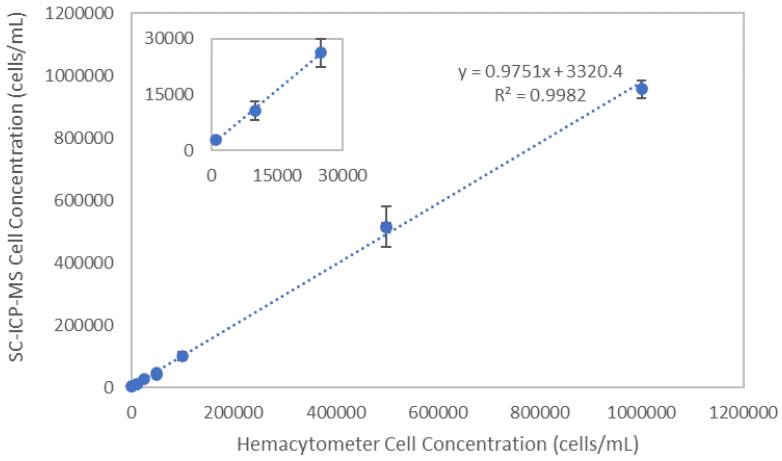

Figure 2. Cell concentrations detected by SC-ICP-MS versus hemacytometer-counted cell concentrations tested on 2 different days. Concentration of cell stock suspension was determined with hemacytometer, and then diluted samples were prepared for analysis. Error bars represent standard deviation (n = 6).

3.2. WASHING METHODS AND THEIR IMPACTS ON AGNP AND YEAST CELL INTERACTIONS

The SC-ICP-MS method cannot distinguish if the AgNPs were in the cells or attached on the surface of the cells. Therefore, cells were imaged using TEM post-dosing with AgNPs to validate the presence of AgNPs on the cell surfaces. Two washing

processes were evaluated: (1) wash with ultrapure water, which leaves the cell surface–adsorbed AgNPs intact, and (2) wash by PBS buffer containing 20 mM $K_3Fe(CN)_6$ and 20 mM $Na_2S_2O_3 \cdot 5H_2O$ to remove the cell surface–adsorbed AgNPs. The procedure for removal of surface-adsorbed nanoparticles from human T-lymphocyte cells is a previously published protocol by Ivask, A, et al. [24, 47], but this procedure has not been used on yeast cells, a microorganism. Therefore, the washing efficiencies by water and the buffer (PBS solution with 20 mM $K_3Fe(CN)_6$ and $Na_2S_2O_3 \cdot 5H_2O$) were evaluated by SC-ICP-MS (Table 3). The washing impacts were evaluated after 1, 3, and 6 washes with H_2O, and no significant effects were observed, indicating that AgNPs loosely attached outside of the cell wall were washed off completely by 3 water washes, and successive washes had no further impact on the total AgNPs associated with yeast cells (Figure S1). Therefore, three-time water wash procedure was used for the determination of total AgNP associated with cells after yeast cell exposure to AgNPs prior to the SC-ICP-MS analysis. When AgNP-dosed cells were washed by PBS containing $K_3Fe(CN)_6$ and $Na_2S_2O_3 \cdot 5H_2O$ for 3 times, the AgNPs adsorbed to the surface of the cells were removed and the AgNP concentration per cell decreased compared with those by water wash. The results from different washes were also confirmed by the TEM. The representative TEM images are shown in Figure S2. No AgNPs were present for the blank control (Figure S2A, no AgNP-dosed). There were many AgNPs associated with the cell surface after 3-time water wash (Figure S2B). The cell surface–adsorbed AgNPs were completely removed from the cell surface after washing 3 times by the PBS buffer containing $K_3Fe(CN)_6$ and $Na_2S_2O_3 \cdot 5H_2O$ (Figure S2C). Our results are in agreement with published literature showing that AgNPs are adsorbed to the cell wall due to attraction to various

functional groups on the cell wall [44]. The insides of cells were not imaged, but prior literature has shown uptake of AgNPs internally in *S. cerevisiae* was kept as nanoparticles. Therefore, for all calculations in this study, it was assumed that any silver taken up by yeast cells and detected by SC-ICP-MS was AgNPs [44]. For samples washed with H_2O, SC-ICP-MS results represent the total AgNPs associated with cells, including AgNPs adsorbed to the cell surfaces and the AgNPs inside the cells. For those washed with PBS buffer containing $K_3Fe(CN)_6$ and $Na_2S_2O_3 \cdot 5H_2O$, SC-ICP-MS results represent only the intracellular AgNPs. One key advantage of this novel SC-ICP-MS method is the accurate quantification of AgNPs inside the yeast cells, the total AgNP associated with the cell, and adsorbed onto the cell surface by calculation. Another major advantage is that it can determine the AgNPs in individual cells and the distribution profile in the cell population as shown in histograms (Figure 1).

Table 3. Quantitative comparison of cell surface adsorbed and intracellular AgNPs. Dosed concentration ratio was 2300 AgNPs/cell and dosing time was 24 hours, *n*=3.

AgNP Size (nm)	AgNP Location on Cell	ag Ag/cell (%RSD)	AgNPs/cell (%RSD)	% Uptake	% Intracellular:Surface-adsorbed AgNPs
10	Total	8903 (5.1)	1621 (5.1)	70.5	-
10	Internal	6359 (1.8)	1158 (1.8)	50.3	71.4
10	External	2544	463	20.1	28.6
20	Total	15603 (2.2)	355 (2.3)	15.4	-
20	Internal	11592 (4.3)	264 (4.2)	11.5	74.3
20	External	4011	91	4.0	25.7

3.3. DOSING TIME IMPACT ON AGNP UPTAKE

To determine the effect of dose time on AgNP uptake, cells were dosed with 10 nm AgNPs at a concentration ratio of 1820 AgNPs/cell and tested at various intervals over the course of 48 h (Figure 3). The majority of the 10 nm AgNP uptake took place in

the first hour, with only slight additional uptake with increasing exposure time up to 48 h. This indicated the fast uptake kinetics of the AgNPs by the yeast cells. It should be noted that we did not collect data shorter than 1 h, and thus could not derive the kinetics constant of the uptake, though the SC-ICP-MS is a potential method to study uptake kinetics. Further study may be conducted to estimate the uptake kinetics using this SC-ICP-MS method.

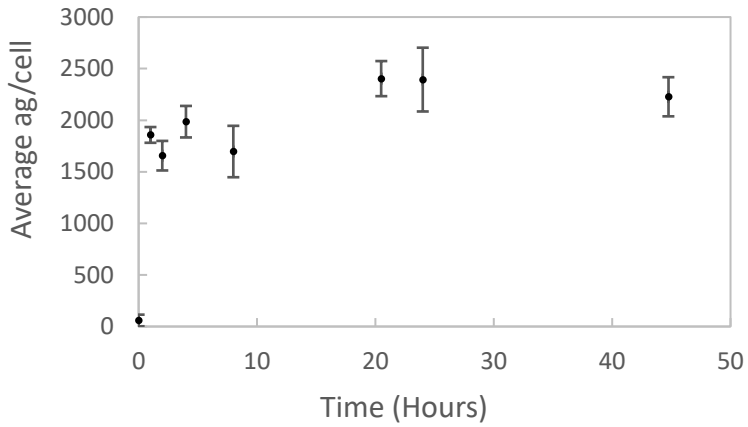

Figure 3. Cellular uptake of 10 nm AgNPs vs exposure time. Dosed concentration ratio was 9997 ag Ag/cell (1820 Ag NPs/cell) concentration ratio. The error bars represent standard deviation (n = 3).

3.4. UPTAKE EFFICIENCIES BY DIFFERENT SIZES OF AGNPS AT DIFFERENT DOSING CONCENTRATIONS

The experiment was conducted to evaluate the correlation of AgNP uptake vs dosing concentration. The correlation of AgNP uptake presented by mass of each cell (ag/cell) vs dosing mass concentration of AgNP (ag/cell) in cell culture is shown in Figure 4. Amounts of uptake by each cell increased quickly with increased AgNP dosing

concentration when the dosing concentrations were low. The uptake increasing slowed down when dosing AgNP concentrations were further increased. It seems that the uptake was driven by mass of Ag per cell where similar mass uptakes per cell were observed for all three AgNPs sizes. However, when the correlation of uptake vs dosing concentration was expressed in terms of particle concentration of AgNPs per cell, differences were observed for different AgNP sizes. The AgNP uptake particle concentration per cell increased with increasing dosing AgNP particle concentration per cell (Figure 5, top), while the uptake percentage of the AgNPs showed a clear optimum dosing concentration for each nanoparticle size tested (Figure 5, bottom). Under these experimental conditions, the highest percentage uptakes were dosing concentrations at approximately 1820, 1000, and 300 AgNPs/cell for 10, 20, and 40 nm AgNPs, respectively.

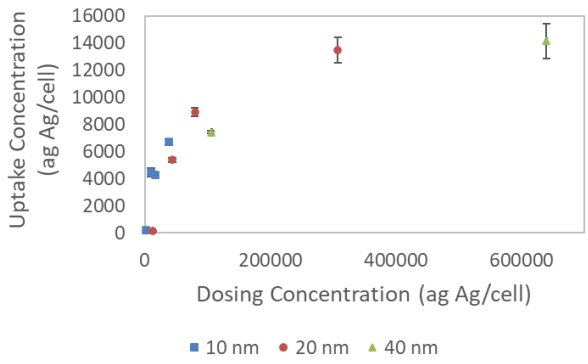

Figure 4. Uptake concentration versus dosing concentration ag Ag/cell for different sizes of AgNPs. Dosing time is about 3 h. The error bars represent standard deviation (n = 3).

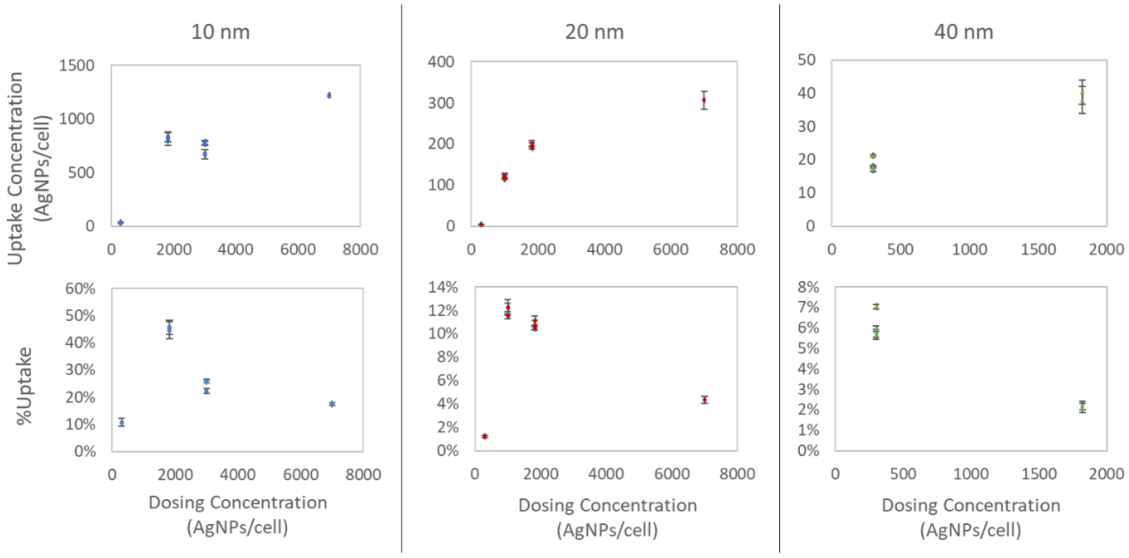

Figure 5. Uptake concentrations and %uptake versus dosing particle concentrations. Dosing time is about 3 h. The error bars represent standard deviation (n = 3).

3.5. INTERNAL UPTAKE VERSUS CELL SURFACE-ADSORBED AGNP

Cells were dosed with a concentration ratio of 2300 AgNPs per cell for 24 h to allow enough time for uptake of the AgNPs. Uptakes of 10 nm and 20 nm AgNPs were tested. Six samples of the same dosing particle concentrations were prepared for each AgNP size. Three samples were washed with H_2O and the other three were washed with PBS containing 20 mM $K_3Fe(CN)_6$ and $Na_2S_2O_3 \cdot 5H_2O$ to distinguish between surface-adsorbed and intracellular AgNPs. The samples were then analyzed by the SC-ICP-MS method and results were used to calculate the total, intracellular, and surface adsorbed AgNPs (Table 3). The total uptake for 10 nm AgNP (1621 particles/cell) was much higher than those for 20 nm AgNP (355 particles/cell), about 4.6 times, based on the particle concentration (particles/cell). However, the total mass uptake of 10 nm AgNP (8903 ag/cell) was lower than those for 20 nm AgNP (15,603 ag/cell), about 0.57 times, based on the mass concentration (ag/cell). Interestingly, despite the differences in

nanoparticle size, the proportions by mass of intracellular and surface-adsorbed AgNPs were similar for both the 10-nm and 20-nm sizes analyzed, at 71.4% intracellular and 28.6% on the cell surface for 10 nm AgNPs, and at 74.3% intracellular and 25.7% on the cell surface for 20 nm AgNPs. These results suggested that the ratio of the cell surface–adsorbed AgNPs and intracellular AgNPs is likely biologically regulated by the mass of the AgNPs, not by the size of the AgNPs. However, more experiments to see if this ratio stays constant or is affected by other variables such as dose time, dose concentration, and NP size would be of interest. This experiment shows that the method works well for quantitatively evaluating intracellular versus surface-adsorbed AgNPs. This could be a useful method for applications in the growing research area of green synthesis of AgNPs where optimal AgNPs per cell can be quantitatively evaluated quickly using the SC-ICPMS technique [36–38].

Overall, this new SC-ICP-MS method was able to quantitate the uptake of AgNPs by yeast cells both adsorbed to the cell surface and located intracellularly. While AgNPs have been reported to be toxic to yeast cells [41], the cell integrity was found to remain intact during the dosing times and concentrations tested in this study, even at the high AgNP dosing concentrations of several thousand AgNPs per cell. Since the SC-ICP-MS can rapidly quantify the cell concentration, silver concentration, and profile of the nanoparticle distribution in a cell population, this makes it a potential asset for green manufacturing applications for the AgNP synthesis using yeast cells where optimal yields per cell can be quickly optimized and evaluated. This new SC-ICP-MS method also can be utilized as a complementary method for nanotoxicity studies, which commonly utilize *S. cerevisiae* as a model [39–41], by quantitatively monitoring the nanoparticle-cell

interactions, fate of nanoparticles, and viability of the cells (pulse signals of the cells will change when cells lyse after death).

4. CONCLUSIONS

A new SC-ICP-MS method was developed for evaluating AgNP interactions with yeast cells as a model. Different TE determination methods were evaluated and the results showed that 40 nm AuNPs were not suitable for TE detection for SC-ICP-MS analysis of yeast cells. Yeast cells in EDTA aqueous solution resulted in similar TEs with the commercial EQ four-element beads, and the beads were used for the daily TE measurement in this study. This SC-ICP-MS method can not only rapidly quantify the cell concentration, silver concentration per cell, and profile of nanoparticle distribution in a cell population, but also quantitatively distinguish the amount of cell surface–adsorbed AgNPs and intracellular AgNPs by washing the dosed yeast cells using a water wash and PBS solution wash (with 20 mM $K_3Fe(CN)_6$ and $Na_2S_2O_3 \cdot 5H_2O$), demonstrating, for the first time, a previously published method used for mammalian cells (human T-lymphocyte cells) [24, 47] which can be applied to remove the cell wall–adsorbed AgNPs from *S. cerevisiae* cells, a microorganism of the fungus kingdom, while leaving the cells intact for analysis. The yeast cell AgNP uptake study demonstrated that the initial uptake of AgNPs was rapid and primarily driven by the mass of Ag per cell, not the nanoparticle size. However, there were optimal dosing concentrations in terms of AgNP particles per cell for each nanoparticle size tested. This model and metrology have high potential to be utilized in many applications, especially for green synthesis method optimization and as a

complementary method for nanotoxicity studies. To the authors' best knowledge, this is the first report for quantifying AgNP uptake in *S. cerevisiae* using SC-ICP-MS methodology.

SUPPLEMENTARY INFORMATION

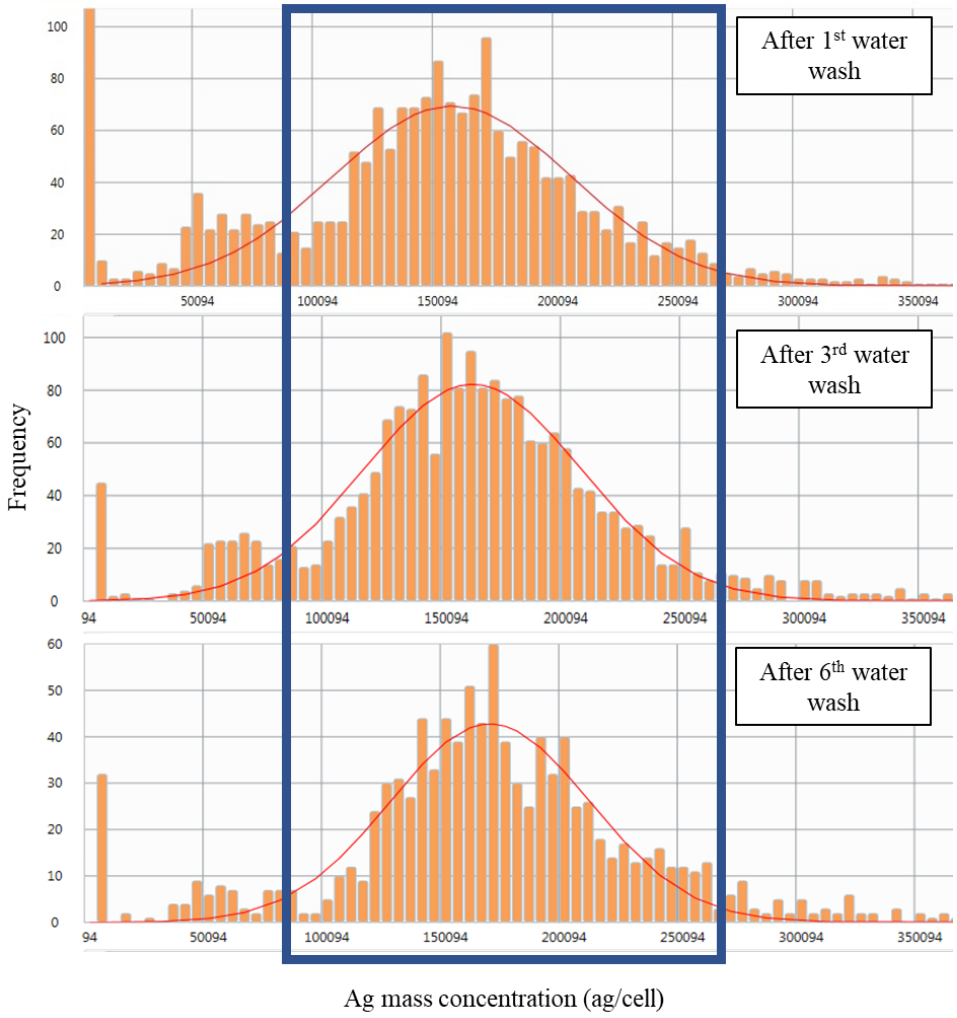

Figure S1. Histograms of AgNP dosed cells after different water washing times. Cells were dosed with 5000 AgNPs/cell for 24 hours. Cells were washed with water to validate that the wash procedure did not remove surface adsorbed AgNPs from the yeast cells.

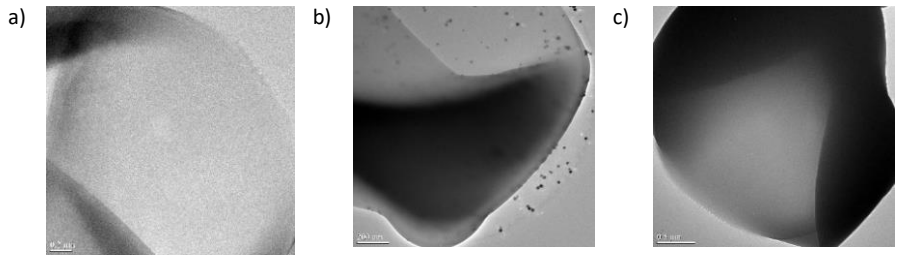

Figure S2. Representative TEM images of 20 nm AgNP dosed yeast cells after different washing processes. a) Control (not AgNP dosed), b) after ultra-high purity water wash, c) after PBS buffer (with 20 mM $K_3Fe(CN)_6$ and $Na_2S_2O_3 \cdot 5H_2O$) wash.

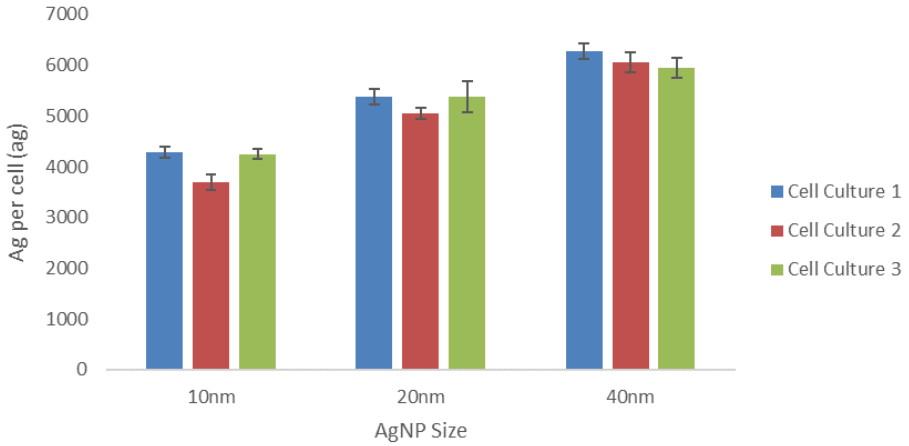

Figure S3. Reproducibility of results where 3 different cell cultures were dosed with 10, 20, and 40 nm AgNPs at 3000, 1000, and 300 AgNPs/cell, respectively for 3 hours. Error bars represent standard deviation (n=3).

ACKNOWLEDGEMENTS

This work was supported by Perkin Elmer, Inc., and the Center for Single Nanoparticle, Single Cell, and Single Molecule Monitoring (CS3M) at Missouri University of Science and Technology. The authors acknowledge the contributions from the following individuals over the course of this project: Chady Stephan and Jack Quade

for assisting and training operators on SC-ICP-MS setup and operation, Ke Li for assisting cell culture procedures used in the project, and Alec Falkenhain and Xing Shen for helping with some preliminary experiments at the early stage of the project.

REFERENCES

1. Taghavi SM, Momenpour M, Azarian M, Ahmadian M, Souri F, Taghavi SA, et al. Effects of nanoparticles on the environment and outdoor workplaces. Electron Physician. 2013;5(4):706–12.

2. Ramos AP, Cruz MAE, Tovani CB, Ciancaglini P. Biomedical applications of nanotechnology. Biophys Rev. 2017;9(2):79–89.

3. Abdelbasir SM, McCourt KM, Lee CM, Vanegas DC. Wastederived nanoparticles: synthesis approaches, environmental applications, and sustainability considerations. Front Chem. 2020;8:782.

4. Lu J, Struewing I, Buse HY, Kou J, Shuman HA, Faucher SP, et al. Legionella pneumophila transcriptional response following exposure to CuO nanoparticles. Appl Environ Microbiol. 2013;79(8):2713–20.

5. Bondarenko O, Juganson K, Ivask A, Kasemets K, Mortimer M, Kahru A. Toxicity of Ag, CuO and ZnO nanoparticles to selected environmentally relevant test organisms and mammalian cells in vitro: a critical review. Arch Toxicol. 2013;87:1181–200.

6. Hulkoti NI, Taranath TC. Biosynthesis of nanoparticles using microbes—a review. Colloids Surf, B. 2014;121:474–83.

7. Ahmed S, Ahmad M, Swami BL, Ikram S. A review on plants extract mediated synthesis of silver nanoparticles for antimicrobial applications: a green expertise. J Adv Res. 2016;7(1):17–28.

8. Hoseinzadeh E, Makhdoumi P, Taha P, Hossini H, Pirsaheb M, OmidRastegar S, et al. A review of available techniques for determination of nano-antimicrobials activity. Toxin Reviews. 2017;36(1):18–32.

9. Kettler K, Krystek P, Giannakou C, Hendriks AJ, de Jong WH. Exploring the effect of silver nanoparticle size and medium composition on uptake into pulmonary epithelial 16HBE14o-cells. J Nanopart Res. 2016;18:182.

10. Wilhelm S, Tavares AJ, Dai Q, Ohta S, Audet J, Dvorak HF, et al. Analysis of nanoparticle delivery to tumours. Nat Rev Mater. 2016;1(5):16014.

11. Sharma A, Kontodimas K, Bosmann M. Nanomedicine: a diagnostic and therapeutic approach to COVID-19. Front Med (Lausanne). 2021;8:648005.

12. Yang D. Application of nanotechnology in the COVID-19 pandemic. Int J Nanomed. 2021;16:623–49.

13. Ashraf S, Hassan Said A, Hartmann R, Assmann MA, Feliu N, Lenz P, et al. Quantitative particle uptake by cells as analyzed by different methods. Angew Chem Int Ed Engl. 2020;59(14):5438–53.

14. FitzGerald LI, Johnston APR. It's what's on the inside that counts: techniques for investigating the uptake and recycling of nanoparticles and proteins in cells. J Colloid Interface Sci. 2021;587:64–78.

15. Despax B, Saulou C, Raynaud P, Datas L, Mercier-Bonin M. Transmission electron microscopy for elucidating the impact of silver-based treatments (ionic silver versus nanosilver-containing coating) on the model yeast Saccharomyces cerevisiae. Nanotechnology. 2011;22(17):175101.

16. Mueller L, Traub H, Jakubowski N, Drescher D, Baranov VI, Kneipp J. Trends in single-cell analysis by use of ICP-MS. Anal Bioanal Chem. 2014;406(27):6963–77.

17. Wang H, Wang M, Wang B, Zheng L, Chen H, Chai Z, et al. Interrogating the variation of element masses and distribution patterns in single cells using ICP-MS with a high efficiency cell introduction system. Anal Bioanal Chem. 2017;409(5):1415–23.

18. Merrifield RC, Stephan C, Lead JR. Quantification of Au nanoparticle biouptake and distribution to freshwater algae using single cell − ICP-MS. Environ Sci Technol. 2018;52:2271–7.

19. Shen X, Zhang H, He X, Shi H, Stephan C, Jiang H, et al. Evaluating the treatment effectiveness of copper-based algaecides on toxic algae Microcystis aeruginosa using single cell-inductively coupled plasma-mass spectrometry. Anal Bioanal Chem. 2019;411(21):5531–43.

20. Ho K-S, Chan W-T. Time-resolved ICP-MS measurement for single-cell analysis and on-line cytometry. J Anal At Spectrom. 2010;25:1114–22.

21. Zheng L-N, Wang M, Wang B, Chen H-Q, Ouyang H, Zhao Y-L, et al. Determination of quantum dots in single cells by inductively coupled plasma mass spectrometry. Talanta. 2013;116:782–7.

22. Meyer S, López-Serrano A, Mitze H, Jakubowski N, Schwerdtle T. Single-cell analysis by ICP-MS/MS as a fast tool for cellular bioavailability studies of arsenite. Metallomics. 2018;10(1):73–6.

23. Virani F, Tanner S. Mass cytometry: an evolution in ICP-MS enabling novel insights in single-cell biology. Spectroscopy. 2015;30(5):14–22.

24. Malysheva A, Ivask A, Doolette CL, Voelcker NH, Lombi E. Cellular binding, uptake and biotransformation of silver nanoparticles in human T lymphocytes. Nat Nanotechnol. 2021;16(8):926–32.

25. Drescher D, Giesen C, Traub H, Panne U, Kneipp J, Jakubowski N. Quantitative imaging of gold and silver nanoparticles in single eukaryotic cells by laser ablation ICP-MS. Anal Chem. 2012;84:9684–8.

26. Wang M, Zheng L-N, Wang B, Chen H-Q, Zhao Y-L, Chai Z-F, et al. Quantitative analysis of gold nanoparticles in single cells by laser ablation inductively coupled plasma-mass spectrometry. Anal Chem. 2014;86:10252–6.

27. Zhai J, Wang Y, Xu C, Zheng L, Wang M, Feng W, et al. Facile approach to observe and quantify the αIIbβ3 integrin on a singlecell. Anal Chem. 2015;87:2546–9.

28. Van Malderen SJM, Vergucht E, De Rijcke M, Janssen C, Vincze L, Vanhaecke F. Quantitative determination and subcellular imaging of Cu in single cells via laser ablation-ICP-mass spectrometry using high-density microarray gelatin standards. Anal Chem. 2016;88:5783–9.

29. Wang H, Chen B, He M, Hu B. A Facile droplet-chip-timeresolved inductively coupled plasma mass spectrometry online system for determination of zinc in single cell. Anal Chem. 2017;89:4931–8.

30. Hong A, Tang Q, Khan AU, Miao M, Xu Z, Dang F, et al. Identification and speciation of nanoscale silver in complex solid matrices by sequential extraction coupled with inductively coupled plasma optical emission spectrometry. Anal Chem. 2021;93(4):1962–8.

31. Miyashita S-i, Fujii S-i, Shigeta K, Inagaki K. Single cell analysis by using ICP-MS. Metallomics 2017. p. 107–24.

32. Corte-Rodríguez M, Álvarez-Fernández R, García-Cancela P, Montes-Bayón M, Bettmer J. Single cell ICP-MS using on line sample introduction systems: current developments and remaining challenges. TrAC Trends Anal Chem. 2020;132:116042.

33. Wei X, Lu Y, Zhang X, Chen M-L, Wang J-H. Recent advances in single-cell ultra-trace analysis. TrAC Trends Anal Chem. 2020;127:115886.

34. Yin L, Zhang Z, Liu Y, Gao Y, Gu J. Recent advances in singlecell analysis by mass spectrometry. Analyst. 2019;144(3):824–45.

35. Yu X, He M, Chen B, Hu B. Recent advances in single-cell analysis by inductively coupled plasma-mass spectrometry: a review. Anal Chim Acta. 2020;1137:191–207.

36. Badhusha MSM, Mohideen MMAK. Biosynthesis of silver nanoparticles using Saccharomyces cerevisiae with different pH and study of antimicrobial activity against bacterial pathogens. Chem Sci Trans. 2016;5(4):906–11.

37. Chen Z, Li Z, Chen G, Zhu J, Liu Q, Feng T. In situ formation of AgNPs on S. cerevisiae surface as bionanocomposites for bacteria killing and heavy metal removal. Int J Environ Sci Technol. 2017;14:1635–42.

38. Li J, Ma G, Liu H, Liu H. Yeast cells carrying metal nanoparticles. Mater Chem Phys. 2018;207:373–9.

39. Narollahi A, Pourshamsian K, Mansourkiaee P. Antifungal activity of silver nanoparticles on some of fungi. Int J Nano Dimens. 2011;1(3):233–9.

40. Sillapawattana P, Gruhlke MCHH, Schäffer A. Effect of silver nanoparticles on the standard soil arthropod Folsomia candida (Collembola) and the eukaryote model organism Saccharomyces cerevisiae. Environ Sci Eur. 2016;28(1):27.

41. Zhang W, Liu X, Bao S, Xiao B, Fang T. Evaluation of nano-specific toxicity of zinc oxide, copper oxide, and silver nanoparticles through toxic ratio. J Nanopart Res. 2016;18(12):372.

42. Sujith A, Itoh T, Abe H, Anas AA, Yoshida K, Biju V, et al. Surface enhanced Raman scattering analyses of individual silver nanoaggregates on living single yeast cell wall. Appl Phys Lett. 2008;92:103901.

43. Sujith A, Itoh T, Abe H, Yoshida K-i, Kiran MS, Biju V, et al. Imaging the cell wall of living single yeast cells using surface-enhanced Raman spectroscopy. Anal Bioanal Chem. 2009;394:1803–9.

44. Bayat N, Rajapakse K, Marinsek-Logar R, Drobne D, Cristobal S. The effects of engineered nanoparticles on the cellular structure and growth of Saccharomyces cerevisiae. Nanotoxicology. 2014;8(4):363–73.

45. Bahadar H, Maqbool F, Niaz K, Abdollahi M. Toxicity of nanoparticles and an overview of current experimental models. Iran Biomed J. 2016;20(1):1–11.

46. Kettler K, Veltman K, van de Meent D, van Wezel A, Hendriks AJ. Cellular uptake of nanoparticles as determined by particle properties, experimental conditions, and cell type. Environ Toxicol Chem. 2014;33(3):481–92.

47. Ivask A, Mitchell AJ, Hope CM, Barry SC, Lombi E, Voelcker NH. Single cell level quantification of nanoparticle−cell interactions using mass cytometry. Anal Chem. 2017;89:8228–32.

48. Cossarizza A, Chang HD, Radbruch A, Acs A, Adam D, AdamKlages S, et al. Guidelines for the use of flow cytometry and cell sorting in immunological studies (second edition). Eur J Immunol. 2019;49(10):1457–973.

49. Validation of analytical procedures: text and methodology [updated November 1, 2005; cited 2021 November 2]. Available from: https://www.ich.org/ page/quality-guidelines.

SECTION

2. CONCLUSIONS

Understanding the interactions and metabolisms of compounds within biological systems is key to progress current research areas to real world applications. The work in this dissertation utilized advanced mass spectrometry instrumentation for cellular analyses in the fields of cancer and nanoparticle research, addressing two key topics: investigation of potential pteridine biomarkers in breast cancer cells and development of a single cell-ICP-MS method to quantitatively investigate the interaction of silver nanoparticles (AgNPs) with *Saccharomyces (S) cerevisiae* yeast cells. The results of these investigations contribute to broader research objectives including the development of a non-invasive breast cancer screening technique and development of green manufacturing in the nanoparticle industry, respectively.

In the first two papers presented in this dissertation, a recently developed HPLC-MS/MS method was advanced to elucidate pteridine metabolism in an isogenic progressive breast cancer cell model that included the sequentially derived MCF10A (benign), MCF10AT (premalignant), and MCF10CA1a (malignant) cell lines. The folate derived pteridine metabolic pathway was established first through dosing folic acid in the cell cultures and monitoring a panel of fifteen metabolic pteridine derivatives. The metabolism was then further confirmed through individual dosing of each pteridine directly in the culture of the breast cancer cell linages to determine the products of each individual step of the metabolic pathway. Furthermore, the changes of metabolites' levels

through progressive tumorigenicity of the breast cancer cells were also evaluated for potential breast cancer biomarkers. The results indicated that pteridines were located predominately in the extracellular media. Folic acid dosing increased extracellular levels of pterin, 6-hydroxylumazine, xanthopterin, 6-hydroxymethylpterin, and 6-carboxypterin. Pterin and 6-hydroxylumazine exhibited a strong correlation with tumorigenicity upon folate dosing. Pterin, isoxanthopterin, xanthopterin, sepiapterin, 6-biopterin, lumazine, 7-hydroxylumazine, and 6-hydroxylumazine were found to have altered metabolism in breast cancer cell lines by individual pteridine dosing. The pteridine biosynthetic pathway in breast cancer cells was established based on these findings. This study provided *in vitro* evidence for the observation of elevated pteridines in the urine of breast cancer patients, and also highlighted several key metabolic reactions within the pteridine biosynthetic pathway that will highly benefit further breast cancer biomarker investigation and clinical applications.

The third paper presented in this dissertation utilized a cutting-edge single cell-ICP-MS technique to investigate the interaction of AgNPs, one of the most broadly utilized type of NP, with *S. cerevisiae* yeast cells, a potential candidate for the green manufacturing of AgNPs. Rapid quantification of cell concentration, silver concentration per cell, and the profile of AgNP distribution in a cell population was used to evaluate dose time, concentration, and size impacts on AgNP uptake and to quantify intracellular versus extracellular AgNP concentrations by washing the dosed yeast cells using a water wash and PBS solution wash (with 20 mM $K_3Fe(CN)_6$ and $Na_2S_2O_3 \cdot 5H_2O$). This high

throughput and ultra-sensitive SC-ICP-MS method is expected to have many potential applications, such as optimization of AgNP green synthesis procedures, drug delivery, nanotoxicity.

BIBLIOGRAPHY

Ahmed, S., Ahmad, M., Swami, B.L. and Ikram, S. (2016) A review on plants extract mediated synthesis of silver nanoparticles for antimicrobial applications: A green expertise. *Journal of Advanced Research* **7,** 17-28. 10.1016/j.jare.2015.02.007

Almatroudi, A. (2020) Silver nanoparticles: synthesis, characterisation and biomedical applications. *Open Life Sciences* **15,** 819-839. 10.1515/biol-2020-0094

Alp, N.J. and Channon, K.M. (2004) Regulation of Endothelial Nitric Oxide Synthase by Tetrahydrobiopterin in Vascular Disease. *Arteriosclerosis, Thrombosis, and Vascular Biology* **24,** 413-420. 10.1161/01.atv.0000110785.96039.f6

Ashraf, S., Hassan Said, A., Hartmann, R., Assmann, M.A., Feliu, N., Lenz, P. and Parak, W.J. (2020) Quantitative Particle Uptake by Cells as Analyzed by Different Methods. *Angew Chem Int Ed Engl* **59,** 5438-5453. 10.1002/anie.201906303

Badhusha, M.S.M. and Mohideen, M.M.A.K. (2016) Biosynthesis of Silver Nanoparticles Using Saccharomyces Cerevisiae with Different pH and Study of Antimicrobial Activity against Bacterial Pathogens. *Chemical Science Transactions* **5,** 906-911. 10.7598/cst2016.1275

Bahadar, H., Maqbool, F., Niaz, K. and Abdollahi, M. (2016) Toxicity of Nanoparticles and an Overview of Current Experimental Models. *Iran Biomed J* **20,** 1-11. 10.7508/ibj.2016.01.001

Bahrulolum, H., Nooraei, S., Javanshir, N., Tarrahimofrad, H., Vasighe Sadat, M., Easton, A.J. and Ahmadian, G. (2021) Green synthesis of metal nanoparticles using microorganisms and their application in the agrifood sector. *Journal of Nanobiotechnology* **19,** 1-26. http://dx.doi.org/10.1186/s12951-021-00834-3

Battelli, M.G., Polito, L., Bortolotti, M. and Bolognesi, A. (2015) Xanthine oxidoreductase in cancer: more than a differentiation marker. *Cancer Medicine* **5,** 546-557. 10.1002/cam4.601

Blau, N., De Klerk, J.B.C., Thöny, B., Heizmann, C.W., Kierat, L., Smeitink, J.A.M. and Duran, M. (1996) Tetrahydrobiopterin Loading Test in Xanthine Dehydrogenase and Molybdenum Cofactor Deficiencies. *Biochemical and Molecular Medicine* **58,** 199-203. https://doi.org/10.1006/bmme.1996.0049

Bondarenko, O., Juganson, K., Ivask, A., Kasemets, K., Mortimer, M. and Kahru, A. (2013) Toxicity of Ag, CuO and ZnO nanoparticles to selected environmentally relevant test organisms and mammalian cells in vitro: a critical review. *Archives of Toxicology* **87,** 1181-1200. 10.1007/s00204-013-1079-4

Braasch, I., Schartl, M. and Volff, J.-N. (2007) Evolution of pigment synthesis pathways by gene and genome duplication in fish. *BMC Evolutionary Biology* **7**. https://doi.org/10.1186/1471-2148-7-74

Brejcha, J., Bataller, J.V., Bosáková, Z., Geryk, J., Havlíková, M., Kleisner, K., Maršík, P. and Font, E. (2019) Body coloration and mechanisms of colour production in Archelosauria: the case of deirocheline turtles. *Royal Society Open Science* **6**. https://doi.org/10.1098/rsos.190319

Burton, C. and Ma, Y. (2017) The role of urinary pteridines as disease biomarkers. *Pteridines* **28,** 1-21. https://doi.org/10.1515/pterid-2016-0013

Burton, C. and Ma, Y. (2019) Current Trends in Cancer Biomarker Discovery Using Urinary Metabolomics: Achievements and New Challenges. *Current Medicinal Chemistry* **26,** 5-28. 10.2174/0929867324666170914102236

Burton, C., Shi, H. and Ma, Y. (2013) Simultaneous Detection of Six Urinary Pteridines and Creatinine by High-Performance Liquid Chromatography-Tandem Mass Spectrometry for Clinical Breast Cancer Detection. *Analytical Chemistry* **85,** 11137-11145. https://doi.org/10.1021/ac403124a

Burton, C., Shi, H. and Ma, Y. (2014) Normalization of urinary pteridines by urine specific gravity for early cancer detection. *Clinica Chimica Acta* **435,** 42-47. https://doi.org/10.1016/j.cca.2014.04.022

Burton, C., Shi, H. and Ma, Y. (2016a) Daily variation and effect of dietary folate on urinary pteridines. *Metabolomics* **12,** 1-10. https://doi.org/10.1007/s11306-016-1019-4

Burton, C., Shi, H. and Ma, Y. (2016b) Development of a high-performance liquid chromatography – Tandem mass spectrometry urinary pterinomics workflow. *Analytica Chimica Acta* **927,** 72-81. https://doi.org/10.1016/j.aca.2016.05.005

Burton, C., Weng, R., Yang, L., Bai, Y., Liu, H. and Ma, Y. (2015) High-throughput intracellular pteridinic profiling by liquid chromatography–quadrupole time-of-flight mass spectrometry. *Analytica Chimica Acta* **853,** 442-450. https://doi.org/10.1016/j.aca.2014.10.044

Cañada-Cañada, F., Espinosa-Mansilla, A., Muñoz de la Peña, A. and Mancha de Llanos, A. (2009) Determination of marker pterins and biopterin reduced forms, tetrahydrobiopterin and dihydrobiopterin, in human urine, using a post-column photoinduced fluorescence liquid chromatographic derivatization method *Analytica Chimica Acta* **648,** 113-122. https://doi.org/10.1016/j.aca.2009.06.045

Cao, Y., Feng, J., Tang, L., Yu, C., Mo, G. and Deng, B. (2020) A highly efficient introduction system for single cell- ICP-MS and its application to detection of copper in single human red blood cells. *Talanta* **206,** 120174. 10.1016/j.talanta.2019.120174

Chalupsky, K., Kračun, D., Kanchev, I., Bertram, K. and Görlach, A. (2015) Folic Acid Promotes Recycling of Tetrahydrobiopterin and Protects Against Hypoxia-Induced Pulmonary Hypertension by Recoupling Endothelial Nitric Oxide Synthase. *Antioxidants & Redox Signaling* **23,** 1076-1091. 10.1089/ars.2015.6329

Chen, Z., Li, Z., Chen, G., Zhu, J., Liu, Q. and Feng, T. (2017) In situ formation of AgNPs on S. cerevisiae surface as bionanocomposites for bacteria killing and heavy metal removal. *International Journal of Environmental Science and Technology* **14,** 1635-1642. 10.1007/s13762-017-1261-y

Corte-Rodríguez, M., Álvarez-Fernández, R., García-Cancela, P., Montes-Bayón, M. and Bettmer, J. (2020) Single cell ICP-MS using on line sample introduction systems: Current developments and remaining challenges. *TrAC Trends in Analytical Chemistry* **132,** 116042. https://doi.org/10.1016/j.trac.2020.116042

Corte Rodríguez, M., García, n., Blanco, E., Bettmer, J. and Montes-Bayo, M. (2017) Quantitative Evaluation of Cisplatin Uptake in Sensitive and Resistant Individual Cells by Single-Cell ICP-MS (SC-ICP-MS). 10.1021/acs.analchem.7b02746

Crabtree, M.J., Tatham, A.L., Hale, A.B., Alp, N.J. and Channon, K.M. (2009) Critical Role for Tetrahydrobiopterin Recycling by Dihydrofolate Reductase in Regulation of Endothelial Nitric-oxide Synthase Coupling. *The Journal of Biological Chemistry* **284,** 28128-28136. https://doi.org/10.1074/jbc.M109.041483

Fan, H., Hitchcock, D.S., Seidel, R.D., Hillerich, B., Lin, H., Almo, S.C., Sali, A., Shoichet, B.K. and Raushel, F.M. (2013) Assignment of Pterin Deaminase Activity to an Enzyme of Unknown Function Guided by Homology Modeling and Docking. *Journal of the American Chemical Society* **135,** 795-803. 10.1021/ja309680b

Fini, M.A., Monks, J., Farabaugh, S.M. and Wright, R.M. (2011) Contribution of Xanthine Oxidoreductase to Mammary Epithelial and Breast Cancer Cell Differentiation In Part Modulates Inhibitor of Differentiation-1. *Molecular Cancer Research* **9,** 1242-1254. https://doi.org/10.1158/1541-7786.MCR-11-0176

Fini, M.A., Orchard-Webb, D., Kosmider, B., Amon, J.D., Kelland, R., Shibao, G. and Wright, R.M. (2008) Migratory activity of human breast cancer cells is modulated by differential expression of xanthine oxidoreductase. *Journal of Cellular Biochemistry* **105,** 1008-1026. 10.1002/jcb.21901

FitzGerald, L.I. and Johnston, A.P.R. (2021) It's what's on the inside that counts: Techniques for investigating the uptake and recycling of nanoparticles and proteins in cells. *Journal of Colloid and Interface Science* **587,** 64-78. https://doi.org/10.1016/j.jcis.2020.11.076

Fukushima, T. and Shiota, T. (1974) Biosynthesis of Biopterin by Chinese Hamster Ovary (CHO K1) Cell Culture. *Journal of Biological Chemistry* **249,** 4445-4451.

Gamagedara, S., Gibbons, S. and Ma, Y. (2011) Investigation of urinary pteridine levels as potential biomarkers for noninvasive diagnosis of cancer. *Clinica Chimica Acta* **412,** 120-128. https://doi.org/10.1016/j.cca.2010.09.015

Gao, L., Chalupsky, K., Stefani, E. and Cai, H. (2009) Mechanistic Insights into Folic Acid-dependent Vascular Protection: Dihydrofolate reductase-mediated Reduction in Oxidant Stress in Endothelial Cells and Angiotensin II-Infused Mice. *Journal of molecular and cellular cardiology* **47,** 752-760. https://doi.org/10.1016/j.yjmcc.2009.07.025

Gibbons, S.E., Stayton, I. and Ma, Y. (2009) Optimization of urinary pteridine analysis conditions by CE-LIF for clinical use in early cancer detection. *ELECTROPHORESIS* **30,** 3591-3597. https://doi.org/10.1002/elps.200900077

Goldberg, M. and Koller, M. (1991) Concentrations and Patterns of Released Pterins of Various Animal Cell Cultures. *Journal of Veterinary Medicine Series A* **38,** 49-53. https://doi.org/10.1111/j.1439-0442.1991.tb00983.x

Gross, S.S. and Levi, R. (1992) Tetrahydrobiopterin synthesis. An absolute requirement for cytokine-induced nitric oxide generation by vascular smooth muscle. *Journal of Biological Chemistry* **267,** 25722-25729.

Halpern, R., Halpern, B.C., Stea, B., Dunlap, A., Conklin, K., Clark, B., Ashe, H., Sperling, L., Halpern, J.A., Hardy, D. and Smith, R.A. (1977) Pterin-6-aldehyde, a cancer cell catabolite: identification and application in diagnosis and treatment of human cancer. *Proceedings of the National Academy of Sciences of the United States of America* **74,** 587-591. https://doi.org/10.1073/pnas.74.2.587

Han, F., Huynh, B.H., Shi, H., Lin, B. and Ma, Y. (1999) Pteridine Analysis in Urine by Capillary Electrophoresis Using Laser-Induced Fluorescence Detection. *Analytical Chemistry* **71,** 1265-1269. 10.1021/ac981218v

Hansen, M.F., Jensen, S.Ø., Füchtbauer, E.-M. and Martensen, P.M. (2017) High folic acid diet enhances tumour growth in PyMT-induced breast cancer. *British Journal of Cancer* **116,** 752-761. https://doi.org/10.1038/bjc.2017.11

Hartmann, L.C., Keeney, G.L., Lingle, W.L., Christianson, T.J.H., Varghese, B., Hillman, D., Oberg, A.L. and Low, P.S. (2007) Folate receptor overexpression is associated with poor outcome in breast cancer. *International Journal of Cancer* **121,** 938-942. https://doi.org/10.1002/ijc.22811

Ho, K.-S. and Chan, W.-T. (2010) Time-resolved ICP-MS measurement for single-cell analysis and on-line cytometry. *Journal of Analytical Atomic Spectrometry* **25,** 1114-1122. 10.1039/c002272a

Hoseinzadeh, E., Makhdoumi, P., Taha, P., Hossini, H., Pirsaheb, M., Omid Rastegar, S. and Stelling, J. (2017) A review of available techniques for determination of nano-antimicrobials activity. *Toxin Reviews* **36,** 18-32. 10.1080/15569543.2016.1237527

Ivask, A., Mitchell, A.J., Hope, C.M., Barry, S.C., Lombi, E. and Voelcker, N.H. (2017) Single Cell Level Quantification of Nanoparticle−Cell Interactions Using Mass Cytometry. *Analytical Chemistry* **89,** 8228-8232. 10.1021/acs.analchem.7b01006

Jayaraman, A., Thandeeswaran, M., Priyadarsini, U., Sabarathinam, S., Nawaz, K.A.A. and Palaniswamy, M. (2016) Characterization of unexplored amidohydrolase enzyme—pterin deaminase. *Applied Microbiology and Biotechnology* **100,** 4779-4789. 10.1007/s00253-016-7513-9

Kettler, K., Krystek, P., Giannakou, C., Hendriks, A.J. and de Jong, W.H. (2016) Exploring the effect of silver nanoparticle size and medium composition on uptake into pulmonary epithelial 16HBE14o-cells. *J Nanopart Res* **18,** 182. 10.1007/s11051-016-3493-z

Kettler, K., Veltman, K., van de Meent, D., van Wezel, A. and Hendriks, A.J. (2014) Cellular uptake of nanoparticles as determined by particle properties, experimental conditions, and cell type. *Environmental Toxicology and Chemistry* **33,** 481-492. https://doi.org/10.1002/etc.2470

Kośliński, P., Bujak, R., Daghir, E. and Markuszewski, M.J. (2011) Metabolic profiling of pteridines for determination of potential biomarkers in cancer diseases. *ELECTROPHORESIS* **32,** 2044-2054. https://doi.org/10.1002/elps.201000664

Kośliński, P., Jarzemski, P., Markuszewski, M.J. and Kaliszan, R. (2014) Determination of pterins in urine by HPLC with UV and fluorescent detection using different types of chromatographic stationary phases (HILIC, RP C8, RP C18). *Journal of Pharmaceutical and Biomedical Analysis* **91,** 37-45. 10.1016/j.jpba.2013.12.012

Leipold, M.D., Obermoser, G., Fenwick, C., Kleinstuber, K., Rashidi, N., McNevin, J.P., Nau, A.N., Wagar, L.E., Rozot, V., Davis, M.M., DeRosa, S., Pantaleo, G., Scriba, T.J., Walker, B.D., Olsen, L.R. and Maecker, H.T. (2017) Comparison of CyTOF assays across sites: Results of a six-center pilot study. *Journal of Immunological Methods* **453,** 37-43. 10.1016/j.jim.2017.11.008

Li, J., Ma, G., Liu, H. and Liu, H. (2018) Yeast cells carrying metal nanoparticles. *Materials Chemistry and Physics* **207,** 373-379. 10.1016/j.matchemphys.2018.01.001

Linder, N., Lundin, J., Isola, J., Lundin, M., Raivio, K.O. and Joensuu, H. (2005) Down-Regulated Xanthine Oxidoreductase Is a Feature of Aggressive Breast Cancer. *Clinical Cancer Research* **11,** 4372-4381. 10.1158/1078-0432.ccr-04-2280

Ma, Y. and Burton, C. (2013) Pteridine detection in urine: the future of cancer diagnostics? *Biomarkers in Medicine* **7,** 679-681. https://doi.org/10.2217/bmm.13.88

Malysheva, A., Ivask, A., Doolette, C.L., Voelcker, N.H. and Lombi, E. (2021) Cellular binding, uptake and biotransformation of silver nanoparticles in human T lymphocytes. *Nature Nanotechnology* **16,** 926-932. 10.1038/s41565-021-00914-3

Merrifield, R.C., Stephan, C. and Lead, J.R. (2018) Quantification of Au Nanoparticle Biouptake and Distribution to Freshwater Algae Using Single Cell − ICP-MS. *Environmental Science and Technology* **52,** 2271-2277. 10.1021/acs.est.7b04968

Miyashita, S.-i., Fujii, S.-i., Shigeta, K. and Inagaki, K. (2017) Single Cell Analysis by Using ICP-MS, *Metallomics*. pp. 107-124. 10.1007/978-4-431-56463-8_5

Montoro Bustos, A.R., Petersen, E.J., Possolo, A. and Winchester, M.R. (2015) Post hoc Interlaboratory Comparison of Single Particle ICP-MS Size Measurements of NIST Gold Nanoparticle Reference Materials. *Analytical Chemistry* **87,** 8809-8817. 10.1021/acs.analchem.5b01741

Montoro Bustos, A.R., Purushotham, K.P., Possolo, A., Farkas, N., Vladár, A.E., Murphy, K.E. and Winchester, M.R. (2018) Validation of Single Particle ICP-MS for Routine Measurements of Nanoparticle Size and Number Size Distribution. *Analytical Chemistry* **90,** 14376-14386. 10.1021/acs.analchem.8b03871

Mueller, L., Traub, H., Jakubowski, N., Drescher, D., Baranov, V.I. and Kneipp, J. (2014) Trends in single-cell analysis by use of ICP-MS. *Analytical and Bioanalytical Chemistry* **406,** 6963-6977. 10.1007/s00216-014-8143-7

Murr, C., Bergant, A., Widschwendter, M., Heim, K., Schröcksnadel, H. and Fuchs, D. (1999) Neopterin Is an Independent Prognostic Variable in Females with Breast Cancer. *Clinical Chemistry* **45,** 1998-2004. 10.1093/clinchem/45.11.1998

Murugesan, T., Velliayadevar, K., Easwaran, M., Kg, K., Ka, A.N., Ramasamy, M., Muthusamy, P. and Jayaraman, A. (2017) Molecular architecture of pterin deaminase from Saccharomyces cerevisiae NCIM 3458. *Pteridines* **28,** 141-151. 10.1515/pterid-2017-0011

Necela, B.M., Crozier, J.A., Andorfer, C.A., Lewis-Tuffin, L., Kachergus, J.M., Geiger, X.J., Kalari, K.R., Serie, D.J., Sun, Z., Aspita, A.M., O'Shannessy, D.J., Maltzman, J.D., McCullough, A.E., Pockaj, B.A., Cunliffe, H.E., Ballman, K.V., Thompson, E.A. and Perez, E.A. (2015) Folate Receptor-α (FOLR1) Expression and Function in Triple Negative Tumors. *PLOS ONE* **10,** 1-19. https://doi.org/10.1371/journal.pone.0122209

Odate, S., Tatebe, Y., Obika, M. and Hama, T. (1959) Pteridine Derivatives in Reptilian Skin. *Proceedings of the Japan Academy* **35,** 567-570. https://doi.org/10.2183/pjab1945.35.567

Oettle, K. and Reibnegger, G. (1999) Pteridines as inhibitors of xanthine oxidase: structural requirements. *Biochimica et Biophysica Acta* **1430,** 387-395.

Off, M.K., Steindal, A.E., Porojnicu, A.C., Juzeniene, A., Vorobey, A., Johnsson, A. and Moan, J. (2005) Ultraviolet photodegradation of folic acid. *Journal of Photochemistry and Photobiology B: Biology* **80,** 47-55. https://doi.org/10.1016/j.jphotobiol.2005.03.001

Rasmussen, L., Foulks, Z., Burton, C. and Shi, H. (2022a) Establishing pteridine metabolism in a progressive isogenic breast cancer cell model. *Metabolomics* **18**. 10.1007/s11306-021-01861-9

Rasmussen, L., Shi, H., Liu, W. and Shannon, K.B. (2022b) Quantification of silver nanoparticle interactions with yeast Saccharomyces cerevisiae studied using single-cell ICP-MS. *Analytical and Bioanalytical Chemistry*. 10.1007/s00216-022-03937-4

Rembold, H., Metzger, H. and Gutensohn, W. (1971) Catabolism of Pteridine Cofactors: III. On the introduction of an oxygen function into position 6 of the pteridine ring. *Biochimica et Biophysica Acta* **230,** 117-126. https://doi.org/10.1016/0304-4165(71)90059-6

Rembold, H. and Simmersbach, F. (1969) Catabolism of pteridine cofactors II. A specific pterin deaminase in rat liver. *Biochimica et Biophysica Acta* **184,** 589-596.

Rosli, N.A., Teow, Y.H. and Mahmoudi, E. (2021) Current approaches for the exploration of antimicrobial activities of nanoparticles. *Science and Technology of Advanced Materials* **22,** 885-907. 10.1080/14686996.2021.1978801

Schoedon, G., Troppmair, J., Fontana, A., Huber, C., Curtius, H.-C. and Niederwieser, A. (1987) Biosynthesis and metabolism of pterins in peripheral blood mononuclear cells and leukemia lines of man and mouse. *European Journal of Biochemistry* **166,** 303-310. https://doi.org/10.1111/j.1432-1033.1987.tb13515.x

Shen, X., Zhang, H., He, X., Shi, H., Stephan, C., Jiang, H., Wan, C. and Eichholz, T. (2019) Evaluating the treatment effectiveness of copper-based algaecides on toxic algae Microcystis aeruginosa using single cell-inductively coupled plasma-mass spectrometry. *Analytical and Bioanalytical Chemistry* **411,** 5531-5543. 10.1007/s00216-019-01933-9

Stea, B., Backlund, P.S., Berkey, P.B., Cho, A.K., Halpern, B.C., Halpern, R.M. and Smith, R.A. (1978) Folate and Pterin Metabolism by Cancer Cells in Culture. *Cancer Research* **38,** 2378-2384.

Stea, B., Halpern, R.M., Halpern, B.C. and Smith, R.A. (1981) Urinary excretion levels of unconjugated pterins in cancer patients and normal individuals. *Clinica Chimica Acta* **113,** 231-242. 10.1016/0009-8981(81)90277-1

Sujith, A., Itoh, T., Abe, H., Anas, A.A., Yoshida, K., Biju, V. and Ishikawa, M. (2008) Surface enhanced Raman scattering analyses of individual silver nanoaggregates on living single yeast cell wall. *Applied Physics Letters* **92,** 103901. 10.1063/1.2891086

Sujith, A., Itoh, T., Abe, H., Yoshida, K.-i., Kiran, M.S., Biju, V. and Ishikawa, M. (2009) Imaging the cell wall of living single yeast cells using surface-enhanced Raman spectroscopy. *Analytical and Bioanalytical Chemistry* **394,** 1803-1809. 10.1007/s00216-009-2883-9

Taghavi, S.M., Momenpour, M., Azarian, M., Ahmadian, M., Souri, F., Taghavi, S.A., Sadeghain, M. and Karchani, M. (2013) Effects of Nanoparticles on the Environment and Outdoor Workplaces. *Electronic physician* **5,** 706-12. 10.14661/2013.706-712

Tanaka, Y.-k., Iida, R., Takada, S., Kubota, T., Yamanaka, M., Sugiyama, N., Abdelnour, Y. and Ogra, Y. (2020) Quantitative Elemental Analysis of a Single Cell by Using Inductively Coupled Plasma-Mass Spectrometry in Fast Time-Resolved Analysis Mode. *ChemBioChem* **21,** 3266-3272. https://doi.org/10.1002/cbic.202000358

Tenchov, R., Bird, R., Curtze, A.E. and Zhou, Q. (2021) Lipid Nanoparticles─From Liposomes to mRNA Vaccine Delivery, a Landscape of Research Diversity and Advancement. *ACS Nano* **15,** 16982-17015. 10.1021/acsnano.1c04996

Tomšíková, H., Solich, P. and Nováková, L. (2014) Sample preparation and UHPLC-FD analysis of pteridines in human urine. *Journal of Pharmaceutical and Biomedical Analysis* **95,** 265-272. 10.1016/j.jpba.2014.03.012

Tomšíková, H., Tomšík, P., Solich, P. and Nováková, L. (2013) Determination of pteridines in biological samples with an emphasis on their stability. *Bioanalysis* **5,** 2307-2326. https://doi.org/10.4155/bio.13.194

Wang, H., Wang, M., Wang, B., Zheng, L., Chen, H., Chai, Z. and Feng, W. (2017) Interrogating the variation of element masses and distribution patterns in single cells using ICP-MS with a high efficiency cell introduction system. *Analytical and Bioanalytical Chemistry* **409,** 1415-1423. 10.1007/s00216-016-0075-y

Watt, W.B. (1967) Pteridine Biosynthesis in the Butterfly Colias eurytheme. *Journal of Biological Chemistry* **242,** 565-572. 10.1016/S0021-9258(18)96242-3

Watt, W.B. (1972) Xanthine Dehydrogenase and Pteridine Metabolism in *Colias* Butterflies. *Journal of Biological Chemistry* **247,** 1445-1451. https://doi.org/10.1016/S0021-9258(19)45578-6

Wei, X., Lu, Y., Zhang, X., Chen, M.-L. and Wang, J.-H. (2020) Recent advances in single-cell ultra-trace analysis. *TrAC Trends in Analytical Chemistry* **127,** 115886. https://doi.org/10.1016/j.trac.2020.115886

Weiss, G., Kronberger, P., Conrad, F., Bodner, E., Wachter, H. and Reibnegger, G. (1993) Neopterin and Prognosis in Patients with Adenocarcinoma of the Colon. *Cancer Research* **53,** 260-265.

Wilhelm, S., Tavares, A.J., Dai, Q., Ohta, S., Audet, J., Dvorak, H.F. and Chan, W.C.W. (2016) Analysis of nanoparticle delivery to tumours. *Nature Reviews Materials* **1,** 16014. 10.1038/natrevmats.2016.14

Yin, L., Zhang, Z., Liu, Y., Gao, Y. and Gu, J. (2019) Recent advances in single-cell analysis by mass spectrometry. *The Analyst*. 10.1039/C8AN01190G

Yu, X., He, M., Chen, B. and Hu, B. (2020) Recent advances in single-cell analysis by inductively coupled plasma-mass spectrometry: A review. *Analytica Chimica Acta* **1137,** 191-207. https://doi.org/10.1016/j.aca.2020.07.041

Zhang, X.-F., Liu, Z.-G., Shen, W. and Gurunathan, S. (2016) Silver Nanoparticles: Synthesis, Characterization, Properties, Applications, and Therapeutic Approaches. *International Journal of Molecular Sciences* **17,** 1534. 10.3390/ijms17091534

VITA

Lindsey Katherine Rasmussen was born in California. She received a dual major in 2015 from the University of Arkansas in Fayetteville, AR with a Bachelor of Science in Chemistry and Biochemistry and a Bachelor of Art in Spanish. After graduation, she started working in the Quality Control department at Brewer Science in Rolla, MO where she continued to work throughout her academic pursuits to the present. In 2016, she started taking classes at Missouri University of Science and Technology. In 2017, she joined Dr. Yinfa Ma and Dr. Honglan Shi's research group for a masters in Analytical Chemistry studying silver nanoparticle uptake in *S. cerevisiae* using SC-ICP-MS. In 2018, she changed programs to work towards a Ph.D. in Analytical Chemistry in the same research group under the direction of Dr. Honglan Shi. Her research shifted focus to the study of pteridine biomarkers in breast cancer cells using HPLC-MS/MS. She received a Ph.D. in Chemistry from Missouri University of Science and Technology in May 2022.